Office of Naval Research

Contract N50RI-76 • Task Order No.1 • NR-071-012

A PROBE SIGNAL STUDY OF THE HULL MAGNETRON DIODE

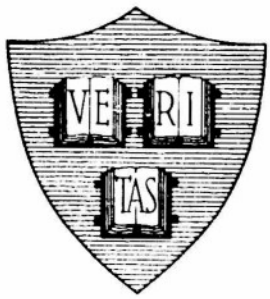

By

John A. Bradshaw

July 20, 1954

Technical Report No. 185

Cruft Laboratory
Harvard University
Cambridge, Massachusetts

TR185

Office of Naval Research

Contract N5ori-76

Task Order No. 1

NR-071-011

Technical Report

on

A Probe Signal Study of the Hull Magnetron Diode

by

John A. Bradshaw

July 20, 1954

The research reported in this document was made possible through support extended Cruft Laboratory, Harvard University, jointly by the Navy Department (Office of Naval Research), the Signal Corps of the U. S. Army, and the U. S. Air Force, under ONR Contract N5ori-76, T. O. 1.

Technical Report No. 185

Cruft Laboratory

Harvard University

Cambridge, Massachusetts

Table of Contents

TR185

A Probe Signal Study of the Hull Magnetron Diode

by

John A. Bradshaw

Abstract

The Hull magnetron diode is a vacuum tube essentially consisting of two concentric metal cylinders. In the diode used to obtain the results herein reported, the inner cylinder was a nickel sleeve 1/4" in diameter and it carried an oxide coating 10 cm long. The outer cylinder was a heavy copper anode. The sleeve could be heated above 1200°K and a steady voltage could be applied between it and the anode.

Anode and sleeve were also sections integrated in a coaxial transmission line between a high-frequency oscillator and a detector. A TEM wave could then pass from the oscillator through the diode to the detector, probing or exciting, as it passed, the space charge of electrons emitted from the hot oxide coating. When a uniform steady magnetic field is imposed on the diode, parallel to its cylindrical axis, the flow of electrons from sleeve to anode may be virtually cut off, and the diode operates as a magnetron.

The probe signal suffers a sharp resonance absorption in transmission through the magnetron when the cyclotron frequency (characteristic of an electron in the magnetic field) lies close to the probe frequency. Near this absorption frequency the transmitted signal suffers changes of phase as well as of amplitude. These were observed over wide ranges of probe frequency, anode voltage, magnetic field and cathode temperature. The changes were correlated with other effects, the disturbance of the residual current by the probe signal, the noise generated in the tube, the signal at the second harmonic of the probe frequency, also generated in the tube and so on. The second half of this report outlines these changes and related effects.

For interpreting these phenomena, the basis is Hull's set of equations of the electronic orbit. In the first half of this report, an examination of the orbit equations yields an expression for the conductivity of the space-charge cloud. The conductivity depends on the ratios of probe and orbit frequency to the cyclotron frequency, u and u_o respectively, on a phenomenological damping parameter τ, and on the average charge density. This density in turn depends on the ratio of anode voltage to the square of the magnetic field.

The probe signal measurements imply a particular distribution of the space charge within the magnetron diode. The features of this distribution form the subject of a companion report, TR 201.

TR185

A Probe Signal Study of the Hull Magnetron Diode

by

J. A. Bradshaw

Cruft Laboratory, Harvard University

Cambridge, Massachusetts

I

The Free Orbit

a. Introduction.

The invention of the magnetron diode is generally credited to A. W. Hull. In a brief letter [1] to the Physical Review in April, 1921, he gave the Hull cutoff relation, and in a twenty-six page article [2] submitted to the same review in July, 1921, he gave a more complete theory, and the results of experiments on over a thousand tubes. The invention presents not only a problem in orbits of free electrons, as Hull realized, but also one in prolonged coulomb interactions of individual charges. The tools for probing a magnetron space charge without disturbing it seriously are not flexible, and the results so far reported are not conclusive. This technical report develops one such tool, the TEM mode probe signal, and attempts to interpret the indications it gives.

We begin, as did Hull, with the basic relations for the orbit of an electron in a magnetron, and develop a rather general solution. This gives the trajectory which an electron will trace after release, between cathode and anode of a cylindrical magnetron, with arbitrary velocity and position in crossed steady electric and magnetic fields. The chief result of the first chapter will be to develop expressions for a coefficient u. If ω is the cyclotron angular frequency, characteristic of an electron in the steady magnetic field in the magnetron and ω_o is the orbit angular frequency, then we define u as

$$u \equiv (\omega_o / \omega) . \qquad (1.1)$$

Since, in general, u is less than 1, the electron lags in its orbit, for reasons

which we will develop. In the first section, we give a treatment in terms of Newtonian velocities, and in the second a relativistic reformulation.

b. Newtonian Motion.

Let us take a coordinate system (r,θ,z) with the z-axis at the center of two concentric conducting cylinders with radii r_a and r_c, $r_a > r_c$, as in Fig. 1-1. Between these cylinders we assume there are static fields:

$$E_r = -\frac{1}{r}\frac{d\phi(r)}{dr} \quad , \qquad B_z = \frac{1}{r}\frac{dr\, A_\theta(r)}{dr} \quad . \tag{1.2}$$

If $B_z = B$ is a constant, then we find

$$A_\theta = \frac{rB}{2} \quad , \quad \omega = \frac{eB}{m} \quad . \tag{1.3}$$

Although the particle moves in three dimensions, in this chapter we consider only the projection of the path on the (r,θ) plane and omit the velocity $\dot{z}$ without further comment here. The equations of motion then are

$$\frac{mv^2}{2} + e\phi = \left(\frac{mv^2}{2} + e\phi\right)_o \quad , \quad r^2\left(\dot{\theta} + \frac{\omega}{2}\right) = \left[r^2\left(\dot{\theta} + \frac{\omega}{2}\right)\right]_o \quad . \tag{1.4}$$

Here the subscript o denotes initial conditions $(t=t_o)$, and $v^2 = \dot{r}^2 + (r\dot{\theta})^2$ is a scalar, the velocity squared. We are interested in steady-state solutions of Hull's equations (1.4), in radial motion between r_b and r_d, and in suitable circumferential motion about the polar axis. The radii r_b and r_d are turning point radii where $\dot{r}$ vanishes. We assume

$$r_a > r_b \geq r_d > r_c \quad . \tag{1.5}$$

We now introduce some unfamiliar notation. The radial equation looks simpler if the independent variable is $s \equiv (r/r_c)^2$. To simplify the initial conditions we assume $r_o = r_d$, so $\dot{r}_o = 0$. We introduce a normalized (dimensionless) potential Φ, and a canonical angular momentum P as follows:

$$\Phi = \frac{e(\phi_d - \phi(r))}{m\omega^2 r_c^2} \quad , \quad P = \left[\frac{2s}{\omega}\left(\dot{\theta} + \frac{\omega}{2}\right)\right]_d = \text{constant} \quad . \tag{1.6}$$

Then we eliminate $\dot{\theta}$ between equations (1.4) and obtain:

$$\dot{s}^2 = \omega^2\left[8s\Phi + \left(\frac{P^2}{s_d} - s\right)(s - s_d)\right] \quad . \tag{1.7}$$

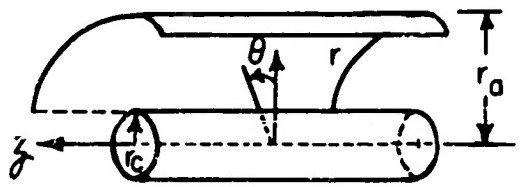

FIG. 1-1 CYLINDRICAL SYSTEM

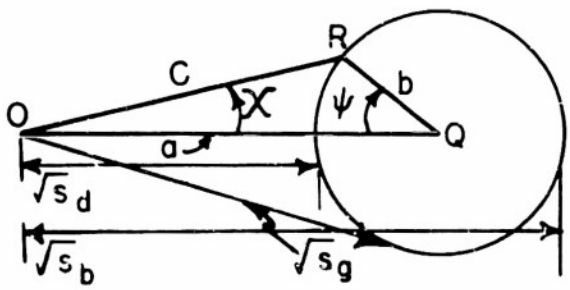

FIG. 1-2 LOCUS OF P

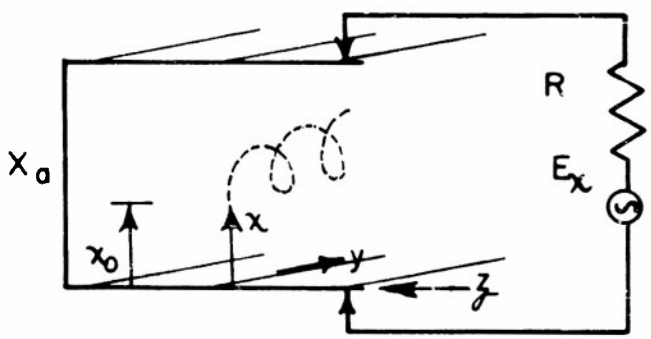

FIG. 1-3 PLANAR SYSTEM

If $\Phi(s)$ is known, then we may integrate the radial equation (1.7) by quadrature, and find s_b and the half period t_b.

We mention first a solution of (1.7) for small radial oscillations. This was given by Allis [3] in 1941. If ξ is a quantity much less than one, we write

$$s = s_g(1+\xi) \quad , \quad s\Phi(s) = s_g^2[\xi \left.\frac{d\Phi}{ds}\right|_g + \frac{\xi^2}{2} \left.\frac{d^2 s\Phi}{ds^2}\right|_g + \ldots] \quad . \tag{1.8}$$

The latter relation is essentially a MacLaurin series for $s\Phi$; the expansion is about the median radius s_g of an individual orbit. Substituting (1.8) in (1.7) we require the coefficient of the term linear in ξ to vanish. We find as $\xi \to 0$ that s_b and $s_d \to s_g$, $\Phi_g \to \Phi_d = 0$ as assumed in (1.8), and:

$$\bar{P}^2 = s_g^2(1 - 8\left.\frac{d\Phi}{ds}\right|_g) \quad , \quad \text{or} \quad \dot{\theta}_g = -\frac{\omega}{2}[1 \pm \sqrt{1 - 8\left.\frac{d\Phi}{ds}\right|_g}] \quad . \tag{1.9}$$

We now distinguish two types of stable orbit: $|\dot{\theta}_1| \geq \frac{\omega}{2} \geq |\dot{\theta}_2|$. As Allis pointed out, in a $\dot{\theta}_1$ orbit the magnetic field has to balance chiefly the centrifugal force on the particle, while in a $\dot{\theta}_2$ orbit, B balances chiefly E_r. The first case resembles the cyclotron, the second applies to the magnetron.

From terms quadratic in ξ we find

$$\dot{\xi}^2 + \omega^2 u^2 \xi^2 = 0, \quad u^2 \equiv 1 - 4\left.\frac{d^2 s\Phi}{ds^2}\right|_g \quad . \tag{1.10}$$

The solution follows: $\xi = \xi_o \cos \omega u(t-t_o)$. This gives the radial oscillation of a particle about a stable secular orbit described by (1.9). There is a corresponding circumferential oscillation which we may describe by η, in $\dot{\theta} \equiv \dot{\theta}_2(1+\eta)$:

$$\eta = -\frac{\omega}{2\dot{\theta}_2}\frac{P}{s_g}\xi \quad , \quad \text{or} \quad \eta^2 = \xi^2(\frac{\omega}{2\dot{\theta}_2})^2[1 - 8\left.\frac{d\Phi}{ds}\right|_g] \quad . \tag{1.11}$$

(Here we have ignored a term $\eta \cdot \xi$.) The sum of these motions is the typical cycloidal path around the magnetron cathode. We have, incidentally, in (1.10) our first expression for the lag coefficient u. Now Poisson's

equation may take the form

$$\frac{d}{ds}\left(s\frac{d\Phi}{ds}\right) = -\frac{\rho(r)r_c^2}{4\epsilon_o} \quad . \tag{1.12}$$

Hence we may rewrite the expression for u^2 as

$$u^2 = 1 - 4\left[\frac{d}{ds}s\frac{d\Phi}{ds} + \frac{d\Phi}{ds}\right]_g = 1 - \frac{e}{m\omega^2}\left[\frac{\rho}{\epsilon_o} + \frac{2E_r}{r}\right]_g \quad . \tag{1.13}$$

Thus as Allis observed (3, page 7) "the oscillation frequency ($\omega_o = \omega u$) is smaller than the cyclotron frequency by an amount which depends on the electric field and the charge density." Moreover, the radial oscillations are unstable if $u^2 < 0$, so we may assume $d^2s\Phi/ds^2 < 1/4$.

We wish next to remove the restriction $\xi \ll 1$, and to generalize the solution of (1.7) to include larger radial oscillations. We can find a simple "closed" solution, if $8s\Phi$ has a particular but fairly flexible form. Allis used a MacLaurin series for $s\Phi$; we propose now a power series in which B and C are constants, at least over the radial extent of the individual orbit under discussion.

$$8s\Phi = \frac{s - s_d}{s_d}[B + C(ss_d + 1)] \quad \text{or} \quad \phi(s) = \frac{-mr_c^2\omega^2}{8e}\left(\frac{s-1}{s}\right)[B + C(s+1)] \quad . \tag{1.14}$$

Since the magnetic field always appears as ω, the constant B need not be confused with it. The factor $(s-1)$ in $\phi(s)$ assures us that $\phi(1) = 0$, so the inner cylinder is our reference for potential.

If this Φ is introduced in (1.7) we find

$$\dot{s}^2 = \omega^2 u^2 (s - s_d)(s_b - s) \quad , \quad u^2 \equiv 1 - C \quad , \quad s_b \equiv \frac{B + C + P^2}{u^2 s_d} \quad . \tag{1.15}$$

Because $\dot{s}$ vanishes if $s = s_b$, and $\dot{s}$ is proportional to $\underline{u}$, it follows that s_b is indeed the outer turning point, and $\underline{u}$ the lag coefficient. The solution of (1.15), as one can show by substitution, is

$$s = \frac{1}{2}[(s_b + s_d) - (s_b - s_d)x] \quad , \quad x = \cos \omega u(t - t_o) \quad . \tag{1.16}$$

Introduction of a parameter k leads to the following modifications of (1.15) and (1.16):

$$k \equiv \frac{s_b - s_d}{s_b + s_d} \quad , \quad s = s_d \left(\frac{1 - kx}{1 - k}\right) \quad , \quad \dot{x}^2 = \omega^2 u^2 (1 - x^2) \quad . \tag{1.17}$$

This radial motion is, then, an oscillation with angular frequency ωu between extreme radii s_b and s_d.

We propose to write (1.15) and its solution in two other forms. The first form has a simple geometric interpretation

$$s = a^2 + b^2 - 2abx \quad , \quad a \equiv \frac{1}{2}(\sqrt{s_b} + \sqrt{s_d}) \quad , \quad b \equiv \frac{1}{2}(\sqrt{s_b} - \sqrt{s_d}). \tag{1.18}$$

This is just the cosine law for the angle $\psi = \omega u(t - t_o)$ in the triangle (abc) in Fig. 1-2, if we take $s = c^2$. There the point R, as a function of ψ, describes a circle with radius b and center Q at a distance a from the origin O. Moreover, from Fig. 1-2, we find

$$d\chi = d\psi \left\{\frac{s_g - s}{2s}\right\} \quad , \quad s_g \equiv \sqrt{s_b s_d} \tag{1.19}$$

Here χ is the angle R subtends at O. The integral of (1.19) we find at once, in part from (1.6):

$$s_g \int_{s_o}^{s} \frac{d\psi}{s} = \psi - \psi_o + 2(\chi - \chi_o) = \frac{s_g}{P}(\psi - \psi_o + 2u[\theta - \theta_o]) \quad . \tag{1.20}$$

The relations (1.20) show two things: first, the average value of (1/s), over a revolution $(\psi - \psi_o) = 2\pi$, is $(1/s_g)$; and second, the rate of change of θ can be expressed in terms of $\dot{\psi}$ and $\dot{\chi}$. The average value of $\dot{\chi}$ is zero, so we have, writing the average value of $\dot{\theta}$ as $\bar{\dot{\theta}}$:

$$\dot{\theta} = \left(\frac{P}{s_g} - 1\right)\frac{\dot{\psi}}{2u} + \frac{P}{u s_g}\dot{\chi} \quad ; \quad \bar{\dot{\theta}} = \left(\frac{P}{s_g} - 1\right)\frac{\omega}{2} \quad . \tag{1.21}$$

Now if B + C = 0, then $P = u s_g$ and $\dot{\theta} = \dot{\chi} + \bar{\dot{\theta}}$. Hence the center, Q, of a radial oscillation moves at a constant angular velocity, $\bar{\dot{\theta}}$, about the polar axis of a cylindrical magnetron, if B + C = 0. Only in this case does the particle move as if fixed on the rim of a wheel with center at Q.

In general, none of the angles ψ, χ or θ changes at exactly the Larmor angular frequency $\omega/2$. When $s = s_g$, we find $x = b/a$, and $|\dot{r}/r_c|$ attains its maximum value, $\omega u b$. We note further that s_g depends on the field parameters and on the canonical momentum, but not at all on the amplitude of the radial motion. We find, indeed,

$$s_g^2 = \frac{B + C + P^2}{1 - C} \tag{1.22}$$

from (1.15), (1.19).

A parameter complementary to s_g is the radial action $J_r = \oint p_r \, dr$, where p_r is the radial momentum $m\dot{r}$. We normalize J_r also as

$$j_r = \frac{4J_r}{m\omega u r_c^2} = \int_0^{2\pi} \frac{\dot{s}^2 d\psi}{s(\omega u)^2} = 4\pi b^2 \quad . \tag{1.23}$$

The second form of equation (1.15) is then in terms of j_r, s_g:

$$\dot{s}^2 = \omega^2 u^2 \left[\frac{j_r s}{\pi} - (s - s_g)^2\right] \quad , \tag{1.24}$$

$$s = s_g + \frac{j_r}{2\pi} - x\sqrt{\frac{j_r}{\pi}}\sqrt{\frac{j_r}{4\pi} + s_g} \quad .$$

The corresponding circumferential action under the same normalization is simply

$$j_\theta \equiv \frac{4J_\theta}{m\omega u r_o^2} = \frac{4\pi P}{u} \quad . \tag{1.25}$$

This same normalization of the energy, $\mathcal{E} \equiv \frac{mv^2}{2} + \phi(r)$, gives

$$\epsilon(j_r, j_\theta) = \frac{\omega u}{2}\left[\frac{j_r}{\pi} - \frac{B}{u^2} - \frac{j_\theta}{2\pi u} + 2\sqrt{\frac{B + C}{u^2} + \left(\frac{j_\theta}{4\pi}\right)^2}\right] \quad . \tag{1.26}$$

In angle-action theory [4], every action has an "angle" whose rate of change is given by $\partial\epsilon/\partial j$. We find then

$$\frac{\partial \epsilon}{\partial j_r} = \frac{\omega u}{2\pi} \quad , \quad \frac{\partial \epsilon}{\partial j_\theta} = \frac{\omega}{4\pi}\left[\frac{u j_\theta}{4\pi s_g} - 1\right] = \frac{\dot{\bar{\theta}}}{2\pi} \quad . \tag{1.27}$$

Both results in (1.27) we have already found by other means.

To complete the application of Hamilton-Jacobi theory to the Hull equations, we develop Jacobi's function $S(q,q_o)$ [4]. S is to generate a transformation of coordinates $q_o \rightarrow q$ such that $\partial S/\partial q_o = -p_o$ are components of the initial momentum, and $\partial S/\partial q = p$ are components of momentum at some point further along the orbit. For S we assume the separated form,

$$S = S_1(r,r_o) + p_\theta(\theta-\theta_o) - \mathcal{E}(t-t_o) \quad . \tag{1.28}$$

We obtain for S_1 an integral over r, since $dS/dr = p_r$:

$$\frac{4S_1}{m\omega u r_c^2} \equiv \sigma_1 = \int_{s_o}^{s} \frac{\dot{s}\,ds}{\omega u s} = \int_{s_o}^{s} \sqrt{\frac{j_r s}{\pi} - (s-s_g)^2}\,\frac{ds}{s} \quad . \tag{1.29}$$

The "angle" corresponding to j_r is then $\partial\sigma_1/\partial j_r$, given by

$$\frac{1}{2\pi}\int_{s_o}^{s} \frac{ds}{\sqrt{\frac{j_r s}{\pi} - (s-s_g)^2}} = \frac{\psi-\psi_o}{2\pi} \quad . \tag{1.30}$$

The "angle" corresponding to j_θ is similarly $\partial\sigma/\partial j_\theta$:

$$\frac{\theta-\theta_o}{2\pi} + \int_{s_o}^{s} \frac{1}{s}\frac{\partial s_g}{\partial j_\theta}\,\frac{(s-s_g)\,ds}{\sqrt{\frac{j_r s}{\pi} - (s-s_g)^2}} = \frac{j_\theta}{4\pi}\left(\frac{\psi-\psi_o}{4\pi s_z}\right) - \frac{\psi-\psi_o}{4\pi u} \tag{1.31}$$

The solution here exhibited consists then of harmonic radial oscillations in s with action j_r and angle ψ about a mean radius s_g, and circumferential motion about the polar axis with action j_θ and angle which breaks in two parts: one part depends only on $\frac{\omega}{2}(t-t_o)$, the other depends on P, B and C as well. We have thus solved for S the equation of Hamilton:

$$H\left(q, \frac{\partial S}{\partial q}\right) + \frac{\partial S}{\partial t} = 0 \quad . \tag{1.32}$$

In the construction of S we referred to initial values $(s_o, \dot{s}_o, \dot{\theta}_o)$ but the relations between these and any of the sets of orbit parameters

(s_b, s_d, x_o), (k, s_d, x_o), $(j_r j_\theta x_o)$ or (a, b, x_o) is not simple nor very significant. We give an example of such relations in Appendix 1-1.

The general radial equation (1.7) yields a closed solution under another type of assumption, which is chiefly of historical interest. The early magnetrons had cathodes of small radius; often a tungsten wire less than one thousandth of an inch in radius served as emitter. For such tubes it seemed reasonable to let $r_c \longrightarrow 0$. Let us then illustrate this type of assumption by renormalizing the radial equation:

$$\sigma \equiv (r/r_b)^2 \equiv 1 \quad , \quad \sigma_d = (r_d/r_b)^2 \quad , \qquad \Phi = \frac{e(\phi_d - \phi)}{m\omega^2 r_b^2} \quad ;$$

$$\dot{\sigma}^2 = \omega^2 [8\sigma\Phi + (\frac{P^2}{\sigma_d} - \sigma)(\sigma - \sigma_d)] \quad . \tag{1.33}$$

If the orbit passes through the polar axis with a zero velocity (!), then $\sigma_d = 0$ and $P = 0$. Then (1.33) reduces to

$$\dot{\sigma}^2 = \omega^2 [8\sigma\Phi - \sigma^2] \quad . \tag{1.34}$$

If we may assume a simple form for Φ, $\Phi = \underline{K^2 \sigma^n / 8}$ then the solution of (1.34) is

$$\sigma = \left\{ K \sin (1-n) \frac{\omega t}{2} \right\}^{\frac{2}{1-n}} \quad . \tag{1.35}$$

This applies if n is less than 1. Since the complete orbit now lies between zeros of the sine, $u = 1-n$. Hull in [2] proposed such a solution, choosing $n = 1/3$ because he assumed a Langmuir potential, $\phi \sim r^{2/3}$. Doehler more recently favored $n = 0.875$ in [5].

This concludes our introductory treatment of the orbit of an electron in a magnetron diode. We have not considered electronic interactions, or other damping mechanisms, and we have assumed fields independent of time. Because the electric field is not linear as it would be in a planar magnetron, the electron lags in its orbit. If the space charge gives the field more curvature it lags even more. Characteristics of an orbit not restricted to small radial oscillations are the canonical circumferential momentum P,

the turning points (s_b, s_d), the median radius s_g and the radial action j_r. We make use of all these in later chapters.

c. Relativistic Formulation.

We turn now to consider relativistic velocities, and effects often visualized as an increase in effective mass. These effects, though small in the fields usually encountered in magnetrons, are of the same sign as the lag already encountered, and increase the orbit period further. This section also introduces a convenient although unrealistic concept, the planar magnetron, and serves to illustrate certain aspects of a Lagrangian derivation of the equations of electron motion. These aspects in a Newtonian treatment would be partly obscured by the double meaning of time, time at a fixed point and time along an orbit.

In a relativistic formulation the parameter τ measures the path length of a particle in space-time, (x,y,z,t) [6]. Its differential $d\tau$ is defined thus:

$$(d\tau)^2 = c^2(dt)^2 - (dx)^2 - (dy)^2 - (dz)^2 = (cdt)^2\,(1 - (v/c)^2) \qquad (1.36)$$

Here c is the velocity of light, which we assume, of course, is the same in every unaccelerating coordinate system (x,y,z,t). The quantity K indicates how far from the domain of Newtonian mechanics, $K \sim 1$, we are.

$$K \equiv \left\{1 - (v/c)^2\right\}^{-1/2} \quad , \quad 1 \leq K \leq \infty \qquad (1.37)$$

To avoid restricting the discussion to cartesian coordinate systems we introduce a metric tensor $g_{\mu\nu}$:

$$g_{\mu\nu} dx^\mu dx^\nu \equiv (d\tau)^2 \; ; \quad \mu, \nu = 1,2,3,4 \qquad (1.38)$$

An index μ or ν which occurs twice in a product (unless bracketed) is equivalent to a summation sign over the values 1 to 4. A coordinate x^μ need not have the dimensions of a length, but x^4 is ct in general. Since our $g_{\mu\nu}$ will be diagonal, we could write

$$g_{\mu\nu} = \delta_{\mu\nu}\, g_{(\mu)} \quad , \quad g_{(4)} = 1 \quad , \quad g_{(i)} < 0 \quad ; \quad i = 1,2,3 \; . \qquad (1.39)$$

Here $\delta_{\mu\nu}$ is the Kronecker symbol, defined as: $\delta_{\mu(\nu)} = 0$, $\mu \neq \nu$; $\delta_{\mu(\nu)} = 1$, $\mu = \nu$.

The proper velocities u^μ are related to Newtonian velocities v^i as follows:

$$u^\mu = \frac{dx^\mu}{d\tau} \quad , \quad K d\tau = c\, dt \quad , \quad \frac{u^\mu}{K} = \left(\frac{v^i}{c}, K\right) \quad . \tag{1.40}$$

In this formulation the mass of the particle m remains constant, while Newtonian substantive derivatives become τ derivatives. These we indicate by a dot, thus:

$$\frac{du^\nu}{d\tau} \equiv \dot{u}^\nu \quad , \quad f_\mu = -mc^2 g_{\mu\nu} \dot{u}^\nu \quad . \tag{1.41}$$

Here f_μ is the inertial force. The proper velocities satisfy an identity which arises directly from (1.36) and the relativistic postulate. We shall find it quite useful:

$$g_{\mu\nu}\, u^\mu u^\nu = 1 \tag{1.42}$$

Maxwell's equations permit one to define a single space-time vector potential $A_\mu = (A_i, -\phi/c)$. The E- and B-fields derivable from A_μ form a single skew-symmetric tensor $F_{\mu\nu}$. The relevant equations are

$$\nabla \cdot B = 0 \quad , \quad \nabla \times E = -\frac{\partial B}{\partial t} \quad ; \quad B = \nabla \times A \quad , \quad E = -\frac{\partial A}{\partial t} - \nabla \phi \; ;$$

$$F_{\mu\nu} = \frac{\partial A_\nu}{\partial x^\mu} - \frac{\partial A_\mu}{\partial x^\nu} \tag{1.43}$$

The components of $F_{\mu\nu}$ can be seen in the array below, where the index μ refers to the column, and ν to the row:

$$F_{\mu\nu} = \begin{matrix} 0 & -B_3 & +B_2 & \frac{-E_1}{c} \\ +B_3 & 0 & -B_1 & \frac{-E_2}{c} \\ -B_2 & +B_1 & 0 & \frac{-E_3}{c} \\ \frac{E_1}{c} & \frac{E_2}{c} & \frac{E_3}{c} & 0 \end{matrix}$$

We can define a scalar $(F)^2 = (B)^2 - (E/c)^2 = F_{\mu\nu} F^{\mu\nu}$. Here $F_{\mu\nu} = g_{\mu\lambda}\, g_{\nu\pi} F^{\lambda\pi}$ illustrates how one moves indices up and down. The scalar $(F)^2$, we shall see, is invariant under a rotation of coordinates in space-time, that is, under a Lorentz transformation.

Another such invariant is the Lorentz equation for the field forces:

$$f_\mu = - e c u^\nu F_{\nu\mu} = - mc^2 g_{\mu\nu} \dot{u}^\nu \quad . \tag{1.44}$$

We can generate (1.44) from a second invariant scalar, the Lagrangian L:

$$L \equiv - \frac{m}{2} g_{\mu\nu} u^\mu u^\nu + \frac{e u^\mu A_\mu}{c} \quad . \tag{1.45}$$

In L the velocities and position coordinates are regarded as on an equal footing, as independent variables under the Euler-Lagrange operation:

$$\frac{d}{d\tau}\left(\frac{\partial L}{\partial u^\mu}\right) - \frac{\partial L}{\partial x^\mu} = 0 \quad , \quad \frac{dA_\mu}{d\tau} = u^\nu \frac{\partial A}{\partial x^\nu} \quad , \tag{1.46}$$

$$\frac{\partial}{\partial u^\mu}\left(g_{\lambda\nu} \frac{u^\lambda u^\nu}{2}\right) = g_{\mu\nu} u^\nu \quad .$$

The operations (1.46) on L do indeed yield (1.44).

The chief purpose of introducing L is to find first integrals of (1.44). If A_μ is not a function of a particular coordinate x^ν, then the corresponding canonical momentum p_ν will be a constant of the motion, and thus provides such an integral. Another such integral is the Hamiltonian, as we have already seen in (1.42):

$$p_\nu \equiv \frac{\partial L}{\partial u^\nu} = - m g_{\mu\nu} u^\mu + \frac{e A_\nu}{c} \quad , \tag{1.47}$$

$$H \equiv p_\mu u^\mu - L = - \frac{m}{2} g_{\mu\nu} u^\mu u^\nu = - \frac{m}{2} \quad .$$

In two cases, considered below, A_μ depends only on x^1, so p_2, p_3, p_4 and H provide constants of the motion. The relation p_4 = constant is like the Newtonian relation for energy (1.4), $\mathcal{E}$ = constant:

$$-p_4 = mu_4 + \frac{e\phi}{c^2} \pm \frac{1}{c^2}\left(mc^2 + \frac{v^2 m}{2} + \frac{3v^4 m}{8c^2} + \ldots + e\phi\right) \qquad (1.48)$$

Let us apply these considerations to determine the electronic orbit in a planar magnetron. We take $x^1 = x$ as the coordinate perpendicular to two conducting planes as in Fig. 1-3, one plane $(x^2, x^3) = (y,z)$ at $x = 0$, and one parallel to it through $x = x_a$. We assume crossed fields, E_1 and B_3, both uniform in space and constant in time, so we have

$$A_\mu = \left(0, x^1 B_3, 0, \frac{x^1 E_1}{c}\right) . \qquad (1.49)$$

For initial conditions when we start to observe the particle, we assume that it lies at $(x_o, 0, 0, 0)$ and has a proper velocity $(0, y_o, 0, K_o)$. Thus x_o is the height of one turning point of the orbit, where the particle's x component of velocity vanishes.

The force equation then has one un-integrated component, the first one:

$$\dot{x}^1 = \frac{e}{mc}\left[\frac{E_1 u^4}{c} + u^2 B_3\right] . \qquad (1.50)$$

We find three integrated components, the momentum relations

$$u^2 = \dot{y}_o - \frac{eB}{mc}(x^1 - x_o) , \quad u^3 = 0 , \quad u^4 = K_o + \frac{eE_1}{mc^2}(x^1 - x_o) . \qquad (1.51)$$

To simplify the notation we introduce the symbols

$$\omega \equiv \frac{eB_3}{m} , \quad \gamma \equiv \frac{eE_1}{mc} , \quad a^2 = \frac{\omega^2 - \gamma^2}{c^2} , \quad r = \frac{K_o \gamma + \dot{y}_o \omega}{c} .$$

On eliminating u^4 and u^2 from (1.50) we obtain

$$\left[\frac{d^2}{d\tau^2} + a^2\right](x^1 - x_o) = r , \quad x^1 - x_o = \frac{r}{a^2}\left[1 - \cos a\tau\right] . \qquad (1.52)$$

Substituting the solution (1.52) in (1.51) we obtain the following table:

Table 1-1. The Complete Relativistic Orbit

$$x^1 - x_o = \frac{r}{a^2}[1 - \cos a\tau] \quad , \quad u^1 = \frac{r}{a}\sin a\tau$$

$$x^2 - \dot{y}_o\tau = -\frac{r\omega}{ca^3}[a\tau - \sin a\tau] \quad , \quad u^2 - \dot{y}_o = -\frac{r\omega}{ca^2}[1 - \cos a\tau]$$

$$x^3 = 0 \quad , \quad u^3 = 0$$

$$x^4 - K_o\tau = \frac{\gamma r}{ca^3}[a\tau - \sin a\tau] \quad , \quad u^4 - K_o = \frac{\gamma r}{ca^2}[1 - \cos a\tau]$$

With the identity $K_o^2 = 1 + \dot{y}_o^2$ and a little algebra, one can show that the complete solution satisfies (1.42). Indeed, one could derive the solution from (1.42) and (1.51) instead of (1.50) and (1.51).

The projection of this electron orbit on the (x^1,x^2) plane is the same type of cycloidal path as one obtains in the Newtonian domain. The projection on the (x^2,x^4) plane satisfies a relation which suggests a Lorentz transformation to a coordinate system $\bar{x}$:

$$\left\{\omega x^4 + \gamma x^2\right\}(ca)^{-1} = \left\{K_o\,\omega + \gamma\,\dot{y}_o\right\}(ca)^{-1}\tau \equiv \bar{x}^4 \qquad (1.53)$$

The rotation tensor $b^\mu{}_\nu$ which makes $\bar{x}^4$ linear in τ appears in the array below:

$$b^\mu{}_\nu = \begin{matrix} 1 & 0 & 0 & 0 \\ 0 & \frac{\omega}{ca} & 0 & \frac{\gamma}{ca} \\ 0 & 0 & 1 & 0 \\ 0 & \frac{\gamma}{ca} & 0 & \frac{\omega}{ca} \end{matrix}$$

With it we find

$$\left|b^\mu{}_\nu\right| = 1 \quad , \quad \bar{x}^\mu = b^\mu{}_\nu x^\nu \quad , \quad \bar{x}^4 \text{ as in (1.53)},$$

$$\bar{x}^1 = x^1 \quad , \quad \bar{x}^3 = x^3 \quad , \quad \text{and} \quad \bar{x}^2 = \frac{r\sin a\tau}{(a)^2} \; . \qquad (1.54)$$

By this transformation we bring the orbit to rest, as it were, in a circle on the $(\bar{x}^1, \bar{x}^2)$ plane, a circle with center $(x_o + r/a^2, 0)$ and radius (r/a^2).

Since the average value of $(\omega u^2 + \gamma u^4)$ is zero, we find the average increment ratio (dy/dt) is $(c\gamma/\omega)$. Thus (γ/ω) equals $(\bar{v}/c)$, where $\bar{v}$ is the velocity of the center of the orbit along the y-axis in the original coordinate system. In it, ω is, of course, the cyclotron frequency, while γ is a similar normalization of the electric field. If B is in gauss, and E in volts/cm, then (γ/ω) is $1/3\,(E/B) \times 10^{-2}$. In general (γ/ω) is a small quantity, but if it exceeds 1, then a is imaginary, and the orbit does not close. This relativistic feature one might not anticipate from the Newtonian equations.

If we equate $ad\tau$ to $\omega u dt$ we find the part of the lag coefficient u which is introduced by relativistic effects alone. We find

$$u^2 = [1 - (\gamma/\omega)^2][1 - (v/c)^2]. \qquad (1.55)$$

Finally we note that a is linear in F, the scalar we defined earlier, while $(F)^2$ is proportional to the difference in energy densities in the magnetic and electric fields:

$$a^2 = \left(\frac{e}{mc}\right)^2 (F)^2 \quad , \quad (F)^2 = \mu\,(H \cdot B - D \cdot E). \qquad (1.56)$$

We return now to consider relativistic orbits in the cylindrical magnetron. In order to derive directly an expression like the Newtonian radial equation (1.7) we choose an unusual coordinate system, $x^\mu = (r^2, \theta, z, ct)$. The corresponding metric is then

$$g_{(\mu)} = \left(-\frac{1}{4x^1} \ , \ -x^1 \ , \ -1 \ , \ +1\right). \qquad (1.57)$$

We start to observe the particle at $(x_o^1, 0, 0, 0)$ when its proper velocity is $(0, u_o^2, 0, K_o)$. The height of one turning point of the orbit is then just $x_o^1 \equiv (r_d)^2$. Between the two coaxial conducting cylinders shown in Fig. 1-1, we assume there is a steady electromagnetic field with potential A_μ,

$$A_\mu = \left(0, \frac{x^1 B}{2} \ , \ 0 \ , \ -\frac{\phi(x^1)}{c}\right). \qquad (1.58)$$

The constants of the motion of a charged particle in this field are then

P_2, P_3, P_4 and from (1.42)

$$(u^4)^2 - x^1 (u^2)^2 - \frac{(u^1)^2}{4x^1} - (u^3)^2 = 1 \ . \tag{1.59}$$

We now substitute in (1.59) the momentum relations

$$u^4 = K_o + \frac{e}{mc^2}[\phi(x_o^1) - \phi(x^1)] \ , \quad u^3 = 0, \quad u^2 = (u_o + \frac{\omega}{2c}) \frac{x_o^1}{x^1} - \frac{\omega}{2c} \ . \tag{1.60}$$

Before transcribing the result, we simplify the notation:

$$\Phi \equiv \frac{e[\phi(x_o^1) - \phi(x^1)]}{m(\omega r_c)^2} \ , \ \frac{x^1}{(r_c)^2} \equiv s \ , \ s_d \equiv \frac{x_o^1}{(r_c)^2} \ , \tag{1.61}$$

$$\overline{m} \equiv \frac{\omega r_c}{2c} \ , \quad P \equiv s_d \left\{1 + \frac{2u_o^2 c}{\omega}\right\} \ , \ (K_o)^2 = 1 + x_o^1 (u_o^2)^2 \ .$$

Then combining (1.59), (1.60) and (1.61), we find

$$(\dot{s})^2 + (\frac{\omega}{c})^2 \left[\left\{\frac{(P)^2}{s_d} - s\right\}(s_d - s) - 8 K_o s \Phi - 16 s (\overline{m} \Phi)^2\right] = 0 \ . \tag{1.62}$$

In (1.62) and in the remainder of this discussion, no superscripts appear, only exponents.

The chief distinction between (1.62) and (1.7) is the term $(\overline{m} \Phi)^2$. It leads to a slight modification in the Hull cut-off equation. To derive the cut-off condition from (1.62) we assume that $\dot{s} = 0$ at $s = 1 = s_d$ and at $s = s_a = s_b$. We also assume that $P = 1$, $K_o = 1$, and write $\Phi(s_a)$ as $\underline{p}$. Then (1.62) becomes

$$p^2 + \frac{p}{2\overline{m}^2} = \frac{(s_a - 1)^2}{16 \overline{m}^2 s_a} \ , \quad p \doteq \frac{(s_a - 1)^2}{8 s_a} - \frac{\overline{m}^2 (s_a - 1)^4}{32 s_a^2} \ \ldots \tag{1.63}$$

In the diode we used for experiments, $(s_a - 1)^2 (8 s_a)^{-1} = 0.42$, so the size of $\overline{m}^2$ relative to this number will determine the importance of relativistic

effects on the cut-off transition. In fact $\overline{m} \leq 0.06$ for the largest magnetic field used in our work. Equation (1.63), in somewhat different notation, was obtained by Page in an article immediately following Hull's main paper of 1921 [7].

Our chief purpose in deriving (1.62) is to obtain an expression for u, the lag coefficient. A solution for the potential $8\Phi = C(s-s_d)$ will show the chief relativistic features and is simple enough to handle. This choice of Φ amounts to setting B = -C in (1.14). It leads us to consider a term of the form $(\overline{m}\ C)^2$, which we wish to show is equivalent to $\left\{4(\gamma/\omega)^2 \cdot s_g^{-1}\right\}$. The demonstration is this:

$$E_1 = -\frac{\partial\phi}{\partial r} = -\frac{2\sqrt{s}}{r_c}\frac{d\phi}{ds} = \frac{2\sqrt{s}\, r_c \omega^2 m}{e}\ \frac{d\Phi}{ds} = \sqrt{s}\ \frac{mc}{2e}\ \overline{m}C \quad . \tag{1.64}$$

Then

$$\left(\frac{eE_1}{mc}\Big/\omega\right)^2 \equiv (\gamma/\omega)^2 = \frac{s(\overline{m}C)^2}{4} \quad ,$$

and for s we take the median value, s_g, assuming also that γ represents a median value of E_1.

We find then for $\tau(s)$, the proper time along an orbit from s_d to s, an elliptic integral,

$$\frac{\omega\tau}{c}\sqrt{g - hs_b} = \int_{s_d}^{s} \frac{ds}{\left\{(s-s_d)(s_b-s)\left(1 - \frac{hs}{g - hs_b}\right)\right\}^{1/2}} \quad . \tag{1.65}$$

Here we have used the notation

$$g \equiv 1 - K_o C + h s_d \ , \ h = \frac{(\overline{m}C)^2}{4} \ , \ s_b = \frac{P^2}{s_d g}\left[1 + \frac{h P^2}{4 s_d g^2} + \ldots\right] \tag{1.66}$$

Here s_b, the outer turning radius, is the smaller solution of the quadratic, $hs^2 - gs + P^2/s_d = 0$. We find from the complete elliptic integral the quantity $\tau(s_b)$ which corresponds to a Newtonian half-period $t(s_b) = \pi/\omega u$:

$$\tau(s_b) = \frac{\pi c}{\omega \sqrt{g - h s_b - \frac{h}{2}(s_b + s_d)}} \tag{1.67}$$

Our conclusion is then the expression for u^2:

$$u^2 = \left\{1 - K_o C - \left(\frac{\gamma}{\omega}\right)^2 \left(\frac{3 s_b - s_d}{2 s_g}\right)\right\} \left\{1 - (v/c)^2\right\} \tag{1.68}$$

The field curvature appears here in $K_o C$ somewhat as it did in (1.15) while the relativistic effects appear in terms (γ/ω) and (v/c) as they did in (1.55). As might be expected, these latter effects are secondary to the curvature.

d. Summary.

The cylindrical magnetron diode is a device, invented by Hull, in which electrons move in crossed magnetic and electric fields. Their radial motions have features of the motion of the harmonic oscillator; however, instead of interchanging energy between elastic (or potential) and kinetic forms, they trace orbits which exchange kinetic energy between orthogonal directions of motion.

The first main section of this chapter exhibits two closed solutions for the orbit, one for small amplitudes of radial motion in an Allis potential and one for arbitrary amplitudes in a quadratic potential. These solutions yield expressions for the lag coefficient u, relating the orbital and cyclotron frequencies.

The second main section derives the relativistic motion from a Lagrangian functional. In a planar magnetron the orbit closes only if the ratio $(\gamma/\omega) = (E/cB)$ is less than one, no matter how large the region available for unimpeded motion. This ratio also appears in relativistic expressions for the coefficient u.

A narrow beam of electrons passing through an inert gas at low pressure may leave a trail of ionized gas. This trail, and in a sense the electronic orbits themselves, can be photographed. In fields such as we assumed the trail has a cycloidal form. Photographs of trails in a cylindrical magnetron such as were published in 1936 by Kilgore [8] provide a convincing demonstration of the correctness of our equations of motion.

References for Chapter I

1. A. W. Hull, "The Motion of Electrons between Coaxial Cylinders in a Uniform Magnetic Field," Phys. Rev. 17, 539-540 (1921).

2. A. W. Hull, "The Effect of a Uniform Magnetic Field on the Motion of Electrons between Coaxial Cylinders," Phys. Rev. 18, 31-57 (1921).

3. W. Allis, Theory of the Magnetron Oscillator, "Electronic Orbits in the Cylindrical Magnetron with Static Fields," Special Report 9S, Section V, Radiation Laboratory, Cambridge, Massachusetts, 1941.

4. C. Lanczos, The Variational Principles of Mechanics, Toronto University Press, Toronto, 1949, pages 231-244.

5. O. Doehler, "On the Properties of Tubes in Constant Magnetic Fields," Ann Radioelectricite, 3, 29-39, 169-183 (1948).

6. J. A. Schouten, Tensor Analysis for Physicists, Oxford University Press, London, 1951, Chap. 9.

7. L. Page, "Theory of the Motion of Electrons between Coaxial Cylinders, taking into account the Variation of Mass with Velocity," Phys. Rev. 18 58-61 (1921).

8. G. R. Kilgore, "Magnetron Oscillators for the Generation of Frequencies between 300 and 600 Megacycles," Proc. I.R.E. 24, 1145 (1936) Fig. 7.

Appendix 1-1

Relations between (a,b,x_o) and $(s_o,\dot{s}_o,\dot{\theta}_o)$.

$$s_o = a^2 + b^2 - 2abx_o$$

$$|\dot{s}_o| = 2\omega\, u\, ab\sqrt{1 - x_o^2}$$

$$\dot{\theta}_o = -\frac{\omega}{2}\left[1 \pm \left\{u^2(a^2-b^2)^2 - (B+C)\right\}^{1/2}\left\{a^2 + b^2 - 2abx_o\right\}^{-1}\right]$$

$$a^2 = D + \frac{s_o}{4}\left(\frac{A}{s_o} + 1\right) \quad , \quad D \equiv \dot{s}_o^2 \Big/ \sqrt{4\omega^2 u^2 s_o}$$

$$b^2 = D + \frac{s_o}{4}\left(\frac{A}{s_o} - 1\right) \quad , \quad A^2 \equiv \frac{s_o^2}{u^2}\left(\frac{2\dot{v}_o}{\omega} + 1\right)^2 + \frac{B+C}{u^2}$$

$$x_o^2 = \underline{M - D \Big/ M + D} \quad , \quad M \equiv \frac{s_o}{8}\left(\frac{A^2}{s_o^2} - 1\right) + \frac{2D}{s_o}\left(\frac{A^2}{2s_o} + D\right)$$

$x_o \equiv \cos\psi_o$ if

$$x = \cos\left[\omega u(t-t_o) - \psi_o\right] \quad .$$

II

The Driven Orbit

a. Introduction.

If a high frequency probe signal is added to the steady fields imposed on a cylindrical magnetron diode, the electric field of the probe signal will exert a harmonic force on electrons in the space charge cloud. The electrons are then said to be "driven." If the probe field is very weak, the driven motion may be added to the free motion. The sum is a motion, along the radial direction, whose amplitude pulsates at a frequency A, equal to the difference between the free orbital frequency and the field frequency.

If this difference is small, the pulsations in amplitude may be large. The electron may leave the space charge cloud and collide with one wall or another and transfer to the wall the energy which it has absorbed from the probe signal field. The effects of electronic interactions and collisions also appear as an absorption of energy from the harmonic field. We now turn to calculate characteristics of the driven motion and the rate of energy absorption, or the conductivity of the space charge cloud.

b. Perturbation of a Free Orbit.

If a particle describes a free orbit of arbitrary amplitude within a magnetron space charge cloud, we may write the motion in terms of s, s_d and k as in (1.17). We ask now for the effects of a small radial alternating field E_1 on the motion given initially by $x = \cos \omega ut$. We first treat E_1 as a small perturbing force on the free orbit. Assuming for E_1 the following form, we find for U, the energy absorbed in one cycle of the orbit, an integral over E_1:

$$E_1 \equiv \frac{E_c r_c}{r} \cos(\bar{\omega}t - \bar{\phi}) \quad , \quad U = -e \oint E_1 \cdot dr = \frac{-er_c E_c}{2} \oint \frac{\cos(\bar{\omega}t - \bar{\phi}) ds}{s} \quad (2.1)$$

Here $\bar{\omega}$ is the angular frequency of the probe field, $\bar{\phi}$ is its phase relative to the orbit, and E_c is the probe field strength at the cathode. On expanding s as in (1.17) we find:

$$U = + \frac{er_c E_c k}{2} \oint \left[\cos(At-\bar{\phi}) \frac{x\,dx}{1-kx} + \sin(At-\bar{\phi}) \frac{(1-x^2)d(\omega ut)}{1-kx} \right]$$

Now if $A \equiv \bar{\omega} - \omega u$ is much less than ωu, we may take the integral sign to the right of the terms in $(At-\bar{\phi})$. The integral following the cosine is zero over a complete orbit, while the integral following the sine can be evaluated by using (1.20). We find then:

$$U = er_c E_c \pi \left\{ \frac{1-\sqrt{1-k^2}}{k} \right\} \sin(At-\bar{\phi}) = er_c E_c \left(\frac{\pi b}{a}\right) \sin(At-\bar{\phi}) \qquad (2.2)$$

For the second form of this expression, $\underline{a}$ and $\underline{b}$ are defined in (1.18). If $(At-\bar{\phi})$ is $\pi/2$, the electric field is in phase to do work on the particle over the whole cycle. Then U is at its maximum as one can see in Fig. 2-1.

To find the effect of U on the turning point radii, s_b and s_d of the free orbit (1.16), we now distinguish initial values with a subscript o: thus s_{bo}, s_{do}. After one cycle in the field E_1, if the particle absorbs energy, then s_b and s_d will move apart to $s_b = s_{bo} + \Delta s_b$, $s_d = s_{do} - \Delta s_d$. Since the canonical angular momentum P is constant during this process, the circumferential velocities at s_{bo} and s_{do} are not affected by the probe field. The absorbed energy then appears at these points entirely as kinetic energy of radial motion: $U = \frac{1}{2} m \dot{r}^2$. Hence:

$$\dot{s}^2\Big|_o = \frac{8Us}{mr_c^2}\Big|_o = \omega^2 u^2 (s_{bo}+\Delta s_b - s)(s - s_d + \Delta s_d)\Big|_{s=s_{bo} \text{ or } s_{do}}$$

Assuming in these relations that Δs is a very small quantity we find an expression for the logarithmic rate of change of either turning point per orbit cycle:

$$\frac{\Delta s}{s}\Big|_{s=s_{bo} \text{ or } s_{do}} = \frac{2\pi e r_c E_c \cdot \sin(At-\bar{\phi})}{m(\omega u \cdot r_c \cdot a)^2} = \frac{2\pi a(t)}{\omega u} \qquad (2.3)$$

Using the abbreviation $a(t)$, over several cycles we find:

$$s_b = s_{bo} \exp\left(\int a\,dt\right), \quad s_d = s_{do} \exp\left(-\int a\,dt\right).$$

In these results the median radius $s_g \equiv \sqrt{s_b s_d}$, a parameter which we

found to be complementary to the radial action j_r, is indeed a constant.

To complete the orbit solution, let us define a constant γ by the ratio of average turning radii: $\left.\underline{s_b/\sqrt{s_d}}\right|_{t_a} \equiv \exp 2\gamma$. Then we have:

$$s = s_g\left\{\cosh\left(\gamma + \int_{t_a}^{t} a\,dt'\right) - x \sinh\left(\gamma + \int_{t_a}^{t} a\,dt'\right)\right\} \tag{2.4}$$

This solution will show beats at the frequency A. Indeed, if $\underline{a}$ is nearly a constant, or if $b \ll a$, then,

$$\int_{t_a}^{t} a\,dt = \frac{eE_c}{m\omega u r_c} \cdot \frac{\sin A(t-t_a)}{A \cdot a^2} \tag{2.5}$$

The constant of integration, suppressed in (2.5), is properly $\gamma(\bar{\phi})$. Incidentally, $k = \tanh\gamma$ and $\underline{b/\sqrt{a}} = \tanh\frac{1}{2}\gamma$.

To give a numerical example, let us assume that a probe signal power W_1, of one microwatt, travels down a transmission line of characteristic resistance R ohms.

$$R = \sqrt{\frac{\mu}{\epsilon}}\,\frac{\ln s_a}{4\pi}\,, \qquad 2RW_1 = \left[\frac{E_c r_c \ln s_a}{2}\right]^2 \tag{2.6}$$

Now let $s_a = 5.14$, At-$\bar{\phi} = \pi/2$, $r_c^2 a^2 = 2.5 \times 10^{-5}$ meters squared and $\omega u = 10^{10}$ radians per second. (These values are appropriate to the experiment we describe in later chapters.) Then $E_c r_c = 12.1\sqrt{W_1} = 1.21\times10^{-3}$ volts, $a = 0.86\times10^{4}$ per second, and $U = 6\times10^{-22}(\frac{b}{a})$ joules per cycle. The rate of absorption depends on the square root of W_1 and is above the level of one quantum, or $\hbar\omega u \doteq 10^{-24}$ joules, per cycle, since b/a is about 10^{-2}.

Now E_1 in (2.1) represents a standing wave, whereas the probe signal we use is a traveling wave, representable with a vector potential component $A_r(r,z,t)$:

$$A_r = -\frac{E_c r_c}{r\bar{\omega}} \sin(\bar{\omega}t - \beta z - \bar{\phi}) \tag{2.7}$$

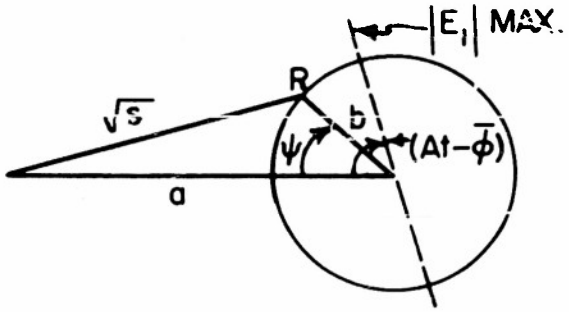

FIG.2-1 PHASES OF ORBIT AND PROBE FIELD

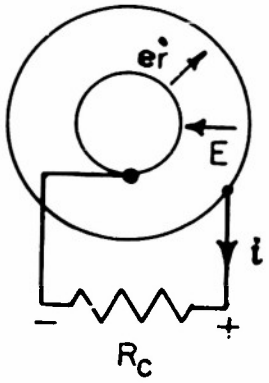

FIG 2-2 IMAGE CURRENT i

Then $E_1 = -(\partial A/\partial t)$ and reduces at z = 0 to the E_1 we used to calculate $\alpha(t)$. The introduction of A_r makes the Lagrangian of the orbit a function of z:

$$L = \frac{1}{2} m \left\{ \dot{r}^2 + (r\dot{\theta})^2 + \dot{z}^2 \right\} + e \left\{ \dot{r} A_r + \frac{r^2 \dot{\theta} B}{2} \right\} - e\phi(r) \quad . \tag{2.8}$$

We have still $\partial L/\partial \dot{\theta} = 0$, so P and s_g remain constants of the orbital motion. However, the correct radial equation is now:

$$\ddot{r} = r\dot{\theta}^2 + r\omega\dot{\theta} - \frac{e}{m}\frac{\partial \phi}{\partial r} + \frac{e}{m}\frac{E_c r_c}{r}\left(1 - \frac{\dot{z}}{c}\right)\cos(\bar{\omega}t - \beta z - \bar{\phi}) \quad . \tag{2.9}$$

We have in addition the z equation:

$$\ddot{z} = \frac{e}{m}\left(\frac{\dot{r}}{c}\right)\frac{E_c r_c}{r}\cos(\bar{\omega}t - \beta z - \bar{\phi}) \quad . \tag{2.10}$$

Equation (2.10) and the term in $(\dot{z}/c)$ in (2.9) represent, of course, the forces exerted by the microwave magnetic field. These forces in (2.10) cause the orbit to wobble slightly back and forth along the z-axis. The factor $(\dot{r}/c)$ is approximately $(b/10)$ and in general $\dot{z}/c \ll 1$.

The introduction of A_r affects then j_r, but not P or s_g. It affects j_r because it modifies $p_r = m\dot{r} + eA_r$, and p_r appears in the definition of j_r. A much more serious modification of the orbit equations arises if the probe field has a circumferential component E_θ as well as E_r. The E_θ-component perturbs P and is strong in cavity magnetrons, of course. We shall avoid problems in which it might arise.

c. Resonance and Damping in the Linear Magnetron.

As the frequency difference A approaches zero, even a weak probe signal field is no longer a small perturbing influence on the electronic orbit. When A = 0, the orbit and field are in resonance and the effects of electronic interactions help to determine the amplitude of radial motion. We examine these complications first in the linear magnetron and in the next section modify the results to fit the cylindrical magnetron.

In a region such as is shown in Fig. 1-3, let us assume a constant and uniform magnetic field $B = B_z$, and a steady electric field $E_x = \frac{x}{x_a} E_a$.

This implies a uniform number density of charges n, given by

$$\frac{ne}{\epsilon_o} = \frac{dE_x}{dx} = \frac{E_a}{x_a} \qquad (2.11)$$

This n depends then only on the anode potential p, defined as

$$p = \Phi(x_a) \ , \ \Phi(x) = -\frac{e\phi}{m\omega^2 x_a^2} \ , \quad \phi = -\int_o^x E_x dx = -\frac{x^2 E_a}{2x_a} \ . \qquad (2.12)$$

If an electron is released in this region at $(x_o,0,0,t_o)$ with velocities $(\dot{x}_o,\dot{y}_o,0)$, its orbit will satisfy the equations, similar to (1.50) and (1.51):

$$\ddot{x} = e(E_x + \dot{y}B) \ , \quad \dot{y} - \dot{y}_o = -\omega(x-x_o) \ , \quad \omega = eB/m \ . \qquad (2.13)$$

These reduce to an equation like (1.52):

$$\left[\frac{d^2}{dt^2} + \omega^2 u_o^2\right](x-x_1) = 0 \ , \ u_o^2 \equiv 1 - \frac{p}{2} \ , \ u_o^2 x_1 \equiv x_o + \frac{\dot{y}_o}{\omega} \ . \qquad (2.14)$$

Here u_o is the lag coefficient discussed in Chapter 1. The subscript has been added to distinguish it from another frequency ratio $u \equiv \bar{\omega}/\omega$, the probe field frequency over the cyclotron frequency. The orbit center x_1, we see, is a function of the initial conditions.

In the presence of a microwave probe field $E_1 \cos \bar{\omega} t$, the orbit equation (2.14) becomes inhomogeneous:

$$\left[\frac{d^2}{dt^2} + \omega^2 u_o^2\right](x-x_1) = \frac{eE_1 \cos \bar{\omega} t}{m} \ . \qquad (2.15)$$

We may write the solution in terms of constants C_1 and C_2, fixed by the velocity and position of the particle at the reference time t_o;

$$x - x_1 = \text{real part of} \left\{\frac{eE_1 \exp j\bar{\omega}t}{m[(\omega_o u)^2 - \bar{\omega}^2]} + C_1 \exp(j\omega u t) + C_2 \exp(-j\omega u t)\right\} \qquad (2.16)$$

Van Vleck and Weisskopf take equations like (2.15) and (2.16) as the foundation for their treatment of collision damping of bound harmonic oscillators[1].

We find our orbits have some similarities to such oscillators and will point out differences as we review their treatment. We make this review in order to develop the effects of damping on the driven orbit.

Van Vleck and Weisskopf take t_o as the time the particle under discussion suffered its most recent collision. They assume all collisions are so strong that the particles carry away no memory of their previous motion. They also assume that each collision lasts a time short relative to $2\pi/\bar{\omega}$. Under these assumptions, they state, the particle's position and velocity just after collision are distributed according to a Boltzmann probability $\exp[-H(t)/kT]$. Here kT is an energy characteristic of the large number of colliding particles and H(t) is the Hamiltonian:

$$H(t) = \frac{1}{2}m[\dot{x}^2 + (\omega u_o)^2 (x-x_1)^2] - e(x-x_1) E_1 \cos \bar{\omega} t \quad .$$

These assumptions make the average value of $\dot{x}_o$ zero, and the average value of $(x-x_1)_o$ is $eE_1 \cos \bar{\omega} t \, (m\omega^2 u_o^2)^{-1}$. If one writes $\theta \equiv t-t_o$, then the probability that the most recent collision lies in the interval $d\theta$ at $t-\theta$ is:

$$dP = \exp\left(-\frac{\theta}{\tau}\right) \frac{d\theta}{\tau} \quad . \tag{2.17}$$

Here τ is a characteristic time between collisions. The authors then average $(x-x_1)_o$ over collision instants t_o by integrating $(x-x_1)dP$ over θ from zero to infinity. Having thus evaluated C_1 and C_2, they find:

$$\underline{(x-x_1)} = \text{real part of} \left\{ \frac{e E_1 \exp j\bar{\omega} t}{m\omega^2 (u_o^2 - u^2)} \right\} \left\{ 1 - \right.$$

$$\left. \frac{u}{2\tau u_o^2} \left[\frac{u_o + u}{1/\tau - j\omega(u_o - u)} - \frac{u_o - u}{1/\tau + j\omega(u_o + u)} \right] \right\} \tag{2.18}$$

In this treatment x_1 is the equilibrium position of a bound particle when E_1 is zero. The x_1 in (2.14), however, depends on $\dot{y}_o$ and x_o. This is an important difference between bound oscillators and orbits in a magnetic field. In the second case the whole space charge drifts in the y-direction, so the average value of $\dot{y}_o$ is not zero. Moreover, the average

value of $(x-x_1)_o$ may depend on x_1. Since a finite leakage current flows from the anode in a magnetron, the particles move on the average toward the anode. Thus x_1 changes in each collision. For these reasons we cannot evaluate C_1 and C_2 in our case. We probably cannot define a uniform average energy kT either. Nevertheless, the form of (2.18) seems to be more general in application than the assumptions used in deriving it. Indeed, Van Vleck and Weisskopf show that the continual patter of weak, long range, coulomb interactions between electrons leads, in the nonresonant case at least, to an expression for phenomenological damping, in formulae for line shape, similar to the τ we have introduced.

We write out (2.18) in order to compare it to the solution of the following linear inhomogeneous differential equation:

$$\left[\frac{d^2}{dt^2}+\frac{2}{\tau}\frac{d}{dt}+\omega^2 u_o^2\right](x-x_1)=\frac{eE_1\cos\bar{\omega}t}{m} \quad . \tag{2.19}$$

The particular solution of (2.19) is

$$(x-x_1)=\text{real part of}\left\{\frac{eE_1\exp(j\bar{\omega}t)}{m\omega^2(u_o^2-u^2+\frac{ju^2}{Q})}\right\}\ ,\quad Q\equiv\frac{1}{2}\tau\bar{\omega}\ . \tag{2.20}$$

In (2.19) τ represents viscous damping rather than a mean time between collisions. Near resonance, $u_o + u \doteq 2u_o$, we may rewrite (2.20):

$$(x-x_1)=\text{real part of}\left[\frac{eE_1\exp(j\bar{\omega}t)}{2m\omega^2 u}\left\{\frac{u_o-u-ju/2Q}{(u_o-u)^2+u^2/(2Q)^2}\right\}\right]. \tag{2.21}$$

Under the same approximation we find (2.18) reduces to:

$$(x-x_1)=\text{real part of}\left[\frac{eE_1\exp(j\bar{\omega}t)}{2m\omega^2 u}\left\{\frac{u_o-u-ju/2Q}{(u_o-u)^2+u^2/(2Q)^2}+\frac{1}{8Qu^2}\cdot\frac{1/4Q-j}{(1/4Q)^2+1}\right\}\right] \tag{2.22}$$

In these expressions the first term is identical, while the second term in (2.22) is negligible if $1 \gg (8Qu^2)^{-1}$. Thus, as Lorentz noted [2], collision broadening and viscous damping lead to nearly identical expressions for the average orbit, if Q is large.

The characteristic decay time τ certainly includes the following process of energy loss: the motion of a charged particle along x may produce a current $i = e\dot{x}/x_a$, an image current in an external circuit such as appears in Fig. 1-3. The power lost to an external resistance R is then:

$$P = \frac{1}{2}|i|^2 R = \frac{e^2\bar{\omega}^2 R|x-x_1|^2_{max}}{2x_a^2} \qquad (2.23)$$

If R is 60 ohms, $\bar{\omega}$ is 10^{10} radians per second and $|x-x_1|_m/x_a$ is 10^{-2}, then P is about 8×10^{-21} watts. The energy stored in the orbit is $W = \frac{1}{2} m\bar{\omega}^2|x-x_1|^2_m$. The quality parameter Q is $\frac{1}{2}\bar{\omega}\tau = \bar{\omega}W \cdot P^{-1} = (m\bar{\omega}x_a^2)(e^2R)^{-1}$. If x_a is about 4 millimeters then Q is about 2×10^{10} and τ is about 4 seconds. Thus the direct losses to an external circuit are a very small part of the orbit damping.

The resonance observed in our magnetron diode depends on many variables beside the obvious orbit parameters. Its exact shape varies even from time to time under otherwise identical conditions. In this situation we prefer a simple model, so we write:

$$(x-x_1) = \text{real part of } \frac{eE_1 \exp j\bar{\omega}t}{m\omega^2 Z}, \quad Z \equiv u_o^2 - u^2 + \frac{ju^2}{Q} \qquad (2.24)$$

The complex image current due to a single driven particle is then:

$$\Delta I = \frac{je^2\bar{\omega}E_1 \exp(j\bar{\omega}t)}{m\omega^2 x_a Z} \qquad (2.25)$$

Assuming that the random free motions of many particles cancel out, we find the image current represents an integral over the driven or coherent motions of the space charge. If the driven orbits have small amplitudes and E_1 is weak, we may ignore convection currents across the surfaces at x = 0 and x_a. In the interval $(0, x_a)$ we assume the n particles per cubic meter move as a unit. If the region of integration has a unit cross section, then the complex current flowing in R is given by:

$$I = j\omega\epsilon_o \cdot \frac{2pE_1 \exp(j\bar{\omega}t)}{Z} \qquad (2.26)$$

Since p and E_1 are known, by measuring I we may find $Z(u^2)$.

The current density within the space charge is, however, a vector:

$$J_1 = nev_1 = \text{real part of} \left\{ \frac{j\bar{\omega} e E_1 \exp j\bar{\omega}t}{m\omega^2 Z} [\hat{i} + \hat{j}\, j/u]\, ne \right\} \qquad (2.27)$$

Here $\hat{i}$ and $\hat{j}$ are unit vectors along the x- and y-directions. The conductivity $\sigma(\bar{\omega})$ of the space charge cloud is then a dyadic. If $J \equiv \sigma \cdot E_1(t)$, by considering various directions for the vector E_1, we find the following array for σ:

$$\sigma = \begin{bmatrix} \frac{2p}{Z} & \frac{2jp}{uZ} & 0 \\ \frac{-2jp}{uZ} & \frac{2p}{Z} & 0 \\ 0 & 0 & \frac{-2p}{u^2} \end{bmatrix} (-j\bar{\omega}) \qquad (2.28)$$

d. Resonance and Damping in a Cylindrical Magnetron Diode.

With the preceding sketch of orbits in Cartesian coordinates as a guide, we return to consider driven orbits in the cylindrical magnetron. If a charged particle is released in a region such as appears in Fig. 1-1, its orbit will follow the radial force equation:

$$\ddot{r} = r\dot{\theta}^2 + \omega r \dot{\theta} - \frac{e}{m}\frac{\partial \phi}{\partial r}\,, \quad \omega \equiv \frac{eB}{m} \text{ as in (1.3)}\,. \qquad (2.29)$$

If the potential ϕ depends on r and on t, then the energy is no longer constant along a given orbit. The Lagrangian of the motion remains, however, independent of θ, so we retain the momentum relation from (1.4). Using this to eliminate $\dot{\theta}$ from (2.29), introducing the radial variable $s \equiv (r/r_c)^2$, and the canonical angular momentum P from (1.6), we find the radial equation takes the form:

$$\frac{s\ddot{s}}{2} - \frac{\dot{s}^2}{4} = \frac{\omega^2}{4}\left[P^2 - s^2\left(1 - 8\frac{\partial \Phi(r,t)}{\partial s}\right)\right] \qquad (2.30)$$

Here Φ is the potential normalized as in (1.6), which we now break in two parts:

$$\Phi(r,t) \equiv \frac{-e\phi(r,t)}{m\omega^2 r_c^2} = \Phi_o(s) + \Phi_1(s,t) \; ; \qquad |\Phi_1| \ll |\Phi_o| \; . \tag{2.31}$$

We wish to solve (2.30), to find the amplitude and phase of the driven radial oscillations, as a function of Φ_o and other parameters. Following the line of development used in Chapter I, we consider first the substitution, $s = s_g(1+\xi)$, $|\xi| \ll 1$, and the expansion:

$$s^2 \frac{\partial \Phi}{\partial s} \doteq s^2 \frac{d\Phi_o}{ds}\bigg|_g + \frac{d}{ds} s^2 \frac{d\Phi_o}{ds}\bigg|_g \xi s_g + \ldots + s^2 \frac{\partial \Phi_1}{\partial s}\bigg|_g \; . \tag{2.32}$$

We use now the identity,

$$\frac{d}{ds} s^2 \frac{d\Phi_o}{ds} \equiv s \frac{d^2 s\Phi_o}{ds^2} \; ,$$

and the relations borrowed from (1.9) and (1.10),

$$P^2 = s_g^2 \left(1 - 8 \frac{d\Phi_o}{ds}\bigg|_g\right) \; , \qquad u_o^2 = 1 - 4 \frac{d^2 s\Phi_o}{ds^2}\bigg|_g \; . \tag{2.33}$$

We find that the terms linear in ξ in (2.30) then yield:

$$\ddot{\xi} + \omega^2 u^2 \xi = 4 \frac{\partial \Phi_1}{\partial s}\bigg|_g \omega^2 \; . \tag{2.34}$$

Making now the appropriate substitution for Φ_1, we find the solution for small amplitudes of probe signal and of driven motion:

$$\Phi_1(s,t) = \frac{eE_c r_c \ln s \cos \bar{\omega} t}{2m\omega^2 r_c^2} \; , \qquad s = s_g + \frac{2eE_c \cos \bar{\omega} t}{m\omega^2 (u_o^2 - u^2) r_c} \; . \tag{2.35}$$

We may now remove to some extent the restriction to small amplitudes, if we assume that Φ_o has the form, quadratic in s, given in (1.14). Equations (2.33) then take the form (1.15):

$$P^2 = u_o^2 s_g^2 - (B+C) \; , \qquad u_o^2 = 1 - C \; . \tag{2.36}$$

If we now add a small term D, independent of time, to $\Phi_1(s,t)$, one can show that $s = a^2 + b^2 - 2ab \cos \bar{\omega} t$ is indeed a solution of (2.30). To

remove entirely the restrictions to small amplitudes we require the special assumptions in (1.14) and the following:

$$\Phi_1(s,t) = \frac{eE_c r_c \ln s(D+\cos\bar{\omega}t)}{2m\omega^2 r_c^2}, \qquad a^2 - b^2 = \frac{P^2+B+C}{u^2},$$

$$D = -\frac{a^2+b^2}{2ab}, \qquad \text{and} \qquad 2ab = -\frac{2eE_c r_c}{m\omega^2 r_c^2}\cdot\frac{1}{u_o^2 - u^2} \tag{2.37}$$

Since our probe signals will be weak, we will not develop the unrestricted solution further.

We note in (2.35) that ξ changes sign when u_o^2 passes through equality with u^2. If u_o^2 is greater than u^2, the natural orbit frequency is greater than the driving frequency, and the velocity tends to lead the driving field. The particle then lies closest to the anode when the electric field pulls it most strongly toward the anode. However, if u_o^2 is less than u^2, the particle's velocity lags behind the driving field and we shall say that b changes sign in (2.37). In the alternative formula, (1.17), we insert the symbol δ to carry the sign of $u^2 - u_o^2$:

$$s = \left(\frac{1-k\delta\cos\bar{\omega}t}{1-k}\right)s_d, \qquad \frac{k\delta s_d}{1-k} = \frac{2eE_c}{m\omega^2 r_c}\frac{1}{u^2 - u_o^2}. \tag{2.38}$$

If damping is present, such as was treated in the last section, we shall replace $u_o^2 - u^2$ in (2.38) by the symbol Z (2.24). We thus assume the damping has the same effects in the cylindrical as in the planar orbit.

We wish finally to derive an expression for the complex conductivity of the space charge in a cylindrical magnetron. We find at once the high frequency components of current driven by a radial field of strength E_c at the cathode:

$$rJ_1 = rnev_1 = ner_c^2\left[\frac{s\hat{r}}{2} + s\dot{\theta}\hat{\theta}\right] = \text{the real part of}$$

$$\left\{\frac{ne^2 E_c r_c e^{j\bar{\omega}t}}{m\omega^2 Z}\, j\bar{\omega}\left[\hat{r} + j\frac{\hat{\theta}}{u}\right]\right\} \tag{2.39}$$

Writing $J_1 = \sigma \cdot E_1(r,t)$, we can identify two terms in the σ dyadic in (2.39), where $\hat{r}$ and $\hat{\theta}$ are unit vectors, and $\underline{n}$, the number density of electrons, may be a function of r. The three other nonzero terms in the σ array may be obtained as for (2.28), but we will have no use for them.

The external effects of a coherent driven radial motion may be represented again by a current of image charges, if we assume the probe signal wavelength is much greater than twice the anode radius r_a. A single particle, moving radially against a field E_r, gives up its energy U to this field and this energy may appear in an external resistance R:

$$\frac{dU}{dt} = -eE\cdot\frac{dr}{dt} = i^2R \text{ as in Fig. 2-2.} \tag{2.40}$$

The voltage V across R is then i R and provides the opposing field within the cylindrical region:

$$E_r = \frac{-2V}{r\ln s_a}, \quad Vi = \frac{2eVt}{r\ln s_a}, \text{ so } i = \frac{e\dot{s}}{s\ln s_a}. \tag{2.41}$$

This argument ignores retardation effects; but it extends well into the microwave region of frequencies, if R is the characteristic resistance of the coaxial region between r_c and r_a. A charged particle in motion will in fact excite a whole spectrum of modes; but only the principal or TEM mode carries away energy, if the others are well beyond cutoff. We will explore the propagating modes in a later chapter.

If a single charge moves in a magnetron orbit, we have from (2.38) and (2.41):

$$i = \frac{e\bar{\omega}k\delta\sin\bar{\omega}t}{\ln s_a(1-k\delta\cos\bar{\omega}t)} = \frac{e\bar{\omega}\delta k}{\ln s_a}\left\{(1+\frac{k^2}{2}+\ldots)\sin\bar{\omega}t + \frac{k\delta}{2}(1+k^2+\ldots)\sin 2\bar{\omega}t+\ldots\right\} \tag{2.42}$$

The expansion of the denominator thus gives rise to higher harmonics of the fundamental driving frequency $\bar{\omega}$. The complex current increment, at the fundamental frequency, due to a single particle is then, if k is much less than one, and we substitute from equation (2.38):

$$\Delta I = \frac{-j\bar{\omega} e\, \delta k}{\ln s_a} \exp(j\bar{\omega}t)\left(1 + \frac{k^2}{2} + \ldots\right) \qquad (2.43)$$

$$\doteq \frac{+j\bar{\omega} e^2 \cdot 2E_c \exp(j\bar{\omega}t)}{m\omega^2 Z r_c s_d \ln s_a}$$

We next integrate ΔI over all charges between anode and cathode, assuming for n(r) the following expression which we will justify in T. R. 201 Chapter 4.

$$\frac{ne^2}{m\omega^2\epsilon_o} = \frac{p}{2p_c}\left(1 + \frac{1}{s_g^2}\right) \quad , \quad \frac{p}{p_c} \text{ a constant} \quad . \qquad (2.44)$$

$$I \equiv \int_{r_c}^{r_a} r\,dr \int_0^{2\pi} d\theta \int_0^h dz\, \Delta I \cdot n(r) \quad ,$$

$$= j\omega\epsilon_o \cdot \frac{E_c r_c \exp(j\bar{\omega}t)}{Z \ln s_a} \cdot 2\pi h \cdot \frac{p}{p_c}\int_1^{s_a} \frac{ds}{2s}\left(1 + \frac{1}{s^2}\right) . \qquad (2.45)$$

Here I is the radial current in an axial length h. It passes through an area $2\pi h r_c$ close to the cathode, so the current density there, J_1, is

$$J_1 \equiv \frac{I}{2\pi h r_c} = \frac{j\omega\epsilon_o p}{Z \cdot 2p_c}\left(1 + \frac{1 - 1/s_a^2}{\ln s_a}\right) E_c \exp(j\bar{\omega}t) \qquad (2.46)$$

Now $rJ_1(r)$ and $rE(r,t)$ are independent of r, if the space charge density does not vary with time. Hence the effective conductivity $\bar{\sigma}(\bar{\omega})$, the ratio of J_1 to E, is independent of r as it should be. On substituting values for s_a and p_c appropriate to the diode used in our experiment, we find

$$\bar{\sigma}(\bar{\omega}) = 1.49\, \frac{j\omega\epsilon_o p}{Z} \quad . \qquad (2.47)$$

This gives the conductivity of a swarm of charges in coherent radial motion in a magnetron diode, if this motion is so small that we may ignore the convection current that passes through the surfaces at r_c and r_a, and if $(\bar{\omega}/c) \ll (2\pi/r_a)$.

References for Chapter II

1. Van Vleck and Weisskopf, "On the Shape of Collision Broadened Lines," Rev. Mod. Phys. 17, 227-236, (1945).

2. H. A. Lorentz, Theory of Electrons, Teubner, Leipzig, 1909, Note 57.

III

Transmission of a TEM Probe Signal

a. Introduction

The high frequency behavior of space charge rotating in a magnetic field has received some attention, in both its experimental and theoretical aspects, for at least fifteen years [1]. Fairly typical theoretical treatments are those given by Lamb and Phillips [2], and by L. Harris [3]. These treatments yield possible resonances of the whole system, — the space charge cloud and the magnetron cavity that confines it. The resonances may be excited by impressing a small signal of appropriate frequency on the output circuit of the (non-oscillating) magnetron. We mention in Chapter IV several experimental studies of these resonances.

A few probe signal measurements have been made on simple Hull diodes with a TEM probe mode. Both Brewer and Geick [4,5] (to mention the two examples I know) used tubes which were coaxial cavities with closed ends. Hence they had axial TEM resonances to disentangle from space charge effects. They both measured the reflection, rather than the transmission of a probe signal, and both used tubes with filamentary cathodes. The space charge cloud about this type of cathode may be expected to yield only a broad resonance (see T.R. 201).

The sharp cyclotron resonance, free of extraneous effects, has apparently gone unobserved. Consequently the incentive to develop a theory of this resonance has been lacking. Previous treatments do not in general consider the behavior of the particles in the space charge cloud in the detail that appears in Chapter II of this report. We found there that a single charged particle in a magnetic field, in its response to a periodic force, resembles a harmonic oscillator. Many such particles in a small region of a space charge cloud behave somewhat like a series RLC circuit, connected between cathode and anode of the diode. We found an expression Z which resembles the impedance of such a circuit and characterizes the resistivity of the cloud.

This suggests analogies which may be worth a brief exposition. We emphasize later the respects in which they fail to resemble the magnetron diode in their transmission characteristics. The transmission T(P) through a section of waveguide coupled to a resonant cavity [6] or through RLC networks such as are shown in Fig. 3-1, can be written as:

$$T(P) \equiv \frac{E_3}{E_1} \quad , \quad \frac{T(P)}{T(\infty)} = \frac{D(1+jPQ)}{1+jDPQ} \quad ;$$

$$P \equiv \left(\frac{\bar{\omega}}{\omega} - \frac{\omega}{\bar{\omega}}\right) \quad , \quad D \equiv \frac{T(0)}{T(\infty)} \quad . \tag{3.1}$$

Here ω is the frequency of cavity resonance, or of network resonance, $\omega = (LC)^{-1/2}$, and $\bar{\omega}$ is the frequency of the applied signal.

As a function of P, T will trace a circle on its complex plane. From this circle the constants Q and D can be determined if D is small relative to one. Then the points $|T(P_1)| = \sqrt{2}\,|T(0)|$ on the T(P) circle lie also on a second circle with radius $|T(0)|$ and center at T(0). At these points $T(P_1)$ in general we find $|P_1|^{-1} = Q\sqrt{1 - 2D^2}$. The quality factor Q can also be found from the so-called tuning rate at resonance. There $\omega = \bar{\omega}$, and P = 0, so we have:

$$dP = -\frac{2d\omega}{\bar{\omega}} = -2d(\ln \omega) \; ; \quad \left.\frac{d \ln T}{d \ln \omega}\right|_{\bar{\omega}} = -2jQ(1-D) \tag{3.2}$$

If, as we assume, the variable in P is ω, rather than $\bar{\omega}$, then in the RLC networks L and C must change so as to hold the ratio $R_o \equiv (L/C)^{1/2}$ constant. We find then, in the first RLC circuit in Fig. 3-1, $Q = R_o/R$, and in the second, $Q = R/R_o$.

The measurement of a complex T(P) in general requires two parallel paths to the detector. One contains the circuit under test, and the other provides the reference signal. The detector then compares this signal with the signal transmitted through the test circuit. We will find that T, determined in this manner for a magnetron diode, also describes a circle or an oval path as a function of $\omega = eB/m$. One can define half-power points on such a curve and a corresponding Q which we will call Q_s. The Q defined for the orbits of electrons is a quite different quality factor.

In Chapter II we found how a TEM probe field effects individual electrons in their orbits. Continuing this development, we now consider how the response of a swarm of electrons modifies the probe signal. In broad outline, the signal suffers a progressive change in phase and in amplitude as it passes down a coaxial guide filled with space charge. The extent and character of this change depend on the length of the cloud relative to the signal wavelength, and on the condition of the space charge within the tube, or in other words on the probe frequency ω, on the static electric and magnetic fields imposed, and on the cathode emission.

One can express the phase and amplitude of the transmitted signal as functions of an effective dielectric constant,

$$\bar{\epsilon} = \epsilon_o - j\sigma/\omega \quad . \tag{3.3}$$

This quantity ϵ, a characteristic of the space-charge filled region in the magnetron diode, will then depend on the static fields, on ω, and on the cathode temperature T_c. It will not depend on time or on the spacial coordinates within the region, because it is an average over them appropriate to the TEM mode.

We thus assume that the probe fields within the diode keep the TEM configuration. Distortion can be regarded as a mixture between TEM and higher coaxial modes. However, such higher modes are far beyond cutoff and they attenuate rapidly in the empty diode at the frequencies we will use. Hence one may feel intuitively that the distortion of the TEM fields must be negligible. We support this intuition in an appendix to this chapter by appropriate calculations for two possible types of distortion.

It is helpful to have an over-all picture of the driven or coherent electronic motion which arises, of course, from electric coupling between particles and the TEM mode. Figure 3-2 contains a sketch of the TEM fields and the corresponding orbit currents for the case $u^2 < u_o^2$, that is, for a steady magnetic field stronger than would be required for orbit resonance with the probe field. The orbits in turn produce a steady magnetic field parallel to the z-axis and directed to oppose the steady external magnetic field. In addition the orbits produce a magnetic vector which

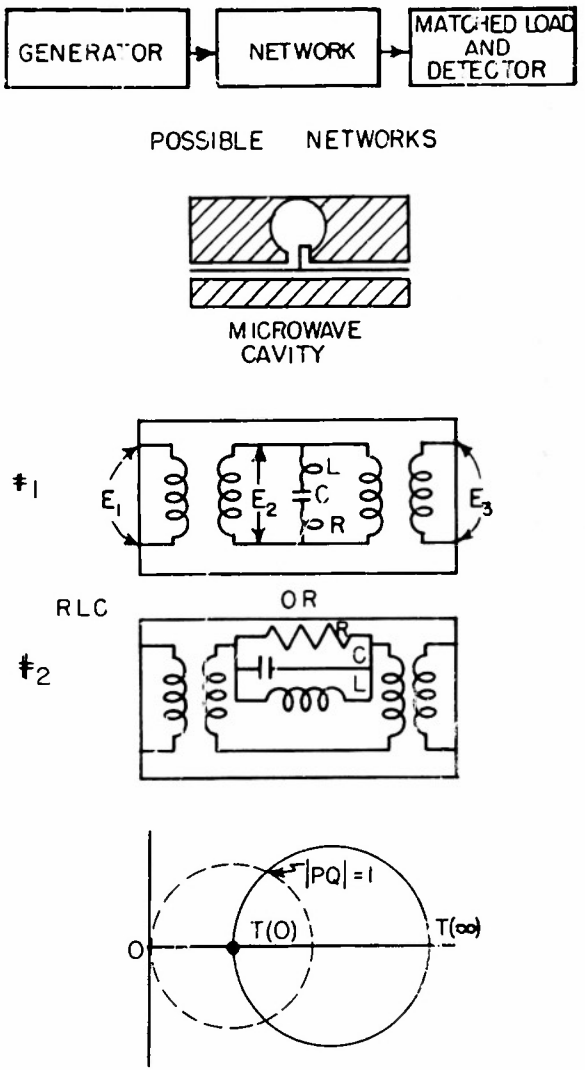

FIG. 3-1 TRANSMISSION CIRCUIT ANALOGUES

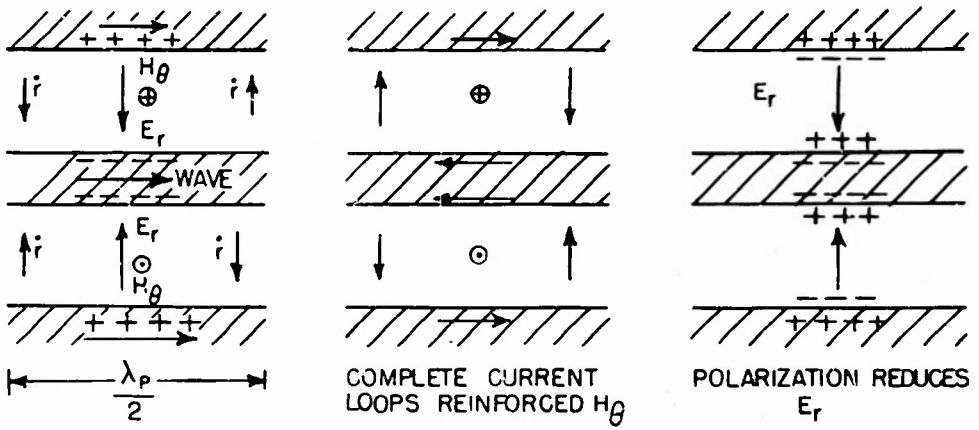

FIG. 3-2 TEM MODE IN MAGNETRON SPACE CHARGE CLOUD, $u^2 < u_o^2$

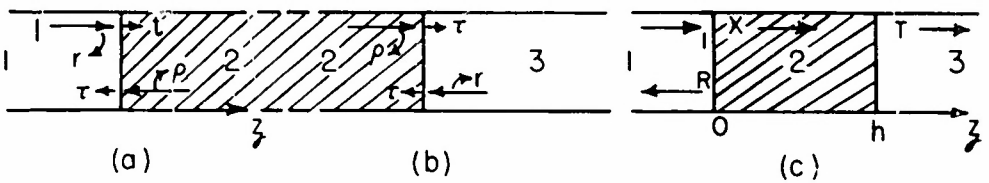

FIG 3-3 TRANSMISSION PARAMETERS

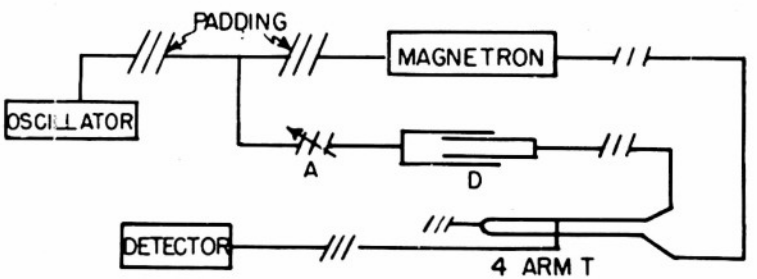

FIG 3-4 TRANSMISSION CIRCUIT

revolves in the (r,θ) plane at the driving frequency.

If the average or coherent radial velocity of the electrons leads the electric field of the probe signal, in space or in time, then the revolving magnetic vector of the orbits lies in the θ-direction when H_θ, the TEM magnetic field, has its maximum. This is the case $u^2 < u_o^2$. The two high frequency magnetic fields then add in the θ-direction, whatever may be the sign of the direction (along the z-axis) of the steady magnetic field or of the propagation of the TEM wave. If the imposed magnetic field is weaker than orbit resonance requires, the probe and orbit fields oppose each other along the θ-direction. Just at resonance they are out of phase in space or in time.

Figure 3-2 also indicates a polarization of the charge cloud along the metal surfaces. This occurs in space or in time between maxima of the radial motion. In this chapter we seek to interpret transmission measurements in terms of such electronic currents, to interpret T in terms of $\bar{\epsilon}$, Z and Q.

b. Transmission and Reflection Formulae.

We wish to find the complex coefficients of transmission T, and reflection R, of a section of coaxial waveguide divided into three regions by discontinuities in the transmitting medium at z = 0 and at z = h. Our treatment follows in most respects one by R. M. Redheffer [7, pages 561-673], but is sufficiently different to justify a sketch of the whole argument. In each region we distinguish fields and certain constants by subscripts i = 1, 2, or 3. The middle region contains, of course, a space-charge cloud, as sketched in Fig. 3-3c.

The fields of a TEM wave traveling forward toward positive z in a coaxial guide are proportional to the real part of $\exp\left\{j(\bar{\omega}t - \beta_i z)\right\} \cdot \frac{1}{r}$. We write their complex amplitudes as $E_r = E_i$, $H_\theta = H_i$. The fields of a wave traveling back toward negative z have a similar dependence on $\exp\left\{j(\bar{\omega}t + \beta_i z)\right\}\frac{1}{r}$, and have similar amplitudes, distinguished, however, by primes, E_i', H_i'. The complex propagation constant β_i, corresponding to z, the axial coordinate, is the same for either direction of propagation.

Within each region, Maxwell's relations,

$$\nabla \times H = \epsilon \dot{E} + \sigma E \quad , \quad \nabla \times E = -\mu \dot{H} \quad , \tag{3.4}$$

reduce, for the forward wave, to the equations,

$$j\beta_i H_i = (j\bar{\omega}\epsilon_i + \sigma_i)E_i, \quad -j\beta_i E_i = -j\omega\mu_i H_i, \tag{3.5}$$

and, for the backward wave, to the equations,

$$-j\beta_i H_i' = (j\bar{\omega}\epsilon_i + \sigma_i) E_i', \quad + j\beta_i E_i' = -j\omega\mu_i H_i' \quad . \tag{3.6}$$

For each wave we have $\beta_i^2 = \bar{\omega}^2 \mu_i \bar{\epsilon}_i$, and by convention $\beta_i = +\bar{\omega}(\mu_i \bar{\epsilon}_i)^{1/2}$. For the first wave we have $E_i/H_i = (\mu_i/\bar{\epsilon}_i)^{1/2}$ and for the second $E_i'/H_i' = -(\mu_i/\bar{\epsilon}_i)^{1/2}$. We shall maintain the distinction between μ_1 and μ_2, although the representation of electronic orbits by $\bar{\epsilon}$ implies $\mu_1 = \mu_2$.

Across the surfaces at z = 0 and z = h we require E_r and H_θ, fields tangent to these surfaces, to be continuous. This requirement can be met at z = 0, for instance, if one satisfies the equations $E_1 + E_1' = E_2$, $H_1 + H_1' = H_2$. These so-called scattering equations represent a wave from region 1 which at z = 0 is partially reflected and partially transmitted into region 2. The transmitted part may suffer further reflection at z = h, but this we treat as a separate problem. The scattering equations take a simpler form if we define the ratios r, t and k:

$$r \equiv \frac{E_1'}{E_1} \quad , \quad t \equiv \frac{E_2}{E_1} \quad , \quad k \equiv \sqrt{\frac{\mu_1 \bar{\epsilon}_2}{\bar{\epsilon}_1 \mu_2}} \quad . \tag{3.7}$$

If $\bar{\epsilon}_i$ is complex, then r, t, and k are also complex. (The symbols r, t, and k will revert to other meanings after the next few pages.) The scattering equations now read:

$$1 + r = t, \quad 1 - r + kt; \quad \text{or } r = \frac{1-k}{1+k}, \quad t = \frac{2}{1+k} \quad . \tag{3.8}$$

Similarly a backward wave in region 2, if it reaches z = 0, is partially reflected and partially transmitted into region 1. Its fields satisfy the scattering relations $E_2' + E_2 = E_1'$, $H_2' + H_2 = H_1'$. We rewrite these equations in terms of ρ, τ and K:

$$\rho \equiv \frac{E_2}{E_2'} \quad , \quad \tau \equiv \frac{E_1'}{E_2'} \quad , \quad K = \sqrt{\frac{\epsilon_1 \mu_2}{\mu_1 \epsilon_2}} \; ; \quad 1 + \rho = \tau \quad , \quad 1 - \rho = K\tau \qquad (3.9)$$

Noting next that $K = 1/k$, we find the relations:

$$\tau = kt \quad , \quad \rho = -r \quad , \quad \tau t - \rho r = 1 \qquad (3.10)$$

The sketch in Fig. 3-3a suggests the application of r, t, ρ and τ.

At the second discontinuity, at z = h, similar reasoning leads to the scattering equations:

$$E_2 + E_2' = E_3 \, , \; H_2 + H_2' = H_3 \quad ; \quad E_3 + E_3' = E_2' \, , \; H_3 + H_3' = H_2' \quad . \qquad (3.11)$$

If regions 1 and 3 have the same constants ϵ and μ, then (3.11) leads to the same type of relations between k r t, $K \rho \tau$ as (3.8), (3.9). However, roles are reversed and we have, for instance, instead of (3.7) and Fig. 3-3a, (3.12) and Fig. 3-3b:

$$r = \frac{E_3}{E_3'} \quad , \quad t = \frac{E_2'}{E_3'} \quad , \quad k = \sqrt{\frac{\epsilon_2 \mu_3}{\mu_2 \epsilon_3}} \quad . \qquad (3.12)$$

To find next the effects of multiple reflections, let us start a forward wave in region 1 towards z = 0. We may take the electric field of this wave to have unit amplitude at z = 0. It will excite a forward wave in region 3; we denote the complex amplitude of its electric field at z = h by T. Within region 2 we denote the complex amplitude of the electric field in the total forward wave by X exp $(-j \beta_2 z)$. Finally R is the reflected field in region 1 at z = 0. These quantities, R, X and T, appear in Fig. 3-3c.

The amplitude X consists of the transmitted part of the unit field incident on z = 0 from region 1, and the part of X which has suffered two reflections, first at z = h and then at z = 0:

$$X = t + \rho^2 X \exp(-2j \beta_2 h) \qquad (3.13)$$

Similarly we have:

$$R = r + \tau\rho \, X \exp(-2j \beta_2 h) \, , \quad T = \tau X \exp(-j \beta_2 h) \qquad (3.14)$$

Then, after eliminating X from (3.14), and r, t, ρ and τ in favor of a quantity

γ, $\exp(-\gamma) \equiv r$, we find:

$$T = \frac{\sinh \gamma}{\sinh(\gamma + j\beta_2 h)} , \quad R = \frac{\sin \beta_2 h}{\sin(\beta_2 h - j\gamma)} . \tag{3.15}$$

If both β and γ are real, then these quantities satisfy the equation $|T^2| + |R^2| = 1$ and no energy is lost in region 2.

Another form for equations (3.15) is the following:

$$T^{-1} = \cos \beta_2 h + \frac{1}{2}(k + \frac{1}{k}) j \sin \beta_2 h , \quad R^{-1} = \frac{1 + k^2 - 2j \cot \beta_2 h}{1 - k^2} \tag{3.16}$$

Here β_2 represents propagation through region 2, and k represents surface effects at the edges of region 2. Formulas (3.16) suggest that, from simultaneous measurements of R and T, one could determine separately the (complex) values of β_2 and k, and then μ_2 and ϵ_2. However, we shall measure chiefly T and shall now assume $\mu_2 = \mu_1 = \mu_o$, $\epsilon_1 = \epsilon_0$.

Finally, it is convenient to introduce a complex quantity δ and a real quantity β_o as follows:

$$1 + \delta \equiv 1 + (x - jy) \equiv k = \sqrt{\epsilon_2 / \epsilon_0} , \quad \beta_o \equiv \omega \sqrt{\epsilon_o \mu_o} , \quad \beta_2 = \beta_o(1+\delta) \tag{3.17}$$

In terms of δ, T and R take the following forms:

$$T^{-1} = \exp\left\{j\beta_o h(1+\delta)\right\} + j \frac{\delta^2 \sin \beta_o h (1+\delta)}{2(1+\delta)} \tag{3.18}$$

$$R^{-1} = \frac{\delta^2 + 2(1+\delta)\left\{1 - j \cot \beta_o h (1+\delta)\right\}}{-\delta(2+\delta)} \tag{3.19}$$

For small δ, $R(\delta) \doteq 0$ and $T(\delta) \doteq \exp(-j\beta_o h)$. The latter is, of course, the transmission through region 2 when the discontinuities at $z = 0$ and $z = h$ vanish. We now drop the subscripts entirely, so $\bar{\epsilon} \equiv \bar{\epsilon}_2$, $\beta \equiv \beta_o$. The symbols r, t, ρ, τ, k and K will not recur with the meanings they had in this section.

c. Interpretation of T Data in Terms of $\bar{\epsilon}/\epsilon_o$ and Q.

The transmission T through the magnetron diode was measured with the circuit sketched in Fig. 3-4 for a variety of values of V_a, ω, and λ_p. The

circuit components are further identified in Chapter V. By bringing the signals transmitted through the tube and through the parallel path (line stretcher and variable attenuator) to agree in phase and amplitude, one obtains a null reading on the detector. The extension D of the stretcher, and the attenuation A in db required to give a null appear in the relations:

$$20 \log_{10} |T| = A , \quad \arg T = \frac{2\pi D}{\lambda_p} \tag{3.20}$$

Figure 3-5a shows the results of three such measurements in curves I, II and III. These examples are extreme ones, for the variable V_a ranges over a ratio of 90 to 1, and λ_p over a ratio of 9 to 1. Curves II and III have been rotated (multiplied by $\exp(-j\,8\pi/9)$) to bring $T(\infty)$ to -1 for all curves and thus make comparison easier. The direction of variation of $T(u^2)$ is the same in curves I and II from $T(\infty)$ to $T = -0.2(1+j)$. Here the curves separate and curve I makes a wide excursion before bending back toward $T = -1$.

To correlate $T(u^2)$ with $\bar{\epsilon}/\epsilon_o$ we will use curve I as an example. For this curve the probe wavelength was 20.18 cm or roughly twice the length of the space-charge region. The substitution $\beta h = \pi$ may then be made in (3.18) to obtain:

$$T^{-1} = -\left\{\exp j\pi\delta + j\,\frac{\delta^2 \sin \pi\delta}{2(1+\delta)}\right\} \tag{3.21}$$

From this formula the grid $\delta = x - jy$ was calculated and imposed on the T-plane in Fig. 3-5b. The actual $T(\delta)$ mapping is a distorted version of the well known one, $T = -\exp(-j\pi\delta)$, which yields radial lines of constant x from $T = 0$ and concentric circles of constant y about $T = 0$. The distortion comes from reflections at $z = 0$ and $z = h$, and is most pronounced in Fig. 3-5b for large values of x.

The same δ-grid on the $\bar{\epsilon}/\epsilon$-plane appears in Fig. 3-6a, plotted from the formula:

$$\bar{\epsilon}/\epsilon_o = (1+x)^2 - y^2 - 2jy\,(x+1) \tag{3.22}$$

The combined grids in Figs. 3-5b and 3-6a permit one to interpret any

measurement of T at $\beta h = \pi$ as a measurement of $\bar{\epsilon}$. (For values of λ_p other than 20 cm, one must calculate other systems of grids on the $T(\delta)$ plane.) Curve I of Fig. 3-5a appears again on Fig. 3-5b, and, interpreted as $\bar{\epsilon}(u^2)$, is replotted in Fig. 3-6a. Experimental points on each figure carry values of the parameter u^2. The critical region near $u_o^2 = 0.895$ opens up enormously as $\bar{\epsilon}(u^2)$. When u^2 is greater than u_o^2, we see in Fig. 3-6a that $\bar{\epsilon}/\epsilon_o < 1$; and on the other wing of the $\bar{\epsilon}(u^2)$ cirve, $u^2 < u_o^2$ implies $\bar{\epsilon}/\epsilon_o > 1$. We recall from Fig. 3-2 that electronic velocities here tend to lead the electronic field of the probe signal.

Figure 3-6b provides a partial test of the analysis in Chapter II that leads to the formula for $\sigma(\bar{\omega})$, (2.47). In this figure we plot, from the data of curve I again, the function $z(u^2)$ as a solid curve, and we compute the function $z(u^2)$ from (2.47) as the dashed line.

$$z \equiv \frac{j\omega\epsilon_o}{\sigma(\bar{\omega})} \; ; \quad z = \frac{1}{(\bar{\epsilon}/\epsilon_o - 1)}(\text{data}), \quad z = \frac{u_o^2 - u^2 + ju^2/Q}{1.49\,p}(\text{theory}) \quad (3.23)$$

In the computation the values u_o^2 and Q are chosen to match the experimental curve at the point marked z_o. Other computed points are joined to corresponding experimental ones by short dashed lines. There is considerable scatter between theory and data, in particular an unexplained salient in the data near $u^2 = 0.925$. Nevertheless the distribution of points, as function of u^2, along the two curves, indicates that 1.49 p is about the correct factor relating z to Z.

Figure 3-6c presents in curve 2 the measured reflection from the diode for the same experimental conditions that apply along curve I of Fig. 3-5a. This curve, labelled $R(u^2)$, clearly changes very little in the whole range of the resonance transition. For comparison, a curve labelled $R(\delta)$, calculated from the transmission measurements of curve I, by means of formula (3.19) and Fig. 3-6a, also appears in Fig. 3-6c. Corresponding points on the two curves are given the same number. The agreement, representing a check of formulae (3.18) and (3.19) and of the assumption $\mu_2 = \mu_o$, is not very good. Mechanical discontinuities such as glass vacuum seals in the tube may cause some of the difference between curves 1 and 2.

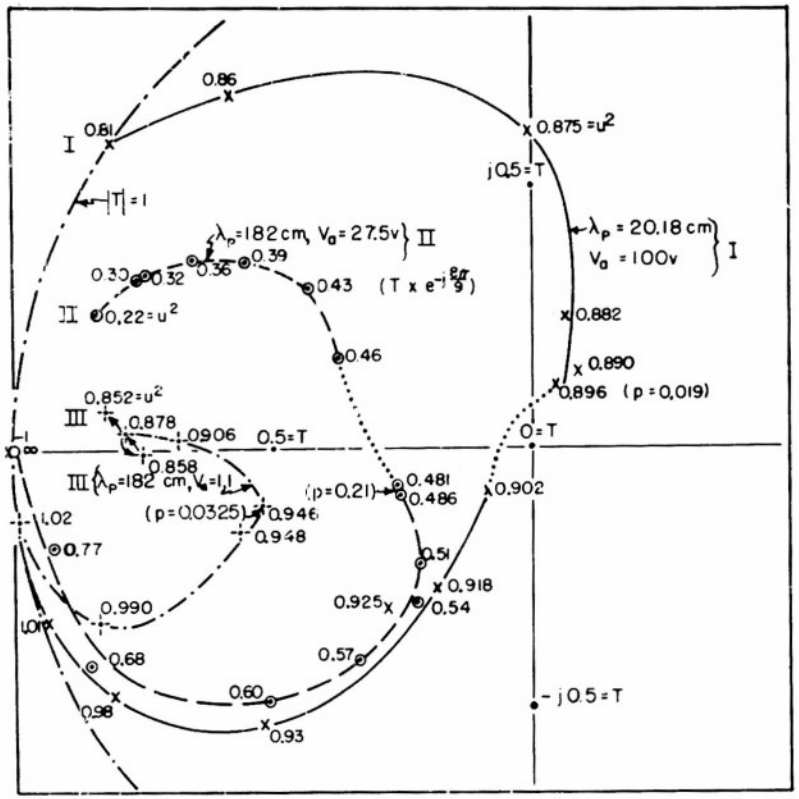

(a)

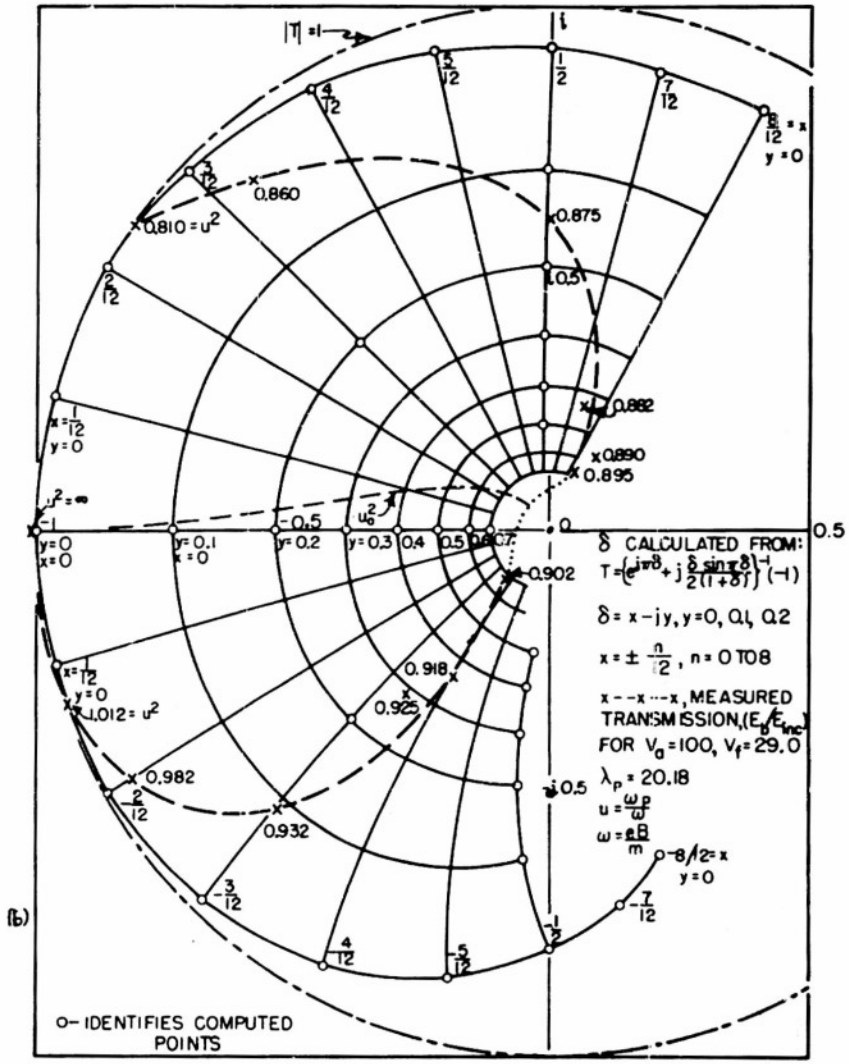

(b)

FIG. 3-5 THE COMPLEX TRANSMISSION COEFFICIENT T
(a) THREE CURVES OF DATA. (b) THE δ GRID

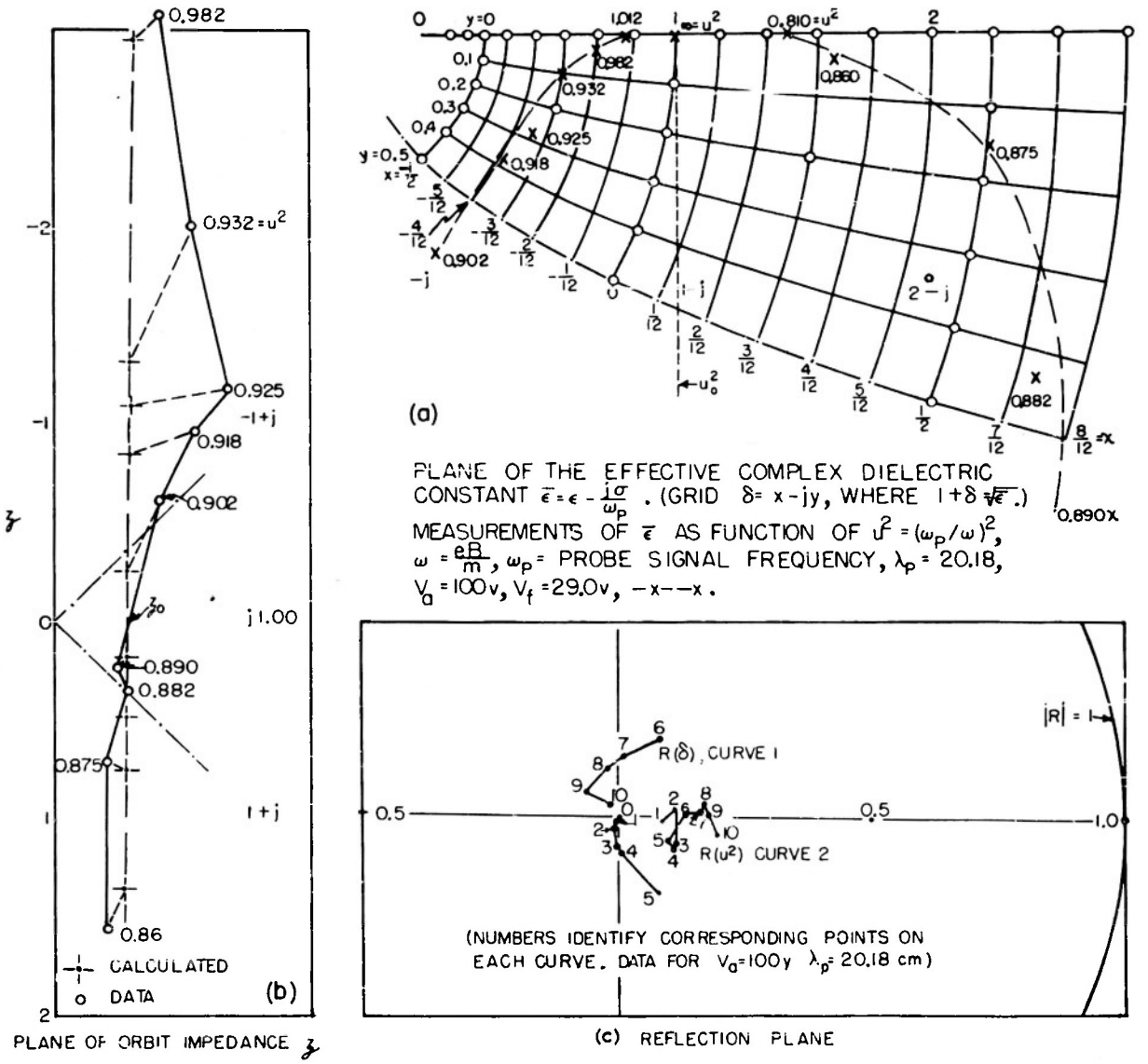

FIG.3-6 TRANSFORMATIONS OF CURVE 1 OF FIGURE 3-5a

We define the transmission at orbit resonance, T_o, as $T(u_o^2)$. This leads us to plot the curve $u_o^2 = u^2$: in Fig. 3-5b on the T-plane it runs from T = -1 to T = 0; and in Fig. 3-6a on the $\bar{\epsilon}/\epsilon_o$-plane it is the line on which the real part of $\bar{\epsilon}/\epsilon_o$ is one. On it, then, we have:

$$y_o^2 + 1 = (x_o+1)^2 \tag{3.24}$$

Using the approximate formula $T = \exp\left\{-j\beta h\,(1+\delta)\right\}$, we find:

$$y_o = -\frac{\ln|T_o|}{\beta h} \quad , \qquad Q = \frac{2u_o^2\, y_o \sqrt{y_o^2+1}}{1.49\,p} \tag{3.25}$$

As the wavelength λ_p is increased, βh decreases, and so does the absorption $\left|\ln|T_o|\right|$ as one can see by comparing curves I and III of Fig. 3-5a. As p decreases, the space-charge thins out and the orbit Q should increase.

To find the tuning rate of $T(u^2)$ near resonance, we consider increments $\underline{dx}$ and $\underline{dy}$ as functions of $\underline{du}$ near $u^2 = u_o^2$ in the equation:

$$(1+x)^2 - y^2 - 2j\,(x+1)\,y = 1 + \frac{1.49\,p}{u_o^2 - u^2 + ju^2/Q} \tag{3.26}$$

We find:

$$(1+x_o)\,dx - y_o\,dy = QKd\ln u \quad , \qquad K \equiv -\frac{1.49\,pQ}{u^2}$$

$$(1+x_o)\,dy + y_o\,dx = K\,d\ln u$$

Solving these expressions for $\underline{dx}$ and $\underline{dy}$ for insertion in the relation $d(\ln T) = -\beta h\,(dy + j dx)$, we find:

$$\left.\frac{d\ln T}{d\ln u}\right|_{u_o} = \frac{K\beta h\,(Q+j)(y_o + j\sqrt{1+y_o^2})}{2y_o^2+1} \tag{3.27}$$

Finally for comparison we recall $Q_s \equiv \omega/\Delta\omega$, where $\Delta\omega$ is the change in normalized magnetic field between points where the transmitted power has twice its maximum value. We present by way of summary the following table. In it we see the methods (3.25) and (3.27) for computing the orbit Q agree that $Q_{III} > Q_I > Q_{II}$.

Table 3-1. Comparisons between Curves of Fig. 3-4a.

Curve	I	II	III
u_o^2	0.895	0.47	0.946
p	0.019	0.21	0.0325
λ_p	20.18	182	182
y_o =	0.67	3.8	1.8
Q_s	95	12.5	20
Q(3.25)	53(100) *	36	150
Q(3.27) =	75	31	83

* The value $Q_I = 100$ can be inferred along the dotted part of curve I near $T = 0$.

References for Chapter III

1. Blewett and Ramo, "High Frequency Behavior of a Space Charge Rotating in a Magnetic Field," Phys. Rev. 57, 635-641 (1940).

2. Lamb and Phillips, "Space-Charge Frequency Dependence of Magnetron Cavity," J. Appl. Phys. 18, 230-238 (1947).

3. L. Harris, "Instabilities in the Smooth Anode Cylindrical Magnetron," J. Appl. Phys. 23, 562-567 (1952).

4. G. Brewer, The Propagation of Electromagnetic Waves in a Magnetron-type Space Charge, Technical Report No. 8, Electron Tube Laboratory, University of Michigan, Ann Arbor, Michigan (1951).

5. G. Geick, Observations of Space-Charge Phenomena in a Diode Magnetron, Technical Report No. 14, Electronics Research Laboratory, Stanford University, Stanford, California (1949).

6. R. Beringer, Ch. 7 in Montgomery Ricke and Purcell, Principles of Microwave Circuits, McGraw-Hill, New York, 1946, Vol. 8 of Rad. Lab. Series.

7. C. G. Montgomery, Technique of Microwave Measurements, McGraw-Hill, New York, 1947, Vol. 11 of Rad. Lab. Series.

8. Suhl and Walker, "Topics in Guided-Wave Propagation through Gyromagnetic Media," B.S.T.J. 33, 579-659 (1954).

Appendix III-1

Stability of the TEM Mode

The distorting influences we wish to consider are the dyadic character of the dielectric constant $\bar{\epsilon}$ of a magnetron space-charge cloud, and the dependence of $\bar{\epsilon}$ on the radial coordinate. We examine the first influence in a linear magnetron with a uniform space-charge density, and the second in a double region between coaxial conducting walls, a region consisting of two concentric shells with distinct scalar dielectric constants, $\epsilon_1 (r_c < r < r_H)$ and $\epsilon_2 (r_H < r < r_a)$. We will conclude that the TEM electric field suffers little distortion in our smooth anode magnetron, at least from these influences and in so far as these models represent our tube.

Following in part a recent treatment by Suhl and Walker [8], we first sketch the general equations for waves in a gyromagnetic medium. Our fictitious medium, introduced to keep the symmetry between E and H in Maxwell's equations, is immersed in a uniform constant magnetic field directed along the z-axis. The wave we study is proportional to the real part of $\exp j(\bar{\omega}t - \beta z)$, and the medium exhibits the following arrays of dielectric and magnetic constants at the frequency $\bar{\omega}$:

$$\bar{\epsilon} = \begin{vmatrix} a & -b & 0 \\ b & a & 0 \\ 0 & 0 & d \end{vmatrix} \qquad \mu = \begin{vmatrix} \alpha & -\gamma & 0 \\ \gamma & \alpha & 0 \\ 0 & 0 & \delta \end{vmatrix} \tag{3.28}$$

(Later we will set $\gamma = 0$ and $\alpha = \delta$, to make the medium represent a charge cloud.)

Let us next denote the z-components of E and H by ψ and χ and introduce k, a unit vector along the z-direction. Then we have:

$$\nabla \times H = j\bar{\omega}\epsilon \cdot E, \quad \nabla \times E = -j\bar{\omega}\mu H;$$

$$\epsilon \cdot E = d\,k\psi - ak \times k \times E + bk \times E, \tag{3.29}$$

$$\mu \cdot H = \delta\, k\chi - \alpha k \times k \times H + \gamma k \times H.$$

Applying the operators ko; kx, kxkx, and $kx\nabla_o$ to Maxwell's equations (3.29) one may obtain two coupled second-order differential equations in ψ and χ,

and eliminate all other components of E and H. In terms of the transverse Laplacian operator ∇_t^2, these equations are:

$$(\nabla_t^2 + R^2)\,\psi = -\,\delta T \chi, \quad (\nabla_t^2 + S^2)\chi = d\,T\,\psi\,. \tag{3.30}$$

In terms of the elements of ϵ and μ we define R, S, and T:

$$R^2 \equiv \bar{\omega}^2\,\alpha d\left(1 + \frac{\gamma^2}{a^2} - \frac{\beta^2}{\bar{\omega}^2 \alpha a}\right), \quad S^2 \equiv \bar{\omega}^2\, a\,\delta\left(1 + \frac{b^2}{a^2} - \frac{\beta^2}{\bar{\omega}^2\,\alpha\,a}\right)$$

$$T \equiv \bar{\omega}\beta\Gamma\,, \quad \Gamma \equiv \left(\frac{\gamma}{a} + \frac{b}{a}\right)\,. \tag{3.31}$$

Both ψ and χ then satisfy the fourth-order equation:

$$(\nabla_t^2 + \lambda_1^2)(\nabla_t^2 + \lambda_2^2)\,(\psi \text{ or } \chi) = 0$$

$$\lambda_1^2 + \lambda_2^2 \equiv R^2 + S^2\,, \quad \lambda_1^2\,\lambda_2^2 = R^2\,S^2 + T^2\,d\,\delta \equiv \Omega\,. \tag{3.32}$$

We write these expressions next in terms of separation constants Λ:

$$\Lambda_i \equiv \lambda_i^2 - R^2\,,\ i = 1 \text{ or } 2\,; \quad \Lambda_1 + \Lambda_2 = S^2 - R^2\,, \quad \Lambda_1\Lambda_2 = T^2\,\delta d \tag{3.33}$$

Then we can express λ_i^2 two ways from (3.31), (3.33);

$$\lambda_i^2 = k^2\left\{\frac{1 + L_i^2}{1 + mL_i}\right\} = k^2\left\{\frac{1 + \mathcal{L}_j^2}{1 + m\mathcal{L}_j}\right\}\,, \quad i \neq j\,. \tag{3.34}$$

$$k^2 \equiv \frac{\bar{\omega}^2\, a\,\alpha d\,\delta\Gamma}{b\delta + \gamma d}\,, \quad m \equiv \frac{a\delta - \alpha d}{b\delta + \gamma d}$$

$$L_i \equiv \frac{\gamma}{a} + \frac{\Lambda_i}{\Gamma\bar{\omega}^2\,\alpha d}\,, \quad \mathcal{L}_i \equiv -\frac{b}{a} + \frac{\Lambda_i}{\Gamma\bar{\omega}^2\, a\,\delta}\,.$$

Finally we eliminate λ_i^2 between (3.31) and (3.33) to obtain the simple relations:

$$(mL_1 + 1)(mL_2 + 1) = (m^2 + 1)\,\frac{a\delta}{\alpha d}\,; \quad (m\mathcal{L}_1 + 1)(m\mathcal{L}_2 + 1) = (m^2 + 1)\,\frac{\alpha d}{a\delta} \tag{3.35}$$

These manipulations serve to show that λ^2, representing the sum of squares

of propagation constants in the transverse directions, may approach infinity if mL+1 or mℒ+1 approaches zero.

However, this can happen only if $m^2 \longrightarrow -1$, since $(\alpha d/a\delta)$ remains in general of the order of unity.

Our gyromagnetic medium is to fill a slab-like region between infinite conducting plates, located at $x = \pm h$, and parallel to the z-axis. We assume our wave represents a TEM-like mode such that, although all three components of the electric field may exist, the chief component is E_x and is nearly constant in the x-direction. We assume further that all field components are independent of the y-coordinate.

As a trial solution we consider the form:

$$\psi = A\left\{\frac{\sin \lambda_2 x}{\sin \lambda_2 h} - \frac{\sin \lambda_1 x}{\sin \lambda_1 h}\right\} \tag{3.36}$$

This form vanishes at $x = \pm h$ as E_z should. It yields for E_z the form:

$$E_y = \frac{\bar{\omega}^2 d\delta}{\Omega}\left\{j\bar{\omega}a\frac{R^2}{\bar{\omega}^2 ad}\frac{d\chi}{dx} + j\beta\Gamma\frac{d\psi}{dx}\right\}.$$

$$\therefore \quad E_y = \frac{jA}{\beta\Gamma}\left[\frac{\Lambda_2 \cot \lambda_2 h}{\lambda_2}\cdot\frac{\cos \lambda_2 x}{\cos \lambda_2 h} - \frac{\cos \lambda_1 x}{\cos \lambda_1 h}\cdot\frac{\Lambda_1 \cot \lambda_1 h}{\lambda_1}\right] \tag{3.37}$$

Since E_y also vanishes at $x = \pm h$, we have the condition:

$$\frac{\Lambda_2 \cot \lambda_2 h}{\lambda_2} = \frac{\Lambda_1 \cot \lambda_1 h}{\lambda_1} = \frac{B}{h} \tag{3.38}$$

Now $kh \doteq \frac{\bar{\omega}h}{c} \leq 0.063 \ll \frac{\pi}{4}$ is an appropriate assumption for the linear magnetron that is to represent our diode. Hence, unless $m^2 \sim -1$, we may take just the first term, $(\lambda h)^{-1}$, in the series expansion of cot λh. We have then:

$$\frac{B}{h} = \frac{\Lambda}{\lambda^2 h} = \frac{(L - \gamma/a)\Gamma\bar{\omega}^2 ad}{hk^2}\left\{\frac{1 + mL}{1 + L^2}\right\} \tag{3.39}$$

Equation (3.39) may be put into the form $(L-L_1)(L-L_2) = 0$. After identifying

L_1+L_2 and $L_1 \cdot L_2$ in this form and inserting them in (3.35), we can solve for β. We find:

$$\beta^2 = \bar{\omega}^2 a\alpha \left(1 + \frac{\gamma^2}{a^2}\right), \quad R^2 = 0, \quad B = 1 \tag{3.40}$$

Then if $\gamma = 0$, β^2 depends on the leading diagonal element in each array (ϵ and μ), but not on any other elements. We also find for λ^2 the expansion, which is real if $\gamma = 0$, if b is pure imaginary, and if α, a, δ, and d are real:

$$\lambda_i^2 = +j\,\bar{\omega}^2 \Gamma \sqrt{a\alpha d\delta}\left\{1 + \frac{\gamma^2}{a^2}\right\}^{1/2}\left\{1 \pm j\frac{P}{2} - \frac{P^2}{8}\ldots\right\} \tag{3.41}$$

$$P \equiv \left(\frac{b}{a} - \frac{\gamma}{\alpha}\right)\sqrt{\frac{a\delta}{\alpha d}}\left\{1 + \frac{\gamma^2}{a^2}\right\}^{-1/2}$$

Here if $\gamma = 0$ and $|b/a| \leq 1$, then $|\lambda h| \doteq \frac{\bar{\omega} h}{c}\sqrt{\left|\frac{b}{a}\right|}$ shows the self consistency in our expansion of the cotangent of λh.

Finally, for the third component of E, E_x, we find:

$$E_x = \frac{\bar{\omega}^2 d\delta}{\Omega}\left\{\frac{j\bar{\omega}\alpha}{\bar{\omega}^2 \alpha a}\left[\frac{R^2 b}{d} + \beta^2 \Gamma\right]\frac{d\chi}{dx} - j\beta\left[\frac{R^2}{\bar{\omega}^2 \alpha d} - \frac{\gamma\Gamma}{a}\right]\frac{d\psi}{dx}\right\}$$

$$\therefore\ E_x = \frac{b}{a}E_y - j\frac{\beta d}{a}\left\{\frac{\cos\lambda_2 x}{\lambda_2 \sin\lambda_2 h} - \frac{\cos\lambda_1 x}{\lambda_1 \sin\lambda_1 h}\right\} \tag{3.42}$$

Expanding now the sines and cosines, as we did the cotangent, we obtain for the six field components of the TEM-like mode:

$$E_x = D + \frac{b}{a}E_y, \quad E_y = D\,\bar{\omega}^2 b\delta\left(\frac{x^2 - h^2}{2}\right), \quad E_z = j\,E_y\left(\frac{b\beta x}{3a}\right);$$

$$H_y = B + \frac{b^2}{a^2}H_x, \quad H_x = B\,\bar{\omega}^2 b\delta\left(\frac{x^2 - h^2}{2}\right), \quad H_z = -j\,B\left(\frac{\beta b x}{a}\right). \tag{3.43}$$

Here D and B are the amplitudes of the constant components of E_x and H_y, and we have assumed $\gamma = 0$. A sketch of these six components, as functions of x, appears in Fig. 3-7.

We can identify from (2.28) the elements of the ϵ-array for the linear magnetron:

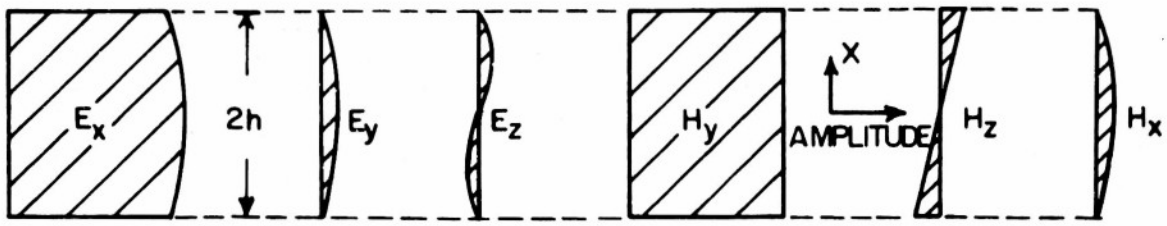

FIG. 3-7 GYROMAGNETIC DISTORTION OF TEM FIELDS

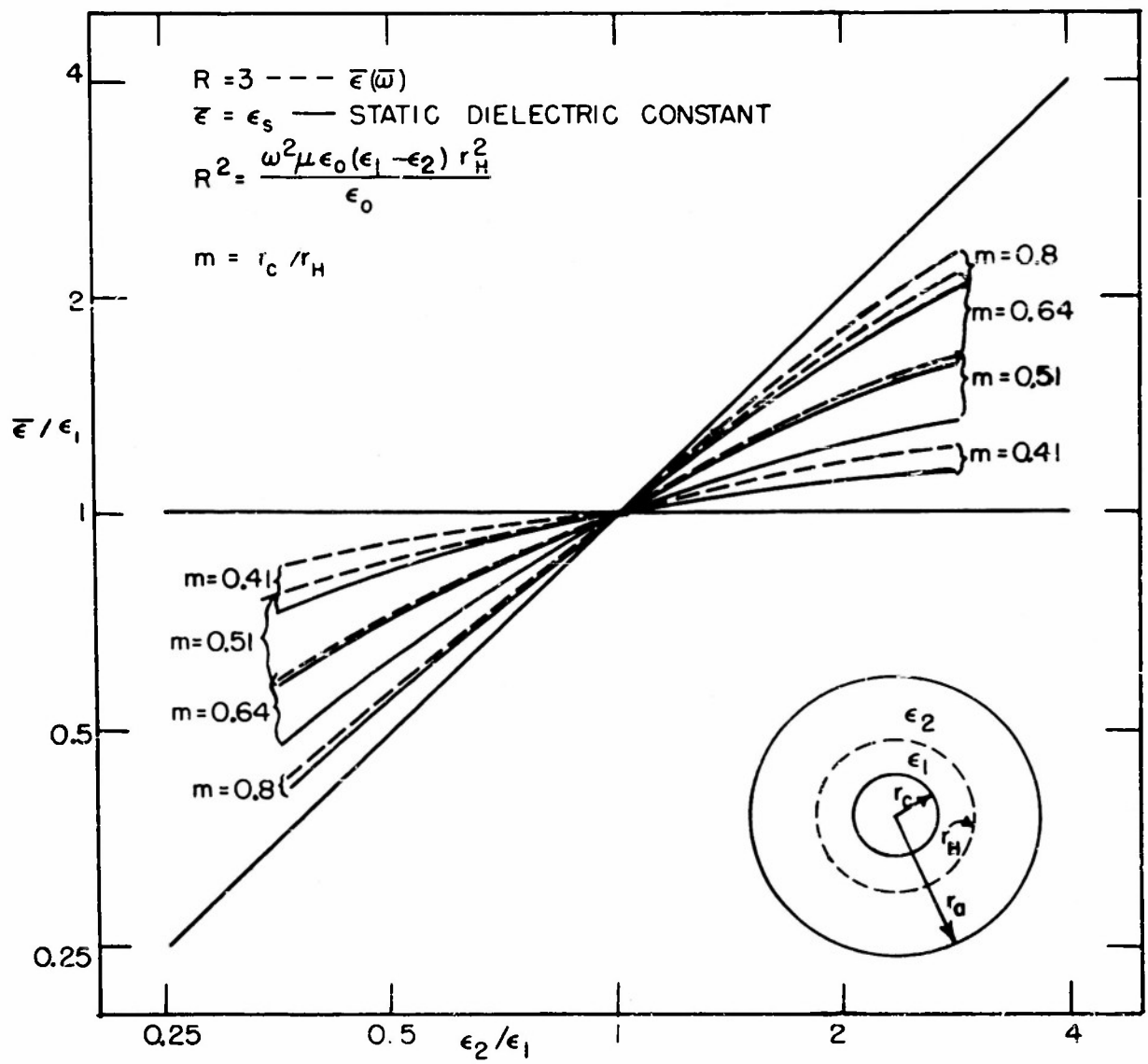

FIG. 3-8 TEM DISTORTION REPRESENTED BY $\bar{\epsilon}$

$$a = \epsilon_o \left(1 + \frac{2p}{Z}\right), \quad b = -\epsilon_o \frac{2jp}{uZ}, \quad d = \epsilon_o \left(1 - \frac{2p}{u^2}\right). \tag{3.44}$$

Moreover, $\underline{m}$ takes the simple form with these elements:

$$m = \frac{j u_o^2}{u} - \frac{u}{Q} \quad . \tag{3.45}$$

From (3.43) we identify the following amplitude ratios:

$$\left|\frac{E_y}{E_x}\right| < \frac{h^2 \bar{\omega}^2}{2c^2} \left|\frac{b}{a}\right| \quad , \quad \frac{E_z}{E_x} = \frac{\beta h}{3} \left|\frac{b}{a}\right| \left|\frac{E_y}{E_x}\right| \tag{3.46}$$

We conclude that the distortion of the TEM electric field is less than 0.002, if $\left|\frac{b}{a}\right| < 1$, $\frac{\bar{\omega} h}{c} < 0.063$ and $m^2 \neq -1$.

The same arguments apply through Eq. (3.35) in the case of the cylindrical magnetron. However, when the x-coordinate passes into r, we lose the symmetry between plus and minus x, and the complications introduced are not worth resolving. We merely take the dimension $r_a - r_c = 0.40$ cm from our diode and equate it to 2h. Then if $\lambda_p > 20$ cm, we have $\frac{\bar{\omega} h}{c} < 0.063$. The complications of cylindrical geometry are less severe, if the dielectric constant is a true scalar. We now turn to consider the distortion caused by a discontinuity in a scalar $\bar{\epsilon}$ at $r = r_H$, $r_c < r_H < r_a$.

In the limit of static fields, the average dielectric constant ϵ_s of a double region between concentric cylinders is given by:

$$\frac{\ln s_a}{\epsilon_s} = \frac{\ln (s_a/s_H)}{\epsilon_2} + \frac{\ln s_H}{\epsilon_1} \quad , \quad s \equiv \left(\frac{r}{r_c}\right)^2 . \tag{3.47}$$

This, we will show, is also the limit of the effective dielectric constant $\bar{\epsilon}$ as determined by propagation measurements, $\bar{\epsilon}/\epsilon_o = \bar{\rho}^2 (\omega^2 \mu_o \epsilon_o)^{-1}$. The extent to which $\bar{\epsilon}$ deviates from ϵ_s we will take as a measure of the distortion of the purely transverse mode into a combination of TM_o modes.

We write the axial component of the microwave electric field in either shell as a TM_o form:

$$E_z = \text{real part of } \left\{ Z_o(kr) \exp j(\bar{\omega}t - \beta z) \right\} . \qquad (3.48)$$

$Z_o(kr)$ is a combination of zero-order Bessel functions:

$$Z_o(kr) \equiv A J_o(kr) + B N_o(kr) \qquad (3.49)$$

Here A, B, and k are constants, which we now distinguish by subscripts i = 1, 2, referring to the inner or the outer region. Since $E_z = 0$ on metal surfaces $s = 1$, $s = s_a$, we have in region 1: $A_1/B_1 = -N_o(k_1 r_c) / J_o(k_1 r_c)$:

$$\therefore \quad Z_o(k_1 r) = \frac{B_1}{J_o(k_1 r_c)} \left\{ N_o(k_1 r)\, J_o(k_1 r_c) - J_o(k_1 r)\, N_o(k_1 r_c) \right\} . \qquad (3.50)$$

In region 2 the same equation applies with $1 \rightarrow 2$, $r_c \rightarrow r_a$. Then E_z is continuous across the boundary s_H between regions, so $Z_o(k_2 r_H) = Z_o(k_1 r_H)$. This defines the ratio B_1/B_2.

The corresponding magnetic field we write:

$$H_o = \text{real part of } \left\{ \frac{-j\bar{\omega}\epsilon}{k} Z_o'(kr) \exp j(\bar{\omega}t - \beta z) \right\} . \qquad (3.51)$$

Here $Z_o' = d Z_o / dkr$. Since H_o is continuous across s_H we have: $\epsilon_1 k_2 Z_o'(k_1 r_H) = \epsilon_2 k_1 (k_2 r_H)$. This equation we may write with suitable definitions in the form:

$$\frac{L(m,x)}{\epsilon_1} = \frac{L(n,y)}{\epsilon_2} \quad , \quad L(mx) \equiv \frac{U(x) - U(mx)}{W(x) - U(mx)\, V(x)} \quad ; \qquad (3.52)$$

$$x \equiv k_1 r_H \quad , \quad y \equiv k_2 r_H \quad , \quad m = r_c / r_H \quad , \quad n = r_a / r_H$$

$$U(x) = \frac{N_o(x)}{J_o(x)} \quad , \quad V(x) = \frac{J_1(x)}{x J_o(x)} \quad , \quad W(x) = \frac{N_1(x)}{x J_o(x)}$$

N_1 and J_1 are Bessel functions here of first order.

In the limit $\epsilon_1 = \epsilon_2$ we wish the TM_o forms to coalesce into a TEM wave. Hence x and y approach zero in this limit. Even for complex x, if $|x| \rightarrow 0$, then:

$$L(m,x) \doteq x^2 \ln m;$$

$$\therefore \quad x^2 |\ln m| / \epsilon_1 + y^2 \ln n / \epsilon_2 = 0, \text{ if } |x|, |y| < \tfrac{1}{2} \qquad (3.53)$$

Equation (3.52) is analogous to (3.38) of the previous development. The analogue of (3.34) requires, if E_z satisfies the wave equation, that the radial propagation constant k must satisfy the eigenvalue equations:

$$k_i^2 = \omega^2 \mu \epsilon_i - \beta^2 , \quad i = 1, \text{ and } 2. \tag{3.54}$$

The waves in each region have, of course, the same β, since E_z is continuous across the interface at s_H. We may then eliminate β from the two equations (3.54) and obtain:

$$x^2 - y^2 = \frac{\bar{\omega}^2}{c^2}\left(r_H^2\right)\frac{(\epsilon_1 - \epsilon_2)}{\epsilon_o} \cdot R^2 \quad . \tag{3.55}$$

Thus, if ϵ_1, ϵ_2 and s_H are given us, we can find both x and y from (3.55) and (3.52), and then β from (3.54). If x and y are small we may substitute (3.54) in (3.53) to eliminate x and y. We obtain, indeed, (3.47). The region of lower ϵ, it turns out, has an imaginary k, in general.

In Fig. 3-8 we present calculations based on (3.47), the case R = 0, and on (3.52) and (3.55), the case R = 3. The ratio $\bar{\epsilon}/\epsilon_1$, plotted against ϵ_2/ϵ_1, should, of course, lie between $\bar{\epsilon} = \epsilon_1$, a horizontal line, and $\bar{\epsilon} = \epsilon_2$, a diagonal line. The static limit ϵ_s appears as solid curves lying between these two limiting lines, with m (or r_H) as a parameter. The dotted curves represent, for corresponding values of m, the extreme case R = 3. This is the case $\epsilon_2 - \epsilon_1 = 520\,\epsilon_o$ for $\lambda_p = 20$ cm and $r_H = 0.42$ cm, or $\lambda_p = 0.1$ cm for $\epsilon_2 - \epsilon_1 = 4\,\epsilon_o$, $r_H = 0.42$.

In summary, then, the microwave fields in the two regions satisfy, near the common boundary r_H, the relation $E_r(1)/E_r(2) = \epsilon_2/\epsilon_1$. The region of lower ϵ has the stronger radial electric field. The extremely slight distortion of the TEM wave toward TM_o waves tends to restore the radial electric fields toward equality. In any case, even if the space-charge cloud actually lies wholly inside r_H, as the simple single and double stream models of the cylindrical magnetron imply, the TEM wave configuration is not altered so as to exclude the microwave fields from the inner region. Indeed, it is scarcely altered at all from the static configuration at the wavelengths we use. The integrals over the shell cross sections of Poynting's vector are then in the ratio:

$$P_1/P_2 = -x^2/y^2 = \varepsilon_2 \ln s_H / \varepsilon_1 \ln (s_a/s_H) \quad .$$

The contrast with ionospheric refraction is instructive. Charge clouds in the ionosphere bend radio waves, in paths several wavelengths long, so the waves may not penetrate far into these clouds. In such cases both the dimensions and shape of the cloud, and the dyadic character of its effective dielectric constant are important. Waves in the cloud are not, however, guided by conducting walls, as the waves through the magnetron diode are.

IV

The Resonance Absorption

a. Introduction.

In recent years many reflection measurements on non-oscillating magnetrons have revealed a high-frequency resonance. In general a probe signal was applied to the output circuit of the tube, while the cathode was held at the temperature of normal emission. The effects were observed as a function of anode voltage V_a, which was, however, held below the level needed to sustain oscillations. These measurements often led to speculation about space-charge behavior, but their inspiration was generally the need for a flexible method of modulating magnetron oscillators.

We should mention briefly several reports of such measurements. At the Massachusetts Institute of Technology Everhart in 1945 [1] and Smullin and Bagnall in 1949 [2] made probe signal tests on commercial magnetrons. On a tunable magnetron QK61 the latter observed that the small leakage current, remaining after cutoff, decreased near resonance. They also observed a saturation effect: the stronger the probe signal, the less the frequency of resonance depended on V_a. We note both effects in our own data.

Smullin and Bagnall hoped to use the input reactance $X(V_a)$ of the non-oscillating magnetron to "pull" an oscillating magnetron, and thus to modulate the latter. Their results were discouraging, for losses in the modulating tube were high. Indeed, these losses, rather than reactive effects, were used in an absorption modulator reported by Gutton in 1947 [3]. Welch at the University of Michigan in 1949 [4] also carried out extensive probe-signal tests on a commercial tube. On the QK59, he found that the frequency of resonance decreases as V_a increases. In our own data the same type of dependence appears.

All probe signals impressed on multi-cavity magnetrons presumably excite electric fields with a strong dependence on the angle θ. In such tubes the cavities are said to "load" the electromagnetic field so that one

wave component propagates slowly in the same circumferential direction as the rotating space charge. This component then interacts strongly with the cloud.

Since our probe signal has neither a θ-component nor a θ-dependence in its electric field, the problems posed thereby need not detain us and a more detailed study of these prior measurements here seems unnecessary. We turn then to present the data we have on the resonance absorption, and show first how it depends on various diode parameters.

b. Dependence on V_a, ω, $\bar{\omega}$, and T_c.

The simple circuit outlined in Fig. 4-1 was used to measure the amplitude of transmission $|T(u^2)|$ through the magnetron diode. Let us first consider the effects on $|T|$ of two variables, the anode voltage V_a and the steady magnetic field $B(I_c)$. These both appear in the normalized potential p, and B also appears in u^2:

$$p \equiv \frac{-e V_a}{m\omega^2 r_c^2}, \quad u^2 \equiv \frac{\bar{\omega}^2}{\omega^2}, \quad \omega \equiv \frac{eB}{m}, \quad \bar{\omega} \equiv \frac{2\pi c}{\lambda_p} \tag{4.1}$$

Hence on a graph whose coordinates are p and u^2, if one changes ω (or B) alone, one traces a straight line through the origin, $(p, u^2) = (0,0)$, with slope:

$$\frac{dp}{du^2} = -\frac{e V_a}{m\bar{\omega}^2 r_c^2} \tag{4.2}$$

The points on curve I, II or III of Fig. 3-5a, if plotted on the (p,u^2)-plane, lie on such a line. The points on curve I appear in Fig. 4-2a, and those on curves II and III in Fig. 4-2c.

In Fig. 3-5b we note that the curves u_o^2 and $T(u^2)$ intersect at the transmission minimum T_m. Thus on curve I $T(u_o^2)$, the transmission where the average electronic orbit is "in tune" with the probe signal lies virtually at the absorption maximum. This may not always occur, for the rate of change of ln T with respect to ln u (3.27) is not in general purely imaginary at $u^2 = u_o^2$. Nevertheless, we now take T_m as defining u_o, and in Fig. 4-2 we plot $u_o^2(T_m)$ as a function of p. In all three sections

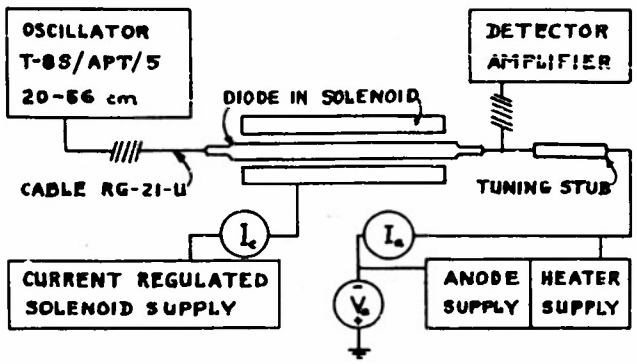

FIG 4-1 CIRCUIT FOR MEASURING |T|.

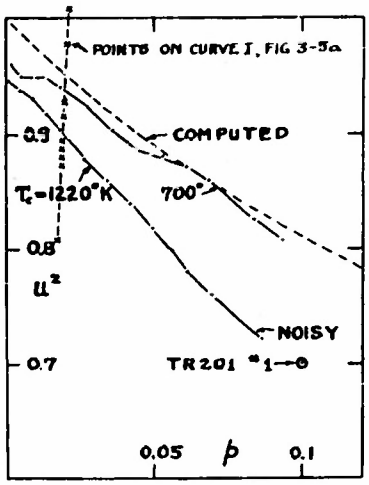

FIG 4-2a RESONANCE ABSORPTION OF A TEM PROBE SIGNAL, λ_p=20.18 cm

$u=\frac{\omega_c}{\omega}$, $\omega=\frac{eB}{m}$, $\beta=\frac{eV_a}{m\omega^2 r_c^2}$.

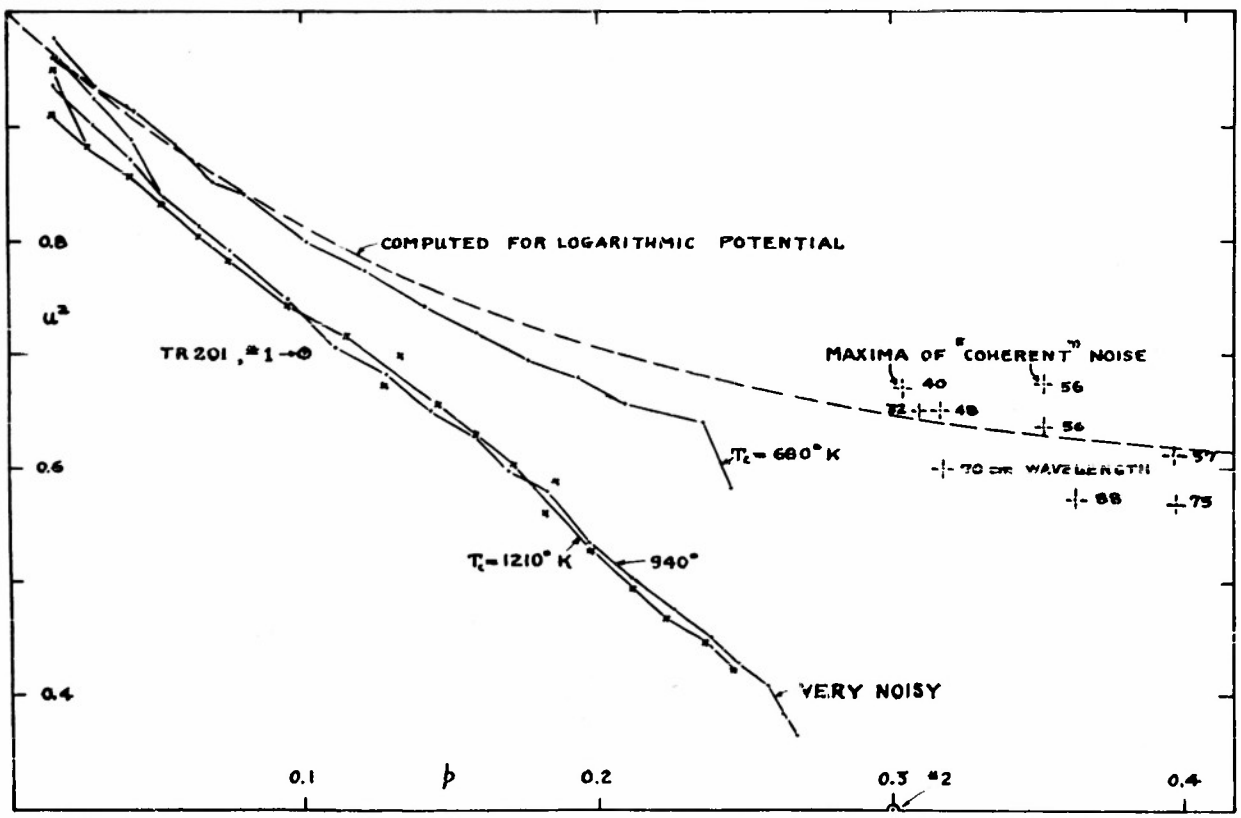

FIG 4-2b RESONANCE ABSORPTION OF A TEM PROBE SIGNAL, λ_p = 46.30 cm

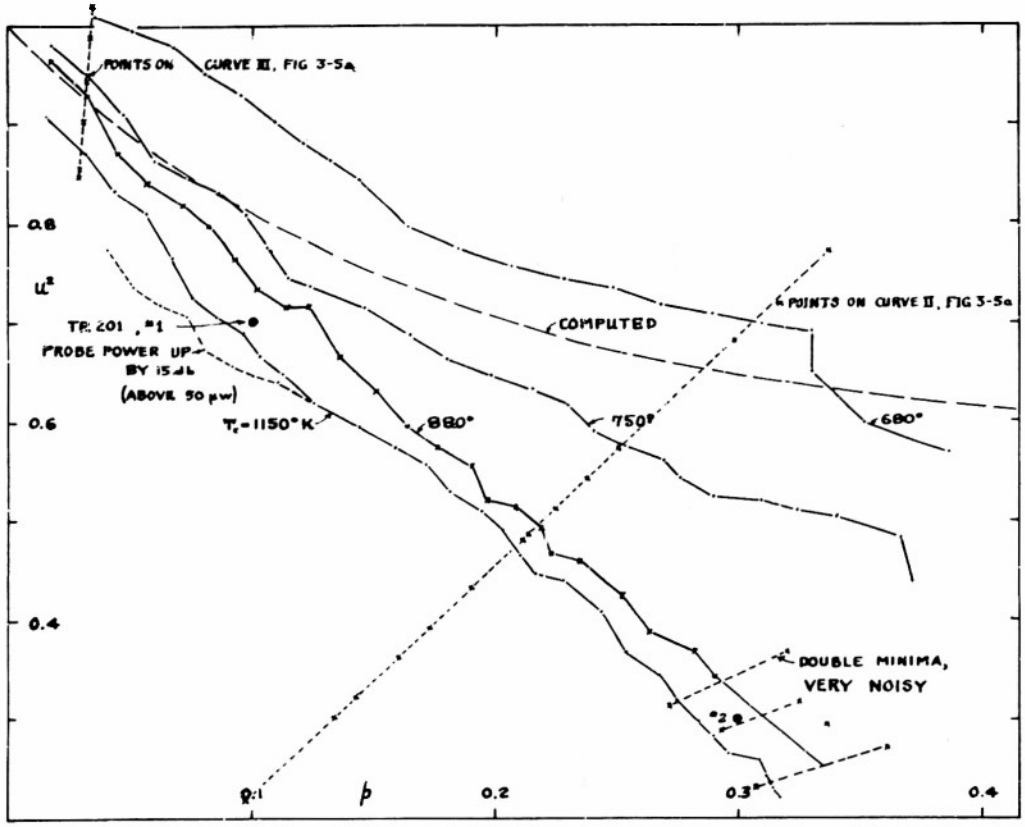

FIG 4-2c RESONANCE ABSORPTION OF A TEM PROBE SIGNAL, $\lambda_p = 186.2$ cm

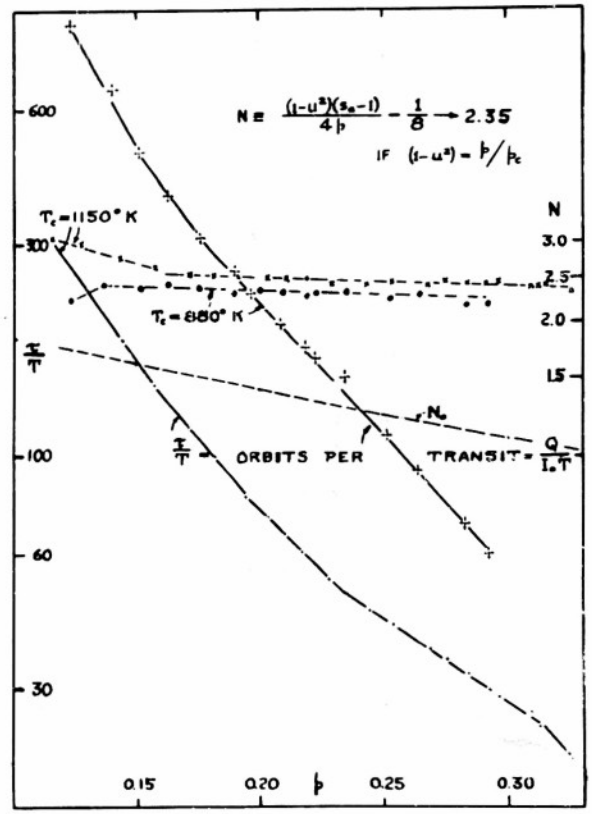

FIG 4-3 TRANSFORMATIONS OF DATA IN FIG 4-2c

of Fig. 4-2 we note this important experimental result: the lines $u_o^2(p)$ tend to lie along the line;

$$1 - u_o^2 = \frac{p}{p_c} \tag{4.3}$$

Here $p_c \doteq 0.42$ is the value of p at magnetron cutoff. For further analysis of $u_o^2(p)$ in T.R. 201 we will take the points numbered 1 and 2 in Fig. 4-2 as representative.

We ask next how the lines $u_o^2(p)$ depend on the cathode emission temperature T_c, and on the probe signal wavelength λ_p. It seems that these parameters interact in $u_o^2(p)$, since as λ_p increases, the variation of $u_o^2(p)$ with T_c increases too. This is reasonable, for temperature effects depend on the ratio $e V_a/\sqrt{kT}$, while V_a at any given point (p,u^2) varies as ϖ^2. Since λ_p in Fig. 4-2c is four times λ_p in Fig. 4-2b, T_c should be sixteen times more significant in Fig. 4-2c. As for the direction of variation of $u_o^2(p)$ with T_c, we note especially in Fig. 4-2c that $u_o^2(p)$ rises as T_c falls. Presumably the space-charge density falls with the cathode emission temperature; if $1 - u_o^2$ is linear in the charge density (1.13), one would expect $u_o^2(p)$ to rise on the (p,u^2) plane as T_c decreases.

In each section of Fig. 4-2, the uppermost line, $T_c \leq 700^\circ$, represents a convenient anomaly. We show in the next chapter that the nickel sleeve, on which the cathode emitting surface lies, becomes ferromagnetic below about 700°K. It then distorts the imposed magnetic field and seems to provide direct paths, near the ends of the tube, down which electrons spiral to the anode. This reduces the space charge almost to the vanishing point. The absorption resonance, just detectable at $T_c = 700^\circ$, represents orbits in a cylindrical region practically free of charge.

The half period T_b of the orbit of a particle, emitted with negligible velocity from the cathode into a region with a logarithmic potential, may be calculated from equation (1.7):

$$\omega T_b = \int_1^{s_b} \frac{ds}{\sqrt{8 s \Phi_o - (s-1)^2}}, \quad \Phi_o = \frac{p \ln s}{\ln s_a}, \quad u_o = \frac{\pi}{\omega T_b}. \tag{4.4}$$

The numerical calculations for T_b yield the line labeled "computed" in each section of Fig. 4-2. The agreement between this line and measured lines $u_o(p)$ for $T_c \leq 700^o$ in Figs. 4-2a and 4-2b is considered a further partial confirmation of the orbit equations.

The position of the line $T_c = 680^oK$ in Fig. 4-7c, above the computed line, is due perhaps to another feature of our diode. This tube was designed for transmission at 10 cm, and at 180 cm each end presents a bad mismatch. This is not serious when the absorption in the tube is large, but a weak absorption resonance could be pulled from its true position by cavity effects.

Figure 4-3 presents two transformations of the lines $T_c = 1150^o$ and $T_c = 880^o$ in Fig. 4-2c. The first transformation, N, in effect measures the deviation of u_o^2 from the line $(1-p/p_c)$. For u_o^2 on this line, N has the value 2.35, while for u_o^2 on the line computed for vanishing space charge, N is N_o. The formula for N and its significance will be developed in T.R. 201.

The second transformation includes data on the leakage current I_a collected by the anode at each point T_m. The ratio of the time τ, of transit from cathode to anode, to the orbit period T, or in other words the number of orbits an average electron complete per transit, is given by $Qf/\sqrt{I_a}$. Here f is $\bar{\omega}/2\pi$, and Q is the total charge in the magnetron charge cloud, as estimated in T.R. 201. Clearly τ/T suggests the function $A\exp(-Bp/\sqrt{p_c})$, while N is nearly constant and close to the value 2.35 in the interval $0.13 \leq p \leq 0.3$. The formulae used involve h, the axial length of the space-charge cloud:

$$Q = \frac{2\pi \epsilon_o h\, m\omega^2}{e}\left\{(s_a-1)(1-u_o^2) - \frac{p}{2}\right\}, \quad N = \frac{Q}{4\pi \epsilon_o h V_a} \qquad (4.5)$$

c. Relation to Other Effects.

Three effects related to the absorption resonance deserve a brief description. Each one reveals aspects of the magnetron space-charge cloud, and merits more investigation than we have been able to give it. These effects are the noise generated in the tube, the decrease in leakage

current I_a sometimes caused by a probe signal near resonance, and the second harmonic generated by the probe signal.

The amplitude of the broad-band noise generated in the magnetron diode tends to be constant along lines $V_a/\sqrt{B}$ = constant, lines of unit slope in Fig. 4-4. One might perhaps expect the noise temperature to reflect the velocity of rotation, $(r\dot{\theta}_2)_g = E_r/B$, (1.9), of the space-charge cloud about the z-axis. The generation of this hot cathode or normal noise increases along any line $u_o^2(p)$ as p increases, and when the noise power overtakes the probe signal power, it obscures the absorption resonances. This explains the early termination of the lines $u_o^2(p)$ in Fig. 4-2b and especially in Fig. 4-2a.

When the cathode cools down below 700° K the noise changes its character. It is no longer broad band, but rather represents fairly coherent oscillations of the remaining space charge at a frequency near the orbit frequency calculated for a charge free diode. Nine peaks of "coherent" or abnormal noise plotted in Fig. 4-2b show this close relation to the computed line. Very early magnetron diodes, called "cyclotron frequency oscillators," apparently delivered truly coherent oscillations based on this type of noise [5, page 3].

A fairly strong probe signal tuned to the orbit frequency may tend to reduce the leakage current I_a. This occurs at the other extreme of the p-axis from the noise phenomena, for p less than 0.1. Figure 4-5a shows this effect, with signal power as a parameter, in a normal region of the magnetron characteristic curve $I_a(p)$, and Fig. 4-5b shows the effect near a pronounced hump in the characteristic. The hump is associated with a kind of drag-loop: as p increases, the leakage current drops abruptly to zero. The value p_i where this happens depends on signal power level. As p decreases from above the sensitive region, on the other hand, I_a falls smoothly to zero, then jumps back suddenly to a normal value at p_d. Since p_i is greater than p_d, in the interval between them we have the dragging effect for which we can offer no good explanation. At the low p-end of the sensitive region, where the electronic velocities tend to lead the signal in phase, the signal increases the leakage current slightly in both parts of Fig. 4-5.

The probe signal then may interfere with the mechanism, whatever it is, that permits charges to flow across the lines of the magnetic field from cathode to anode. Further study of this interference should reveal more about the transport process. As we explain in Chapter 5, we do not favor the suggestion that I_a represents charges leaking around from beyond the ends of the active cathode, so in a sense "leakage" current is a poor description of I_a. We develop indications of the transport process further in T.R. 201.

These first two effects, in summary, appear to divide the normal data on the (p^2,u)-plane into three sections: for small p the probe signal affects I_a, and the transit time is relatively long. For somewhat larger p the absorption at resonance is strong and sharp, and $u_o^2 = 1 - p/p_c$. For still larger p the noise generated in the tube tends to obscure the absorption. These three sections contract toward the origin, p = 0, as one reduces λ_p, the probe-signal wavelength.

To describe the third effect, we recall the formula (2.42) for the second harmonic content in the current due to the radial motion of a single electron:

$$i_2 \doteq \frac{e\bar{\omega}(\delta k)^2 \sin 2\bar{\omega}t}{2 \ln s_a}, \quad \frac{k\delta}{1-k} = \frac{-2e E_1}{m\omega^2 r_c s_d Z} \tag{4.6}$$

If this motion is driven by a probe field E_1 of angular frequency $\bar{\omega}$, then we have by (2.38) the formula given above for $(k\delta)$. We then integrate i_2 over all particles in the space-charge cloud, which is assumed to move coherently with very small radial amplitude, and find I_2, the total second harmonic current.

$$\left| \frac{I_2}{2\pi h r_c} \right| = 0.56 \left| \frac{\sigma E_1}{Z} \right| \left\{ \frac{eE_1}{m\omega^2 r_c} \right\} . \tag{4.7}$$

Here σ is the space-charge conductivity at the fundamental frequency as in (2.47), and the numerical factor represents the integration over the radial interval $1 \leq s \leq s_a$.

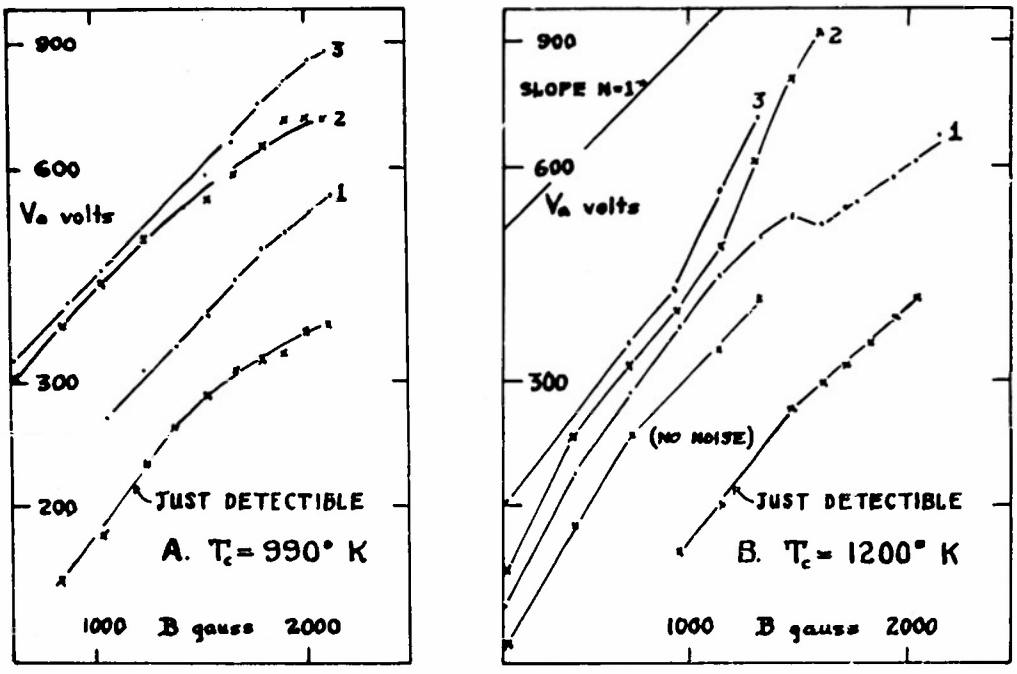

FIG 4-4 BROADBAND NOISE GENERATION, 3 db CONTOURS

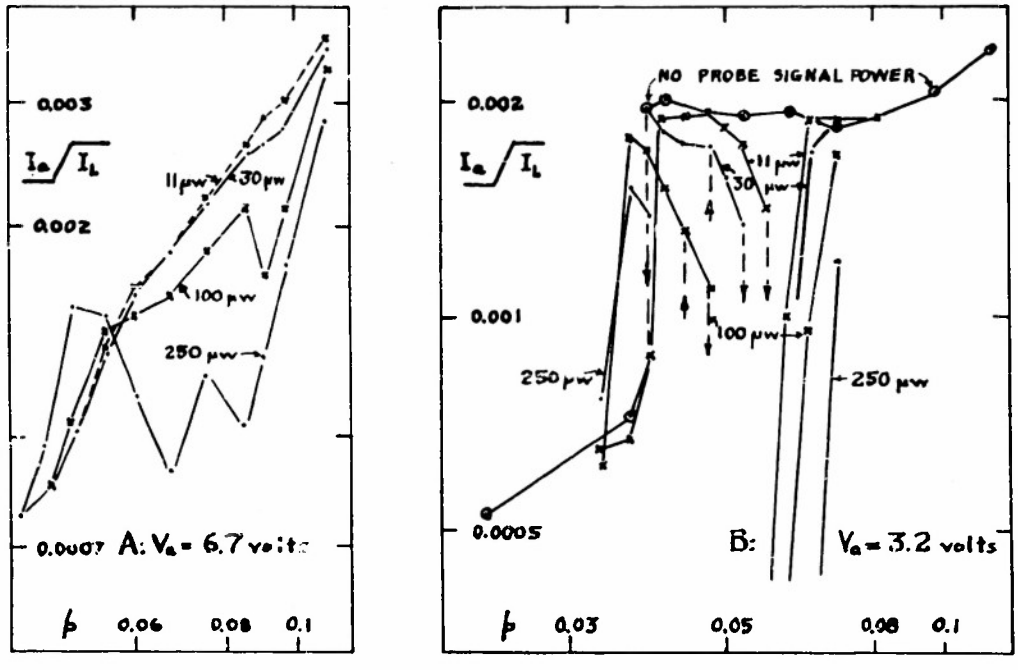

FIG 4-5 EFFECTS OF PROBE SIGNAL ON LEAKAGE CURRENT
CONDITIONS: λ_p = 182 cm, T_c = 1220° K

The power in this second harmonic, $W_2 = \frac{1}{2}|I_2|^2 R_c$, will then depend on E_1 to the fourth power, or on the square of the probe signal power W_1. Indeed, for λ_p of 20.18 cm we find:

$$W_2 = 11.7 \times 10^{-6} \left\{ \frac{u_o^2 p}{p_c} \right\}^2 \frac{W_1^2}{|Z|^4} \qquad (4.8)$$

If the probe signal carries 63 $\mu\omega$, $p = 0.02$, and $u_o^2 = 0.9$, then $|Z|$ is about 0.024 and W_2 about 25 $\mu\mu$W. This type of calculation led us to look for the second harmonic with a spectrum analyzer capable of measuring micro-microwatts. The results, presented in Figs. 4-6 and 4-7, seem to confirm the orbit concepts.

Figuratively it seems that the probe signal sets up along the tube a line of individual generators of the second harmonic current, and that it determines the phases of these generators. The second harmonic signal from each generator propagates in both directions without affecting the space-charge motion at all. (A probe signal of a frequency corresponding to the second harmonic of the orbit frequency shows no resonance effects in transmission through the diode.) The generators, if in correct phase, will reinforce each other rather like the holes in one type of directional coupler. However, if the probe signal has a rate of propagation differing from the rate of these second harmonic signals, the generators will not be phased correctly and will interfere with each other. This is the case near the absorption resonance and one finds interference effects in Fig. 4-6 near $u^2 = u_o^2$. In this figure, the distribution of the second harmonic output over the (p,u^2)-plane is presented, both for a rather cold cathode (6a), and a normal cathode temperature (6b). In each case, near the dotted resonance line, the second harmonic has a minimum, or valley, flanked on each side by roughly equal ridges, or maxima of second harmonic output.

Figure 4-7 shows in curves 1 and 2 a cross section of data similar to that presented in the form of amplitude contours in Fig. 4-6b. Curve 1 gives $|T|$ for the probe signal and curve 2 gives the corresponding second harmonic or 2f amplitude generated in the tube, both as functions of u^2. For this data microswitch T in the circuit sketched below the curves in

Fig. 4-7 was in position 1. The trap for 10 cm or 2f signals, an absorption wavemeter cavity, effectively removed from the oscillator output the small 2f content normally present with the probe fundamental.

With microswitch T in position 2 the probe signal and its 2f content were reunited ahead of the diode, but the relative phases of the two could be controlled by the line stretcher in the path of the fundamental. Curves 3 and 4 represent the addition, as seen by the 2f detector with due regard for relative phase, of 2f waves from two sources, the probe signal source and the magnetron diode. We see that a shift of $\lambda/8$ in the path length of the fundamental changes this addition from an effective and symmetric cancellation, curve 3, to a function of u^2 antisymmetric about u_o^2, curve 4. This reflects the fact that the fundamental probe signal has in the diode a propagation function $\beta(u^2)$ whose real part is antisymmetric about the resonance $u^2 = u_o^2$.

References in Chapter IV

1. E. Everhart, The Magnetron as a Reactance Tube, No. 52. Radiation Laboratory, Cambridge, Massachusetts, 1945.
2. Smullin and Bagnall, Some Measurements of the Characteristics of a Cutoff Magnetron, T.R.9A, Research Laboratory of Electronics, Massachusetts Institute of Technology, Cambridge, Massachusetts, 1949.
3. Gutton and Ortusi "Modulation on Guides for Centimeter Waves," Onde Elect. 27, 307-317 (1947).
4. H. Welch, Jr., "Effects of Space Charge on Frequency Characteristics of Magnetrons," Proc. Inst. Radio Engr. 38, 1434-1449 (1950).
5. G. Collins, Microwave Magnetrons, McGraw-Hill, New York, 1948, Vol. 6 of Rad. Lab. Series.

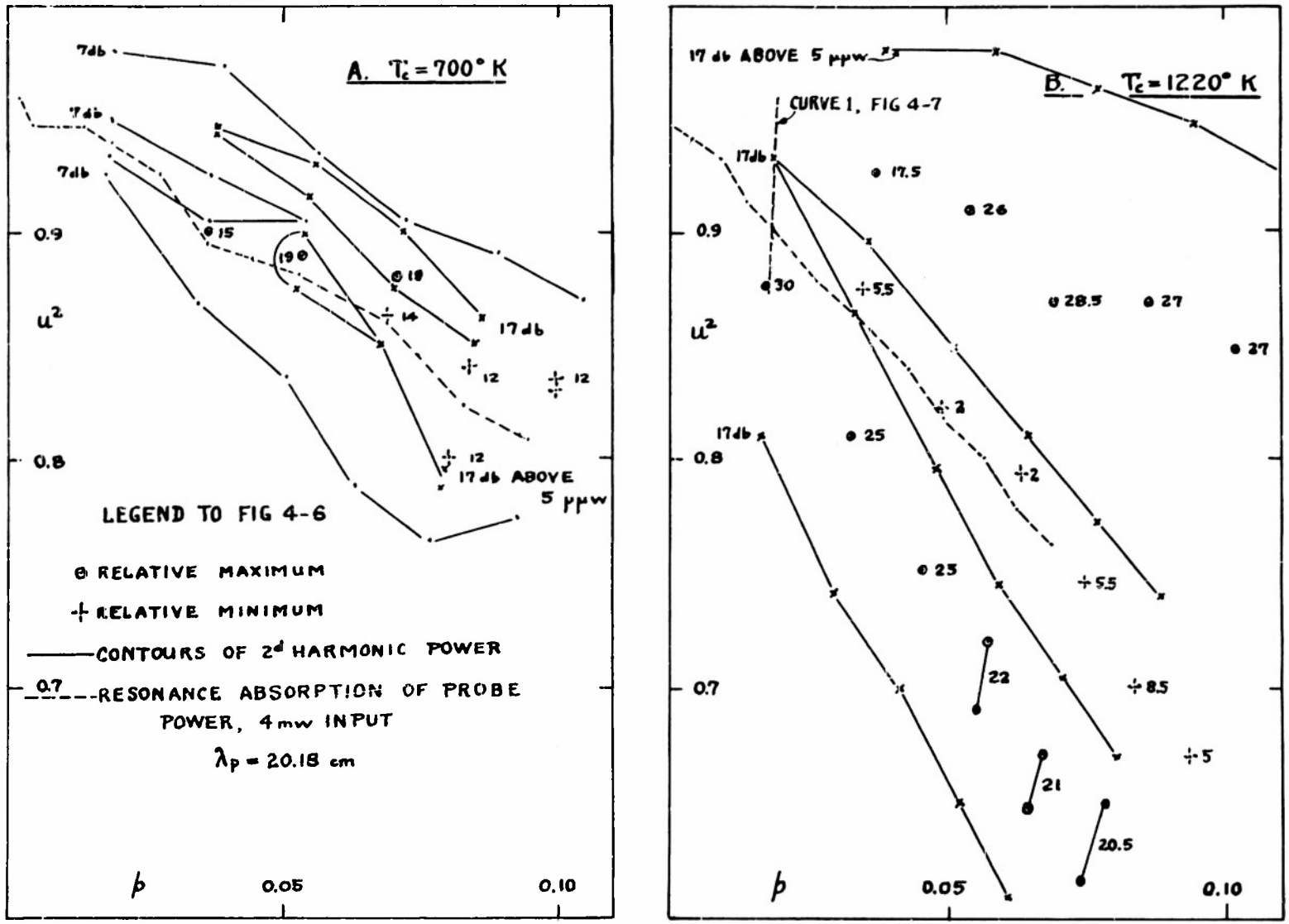

FIG 4-6 CONVERSION OF PROBE SIGNAL INTO ITS SECOND HARMONIC

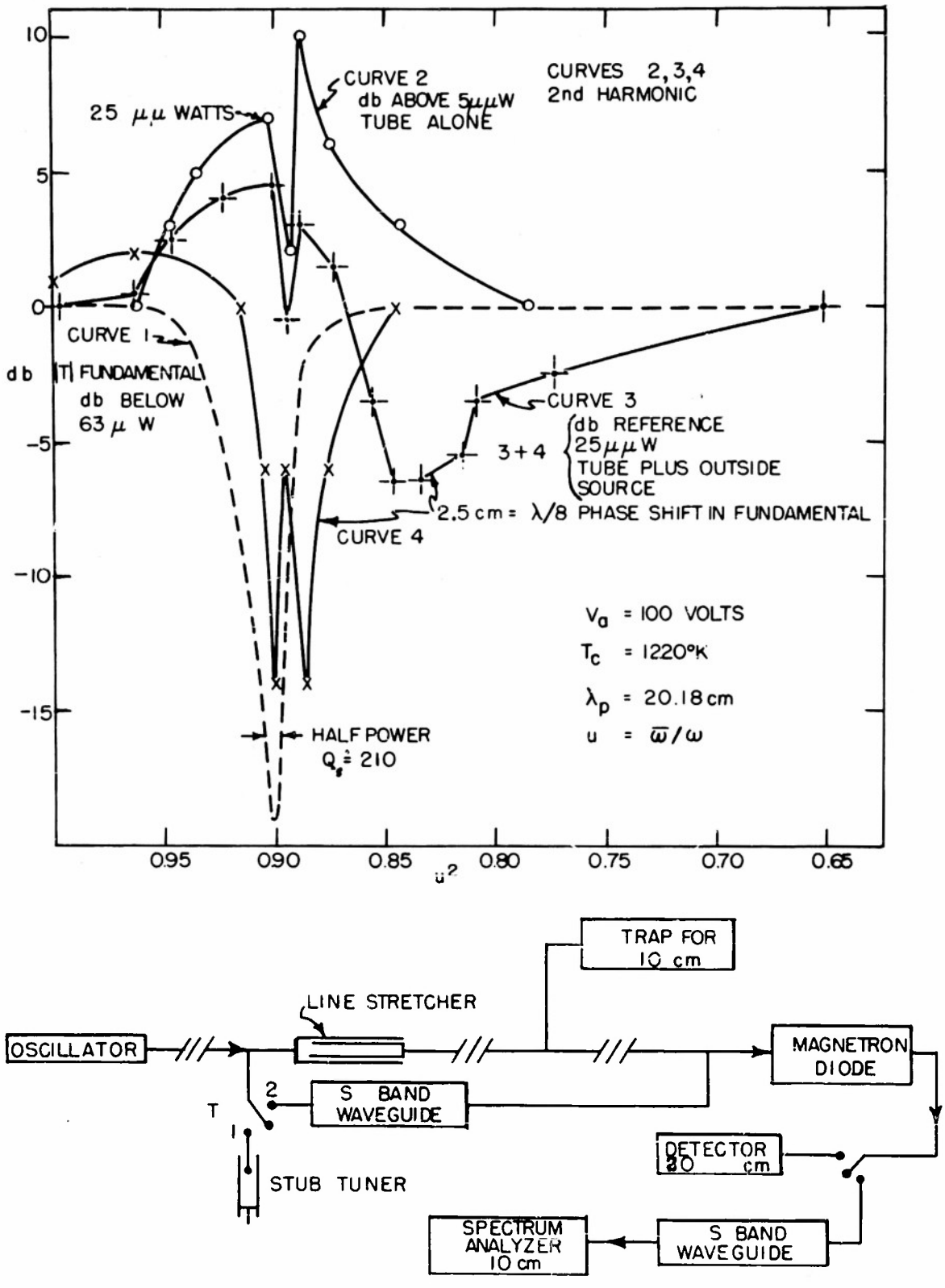

FIG.4-7 INTERFERENCE EFFECTS IN 2d HARMONIC GENERATION

V

Equipment

a. Magnetron Diode.

The central element in the experiments described in this report is a coaxial diode. Professor Sanai Mito of Osaka City University, Japan, designed and built this diode while he was at Harvard University in the period October 1951 to August 1952. He planned that it should amplify a microwave signal by a "distributed negative conductance," either as a transit time diode or as a magnetron diode.

A drawing of the tube appears in Fig. 5-1. The electrons are emitted from an oxide coating on the nickel sleeve which forms the inner conductor. "Several tests were carried out to obtain a uniform temperature distribution along this cathode, which is ten centimeters in length. This was achieved by properly spacing the heater coils along the nickel sleeve, and also by thinning down both ends of the sleeve to a wall thickness of 0.21 mm for a length of 3.8 cm. The temperature was then uniform along the cathode within 1.7 per cent.

"In order to take care of the thermal expansion of the cathode, a trombone slide was adopted. This slide was designed to take care of a maximum expansion of about 2.7 mm at the flashing temperature of the cathode and at the same time was designed to serve as d-c insulation as well as an r-f choke. Several test diodes were made to determine a suitable breakdown schedule. This was necessary because of the unusual cathode length in the final tube."[1]

The side arm in Fig. 5-1 terminates in a bottle enclosing a getter. The cathode sleeve, at the end of the tube labeled "IN," slides on a quartz tube which insulates the sleeve from the inner conductor of Kovar, as noted in the quotation above. The capacity between Kovar and nickel parts is between 4 and 7 $\mu\mu$f. The impedance of this coaxial condenser is of the order of the characteristic impedance of the coaxial line, if the wavelength λ_p of the probe signal lies in the range 45 to 80 cm. Consequently, the measurement of reflection from the space charge in the tube is possible

only at short wavelengths. At longer wavelengths it is hard to match the tube input impedance to the line.

The emission of this tube has held up well over the past two years. The diode characteristic obtained from the tube soon after activation, as it appears in Fig. 5-2, satisfies well Langmair's relation for space-charge limited current, which in this case reduces to:

$$I_L = 0.577 \times 10^{-3} V_a^{3/2} \text{ amperes, } V_a \text{ in volts.} \qquad (5.1)$$

The experimental points in Fig. 5-2 leave this curve when the anode current I_a reaches saturation values; the points branch off along curves identified by T_c and by V_f, the voltage applied to the heater circuit.

The branching of the V_f curves in Fig. 5-2 is so gradual that it does not allow us to calculate I_o, the saturation emission current at zero cathode field. For values of V_f under 12 volts, however, following Hermann and Wagener, [2, page 177, Vol. II] we plot $\ln I_a$ against $\ln (V_a+1)$ in Fig. 5-3 and extrapolate to I_o at $V_a = 0$. I_o seems to depend somewhat on the recent history of the tube, on whether light or heavy currents were drawn, and on the magnetization of the cathode sleeve as well as on T_c.

The slope of the "straight" section of each curve in Fig. 5-3 is apparently nearly independent of temperature and is reported to depend chiefly [2] on the surface roughness of the cathode. The temperature T_c for higher values of V_f was found from the slopes of curves such as appear in Fig. 5-4, where the ordinate is $\ln I_a$ and the abscissa a retarding voltage V_a. From Schottky's formula, we have [3]:

$$\frac{d(\ln I_a)}{d V_a} = -\frac{e}{kT_c} \qquad (5.2)$$

In order to find this slope, two points within the linear portion of each curve were noted in alternation until a succession of identical pairs of readings showed that I_o was momentarily constant.

Most of the data given in Figs. 5-3 and 5-4 reappear in Fig. 5-5 as functions of V_f. The curve $T_c(V_f)$ depends in its upper linear part on

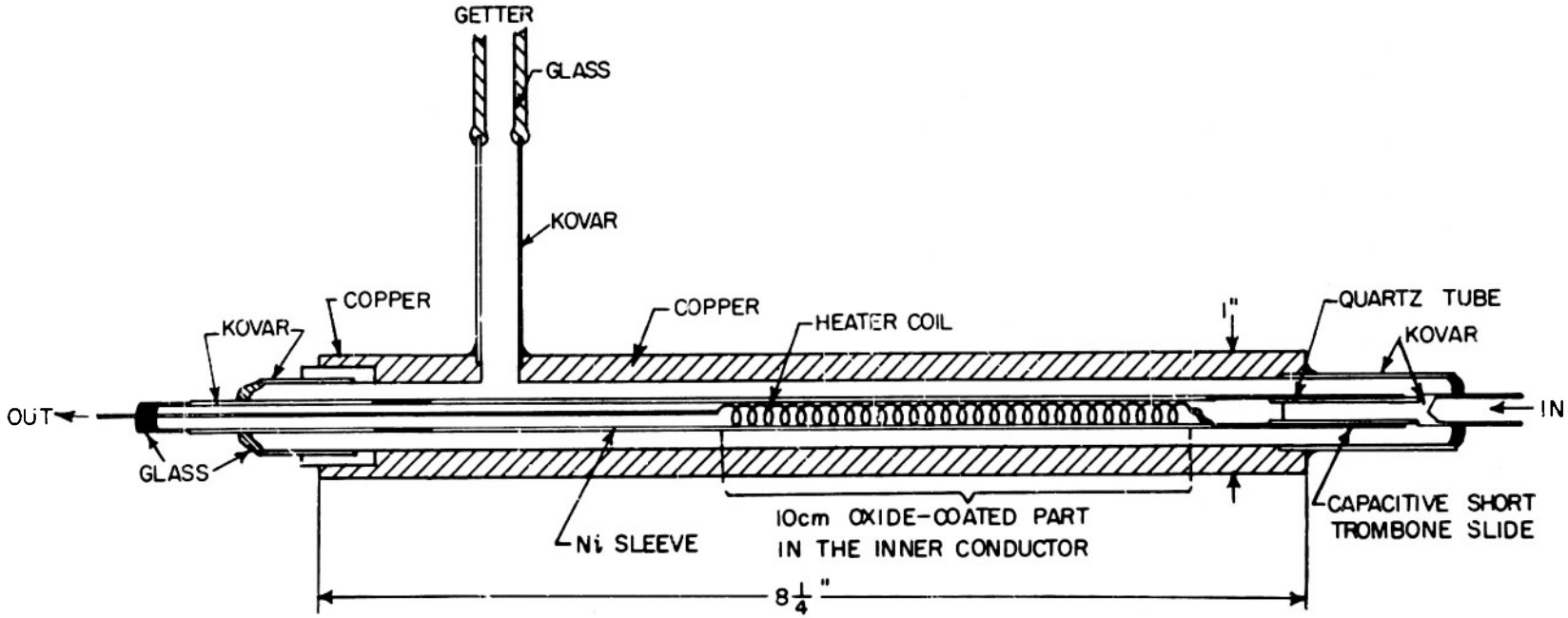

FIG. 5-1 TRANSMISSION DIODE

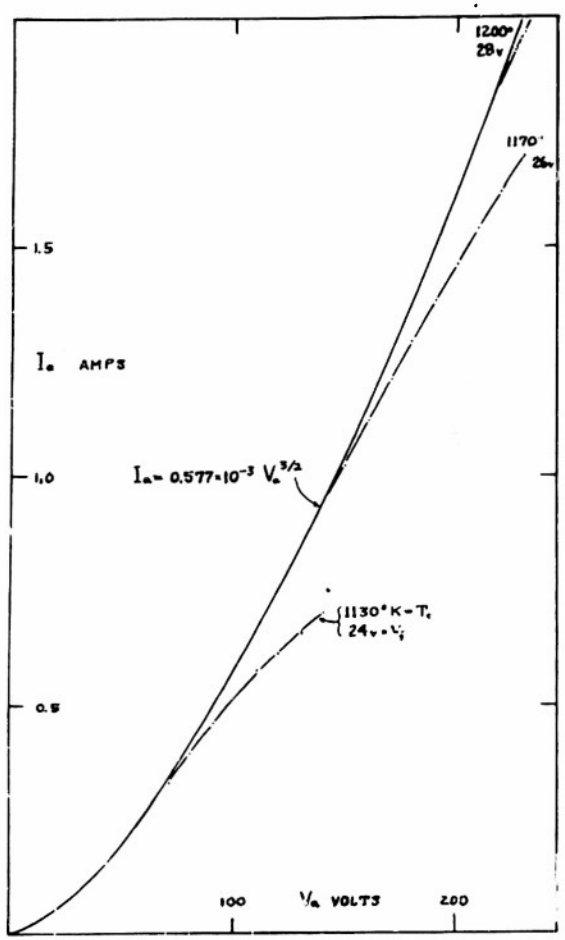

FIG 5-2 SPACE CHARGE LIMITED CURRENT

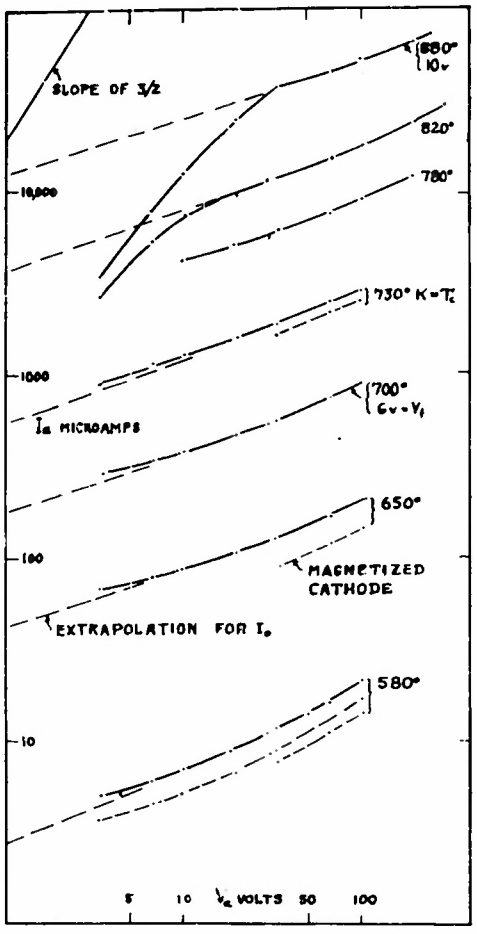

FIG 5-3 TEMPERATURE LIMITED CURRENT

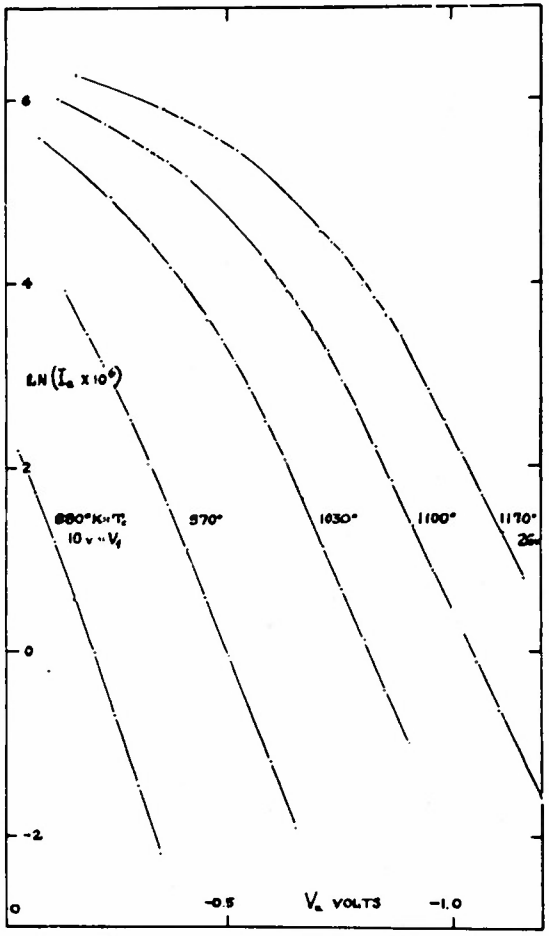

FIG 5-4 CURRENT IN A RETARDING FIELD

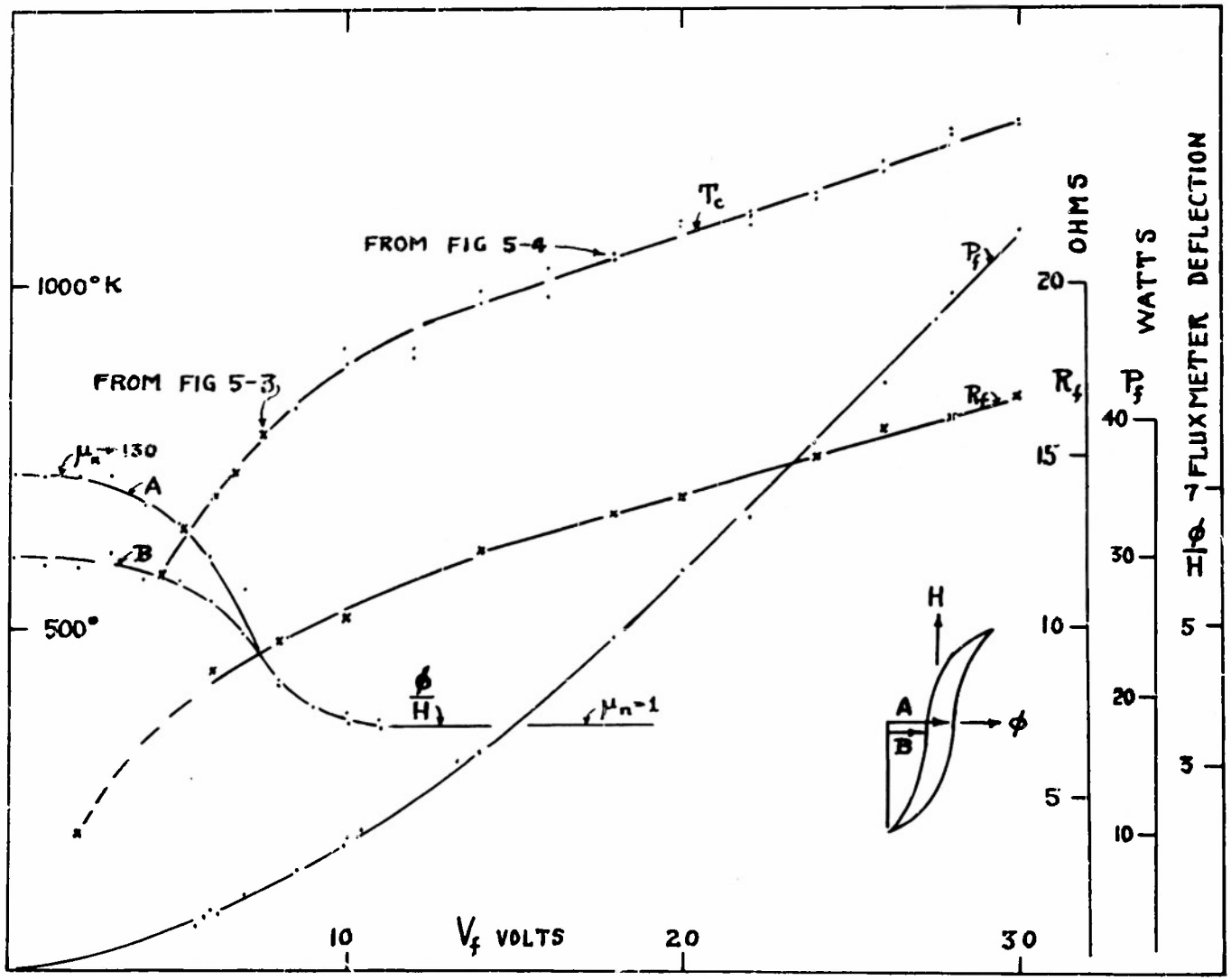

FIG 5-5 FUNCTIONS OF HEATER CIRCUIT VOLTAGE V_f

measurements of I_a into a retarding potential, and in its lower section on estimates from saturation emission data. The curves of heater power $P_f(V_f)$ and resistance $R_f(V_f)$ need no comment. The fourth curve, ϕ/H as a function of V_f, shows the Curie transition in the nickel of the cathode sleeve and will be described later.

Figure 5-6 presents curves of leakage current I_a (T_c, p) for p less than the cutoff value p_c. (Here, as in Chapter IV, p is the anode voltage normalized with respect to the steady magnetic field.) As the cathode cools down, I_a falls until T_c reaches 750°K, and then I_a rises to a maximum close to the saturation value. The maximum occurs in the region of the Curie transition shown in Fig. 5-5. We conclude that the anomalous behavior of I_a arises from progressive magnetization of the cathode and from the appearance of fringing magnetic fields near the ends of the nickel sleeve. These fields will have radial components which distort the lines of B within the tube. Electrons then find paths along the distorted lines down which they can readily spiral from cathode to anode.

The Curie transition shown in Fig. 5-5 was actually measured with the circuit shown in Fig. 5-7a. The measured current I_c through the large solenoid S gave, when the diode was withdrawn from S, a field of about 40 gauss. The switch W permitted one to cut off and to reverse I_c. When this was done, the changing lines of the field cut the turns of a probe solenoid and the deflection registered on the flux-meter indicated the strength of the collapsing (or increasing) B-field. When the magnetron diode was reinserted in S, it had little effect on the deflections obtained unless the cathode temperature was below 900°K. Curve B in Fig. 5-5 gives the deflection obtained by opening W and curve A that obtained by closing W so as to reverse I_c. The sketch of the hysteresis loop shows the relation of amplitudes A and B to the whole loop.

Figure 5-7b shows the magnetic circuit used to calculate the changes in the reluctance R_n of the nickel sleeve and from these the permeability μ_n. The reluctance R_e of the magnetic path outside the solenoid is concentrated mainly at the two ends of S. The reluctances inside the solenoid are in the inverse ratio of the cross-sectional areas of the nickel and the

diode, $R_o/R_n = 0.0088$, when the cathode is hot and $\mu_n = \mu_o$. Similarly, R_o/R_e is in the ratio of solenoid radius to length $r_a/h = 0.072$. Finally,

$$NI_c = R\phi\ , \quad \text{and} \quad \frac{1}{R_o} + \frac{1}{R_n} = \frac{1}{R - R_e}\ . \tag{5.3}$$

We conclude that μ_n for the cold nickel is 130 μ_o for the coercive force NI_c used. For higher values of coercive force, as the nickel saturates, μ_n will decrease and so will the changes in total flux in the Curie transition from above $T_c = 700^oK$ to below it. The values for the transition temperature and μ_n are reasonable [7].

b. Other Equipment.

Except for the magnetron diode the equipment used in the experiments herein reported was fairly standard and has little intrinsic interest. It was chosen to survey the ramifications of the absorption resonance, rather than to refine the accuracy or examine the details of any one aspect.

Figure 5-8 represents the microwave receiver. The signal passed through lossy cable to a tuning piston in parallel with a IN-23 crystal. On this crystal a Hewlett Packard and crystal-controlled oscillator imposed a 100 kc signal. This signal modulated the crystal characteristics seen by the microwave signal, so that, in effect, the crystal appeared as a variable admittance at the point X. Thus it modulated the amplitude of the microwave power transmitted to a second crystal. This crystal also was in parallel with a shorting piston, and the two pistons were tuned to provide a high-pass filter. The filter in effect shields crystal number 2 from the direct effects of the 100 kc signal applied to number 1, yet passes the modulated microwave signal. If the probe wavelength was changed, pistons numbers 1 and 2 and the three line stretchers had to be readjusted.

Crystal number 2 detected the modulation on the microwave carrier and its output was amplified in the r-f stages of a Navy radio receiver RBA-1. Readings on a Ballantine amplifying meter connected to the receiver proved to be proportional to the microwave power, so the system had a square-law response over the range 0.002 to 0.2 volts on the Ballantine. However, the detecting system was used to obtain null readings

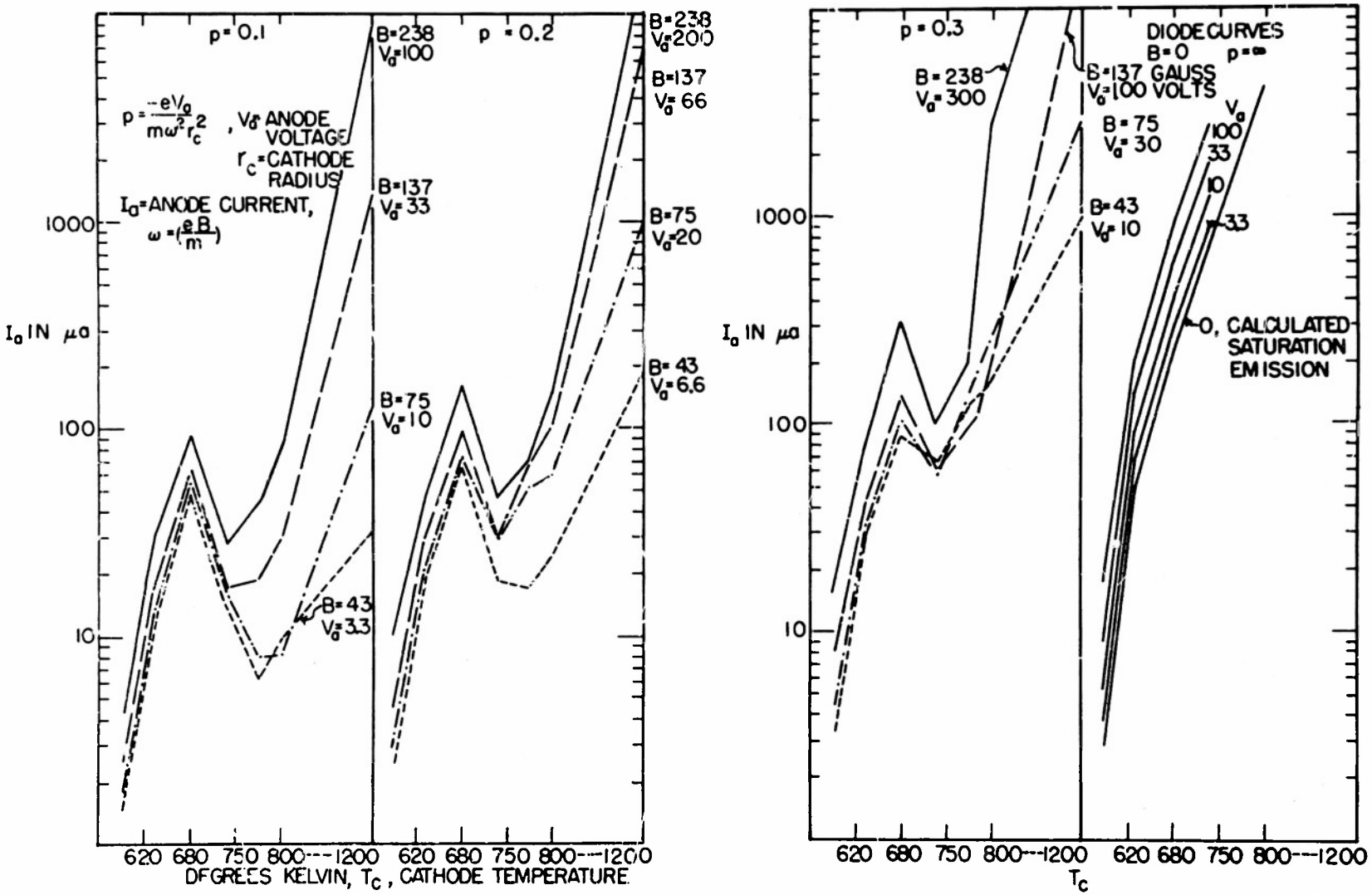

ANODE LEAKAGE CURRENT ANOMALY AT LOW EMISSION TEMPERATURES IN CYLINDRICAL MAGNETRON DIODE

FIG. 5-6

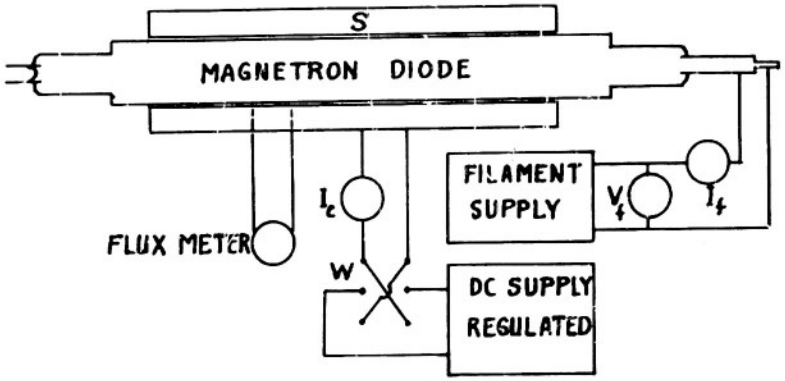

5-7A ELECTRICAL CIRCUIT

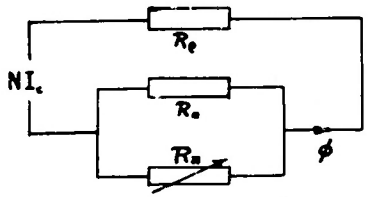

5-7B MAGNETIC CIRCUIT

FIG 5-7 CURIE TRANSITION MEASUREMENT

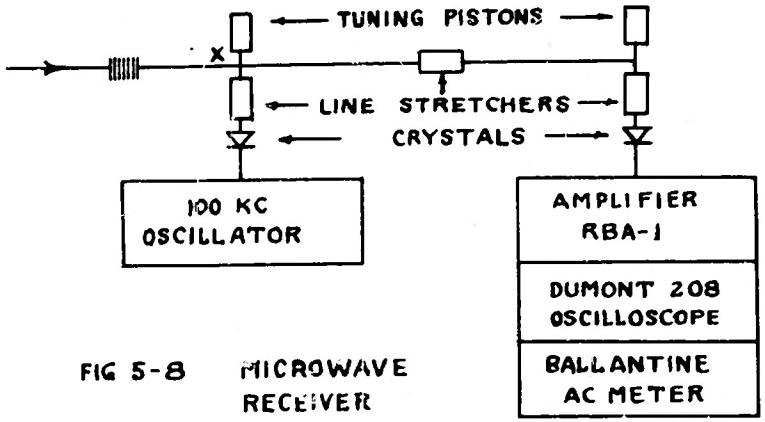

FIG 5-8 MICROWAVE RECEIVER

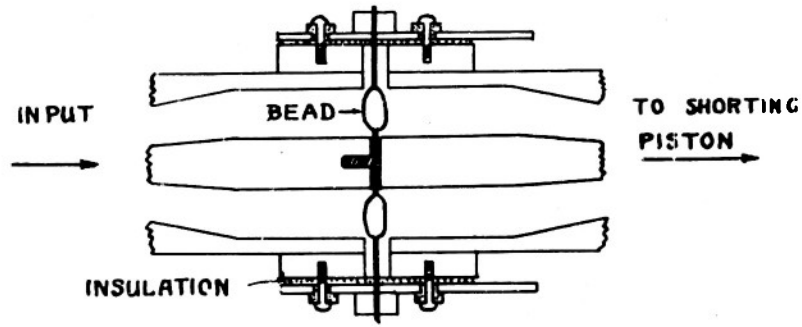

FIG 5-9 THERMISTOR MOUNT

and no accurate calibration was attempted. Minima below the level of 0.1 μw could not be measured because the filter did not remove completely the direct effects of the 100 kc signal on crystal number 2.

The receiver output could be displayed on a Dumont 208 oscilloscope and there presented a solid rectangle of 100 kc tracings. If noise from the diode magnetron mixed with the transmitted probe signal, the top and bottom of the rectangle showed violent ripples. The coherent noise associated with a cold cathode appeared as a smooth envelope with one or two sharp valleys.

A double thermistor circuit, mounted as shown in Fig. 5-9 served to calibrate the probe signal power. The circuit terminated in a shorting piston which was adjusted to maximize the readings. The thermistor mount, with thermistors in place and in operation presented a standing-wave ratio less than two. Hence about 90 per cent of the power incident on the mount was absorbed in it; most of this absorption presumably occurred in the thermistors. These thermistors were chosen from a group of six to obtain a good match of d-c characteristics. The power they absorbed from the probe signal was compared in a W bridge [6, page 118] with a standard 100 μw of d-c power.

A microwave transition section of brass, approximately the standard transition from 7/8" coaxial line to type N cable connection [4, Fig. 1.12] was fitted to the diode input end and secured by four radial screws. The similar transition at the output end of the diode also made connection to the diode filament leads. Figure 5-10 indicates how the filament leads came out through the hollow center conductor which extended the coaxial configuration of the diode. The extension ended beyond a movable shorting piston. The piston was always adjusted to maximize transmission through the type N fitting on the top of the section.

The current I_c through the windings of the solenoid sketched in Fig. 5-11 provided the steady magnetic field imposed on the diode. The windings, 6575 turns of number 24 copper wire coated twice with Formex, were wound on a copper tube 17 cm long and 2.6 cm in diameter. Each of the 21 layers was wound in the same direction, and the ends came out through

holes in insulating end-plates crimped to the copper tube. The inner layer was used for calibration, and the other twenty were connected externally in series. Each interior turn in the winding had continuous contacts with its six neighbors. This, the result of winding each layer in the same direction, presumably improves the thermal contact between layers. A similar solenoid, wound as one continuous wire, would have 10 per cent larger volume.

Two correction coils, each 5.9 cm ID and 2.6 cm long, and each of 222 turns of number 24 wire, were placed around the solenoid 1.5 cm in from its ends, and connected in series with it. They served to increase the strength of the axial magnetic field near the ends of the active cathode of the diode. At points on the axis and 4 cm from the center of the cathode the field was 1.4 per cent stronger than at the center. Thus the magnetic field serves in place of end hats to prevent electrons from leaking out to the anode at the ends of the diode.

The field along the solenoid axis was calibrated with a proton resonance circuit available in the laboratory. The first layer of the solenoid carried a 60 cycle modulating current for this calibration. The average B(gauss) corresponded to 466 I_c(amps). The ammeter used to measure I_c for the calibration was also used in the rest of the experiment to measure I_c.

The four arm junction in the circuit in Fig. 3-4 appears in the sketch in Fig. 5-12 and is similar to one given by Pound [6, Fig. 6.10, p. 268]. A null signal E_{o4} out of arm 4 of the T was taken to indicate that the signals E_{i1} and E_{i2} imposed on arms 1 and 2 were equal. In terms of the elements S_{14} and S_{24} of the scattering matrix S of the T [5, p. 548], the equation is:

$$E_{04} = S_{14} E_{12} + S_{24} E_{12} \doteq 0 \qquad (5.4)$$

The equation as it stands requires only that $S_{14} + S_{24} = 0$. At λ_p of 40 cm we found $S_{24} = -S_{14} = 0.55$, and at 180 cm $S_{24} = -S_{14} = 0.45$, while the ideal values are 0.71. This indicates that equation (5.4) is incomplete, and in fact S_{34} and S_{44} are not zero. The equation will still apply, however, if no signals enter arms 3 and 4. Arm 3 was terminated by fifty feet of lossy cable, Amphenol RG-21/u, and another length of this cable was inserted ahead of arms 1 and 2 to reduce the effect of reflections from them. The T-junction

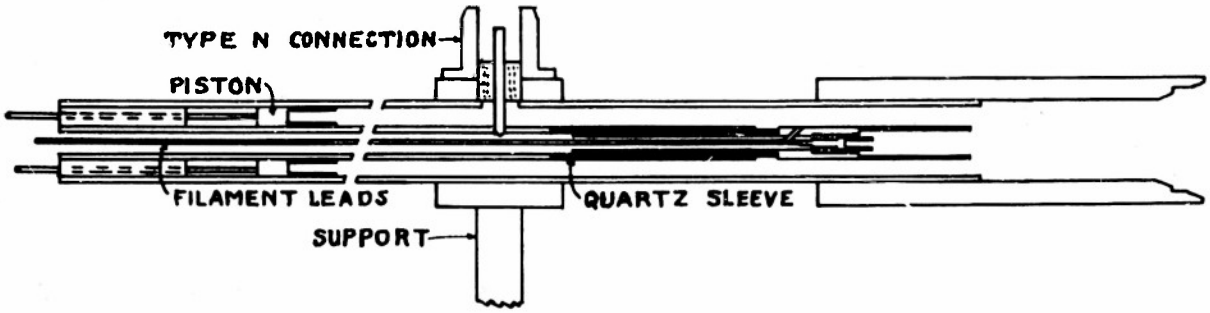

FIG 5-10 MICROWAVE COUPLING TO DIODE

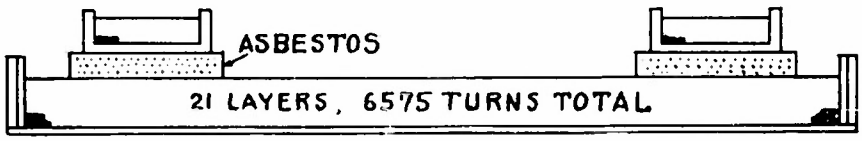

FIG 5-11 SOLENOID

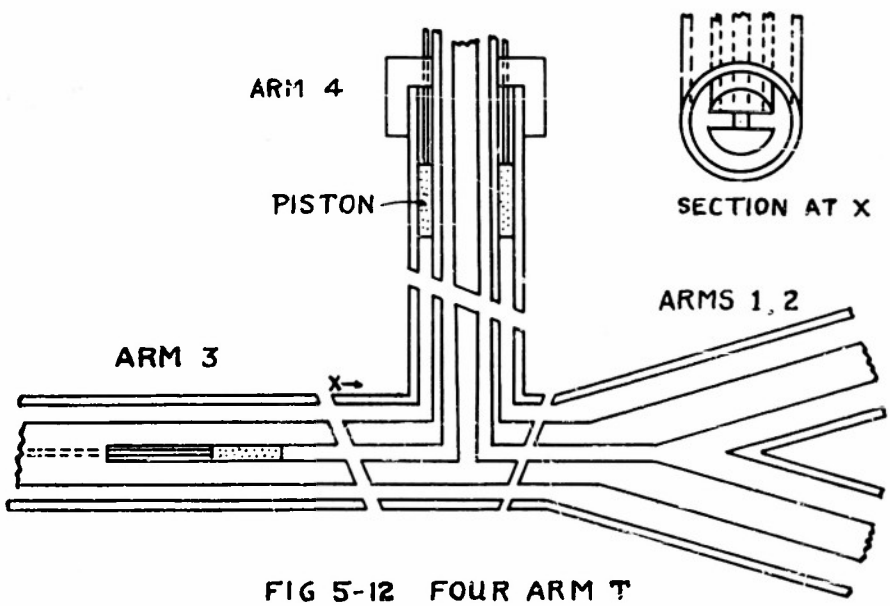

FIG 5-12 FOUR ARM T

does not have the good S matrix that Morita and Sheingold claim for a similar design [6, Fig. 10]; but the range of frequencies over which it gave adequate performance is 9 to 1, whereas they investigated a range of 1 to 1.13 with their design.

To measure attenuation, a cutoff attenuator TPS-15 [5, Fig. 11-16] was used. It proved, on calibration by the standing-wave method [5, page 816], to be consistent and accurate between settings zero and 20 db at all wavelengths used, but the insertion loss was over 20 db. Phase measurements by extension of a line stretcher require a single free progressive wave without reflections within the stretcher. Each end of a 70 cm stretcher (130 cm extension) was padded with lossy cable for our phase measurements and two such stretchers along parallel paths were in agreement. This is not, however, conclusive. The null setting of the stretcher was always the average of settings of equal signal level either side of the minimum, which was often relatively broad.

In summary, the measurements of frequency and of magnetic field we claim to be accurate within 0.2 per cent. The squares of these parameters, as plotted on the (p,u^2)-plane are then known to 0.4 per cent, the voltage V_a, and current I_a to 1 per cent. Over the range of variation of probe signal power, 1 to 400 μw, we cannot claim absolute accuracy closer than 20 per cent, and relative accuracies of 10 per cent. The signal sources were two: a military APT-5 radar jamming transmitter in the range λ_p from 20 to 66 cm, and a commercial General Radio 857A oscillator using a WE 316A (pre-war) triode at 180 cm.

Acknowledgments

This experimental study was carried out in part under the guidance of Professor E. L. Chaffee, and more recently under that of Professor N. Bloembergen. The diode was designed and built by Professor Mito, and the cyclotron resonance absorption first observed with it by Mr. L. M. Pease. Dr. F. K. Willenbrock made his wall-regulated current source available for the steady magnetic field. Professor C. L. Hogan suggested the work which led to Appendix 3-1.

References

1. Progress Report 23, Project III-A-7, Cruft Laboratory, Cambridge, Massachusetts, April, 1952.

2. Hermann and Wagener, The Oxide Coated Cathode, Chapman and Hall, London, 1951.

3. W. Schottky, "On the Emission of Electrons from Hot Wires in Retarding Potentials," Ann. Phys. Lpz. 44, 1011-1032 (1914).

4. R. V. Pound, Microwave Mixers, McGraw-Hill, New York, 1946, Vol. 16 of Rad. Lab. Series.

5. C. Montgomery, Technique of Microwave Measurements, McGraw-Hill, New York, 1947, Vol. II of Rad. Lab. Series.

6. Morita and Sheingold, A Coaxial Magic-T, T.R. 162, Cruft Laboratory, Cambridge, Massachusetts, October 10, 1952.

7. R. Bozorth, Ferromagnetism, D. Van Nostrand, New York, 1951 (page 271, Fig. 8-11 and page 721, Fig. 14-11).

DISTRIBUTION LIST

Technical Reports

2	Chief of Naval Research (427) Department of the Navy Washington 25, D. C.
1	Chief of Naval Research(460) Department of the Navy Washington 25, D. C.
1	Chief of Naval Research (421) Department of the Navy Washington 25, D. C.
6	Director (Code 2000) Naval Research Laboratory Washington 25, D. C.
2	Commanding Officer Office of Naval Research Branch Office 150 Causeway Street Boston, Massachusetts
1	Commanding Officer Office of Naval Research Branch Office 1000 Geary Street San Francisco 9, California
1	Commanding Officer Office of Naval Research Branch Office 1030 E. Green Street Pasadena, California
1	Commanding Officer Office of Naval Research Branch Office The John Crerar Library Building 86 East Randolph Street Chicago 1, Illinois
1	Commanding Officer Office of Naval Research Branch Office 346 Broadway New York 13, New York
3	Officer-in-Charge Office of Naval Research Navy No. 100 Fleet Post Office New York, N. Y.

1	Chief, Bureau of Ordnance (Re4) Navy Department Washington 25, D. C.
1	Chief, Bureau of Ordnance (AD-3) Navy Department Washington 25, D. C.
1	Chief, Bureau of Aeronautics (EL-1) Navy Department Washington 25, D. C.
2	Chief, Bureau of Ships (810) Navy Department Washington 25, D. C.
1	Chief of Naval Operations (Op-413) Navy Department Washington 25, D. C.
1	Chief of Naval Operations (Op-20) Navy Department Washington 25, D. C.
1	Chief of Naval Operations (Op-32) Navy Department Washington 25, D. C.
1	Director Naval Ordnance Laboratory White Oak, Maryland
2	Commander U. S. Naval Electronics Laboratory San Diego, California
1	Commander (AAEL) Naval Air Development Center Johnsville, Pennsylvania
1	Librarian U. S. Naval Post Graduate School Monterey, California
50	Director Signal Corps Engineering Laboratories Evans Signal Laboratory Supply Receiving Section Building No. 42 Belmar, New Jersey

3	Commanding General (RDRRP) Air Research and Development Command Post Office Box 1395 Baltimore 3, Maryland
2	Commanding General (RDDDE) Air Research and Development Command Post Office Box 1395 Baltimore 3, Maryland
1	Commanding General (WCRR) Wright Air Development Center Wright-Patterson Air Force Base, Ohio
1	Commanding General (WCRRH) Wright Air Development Center Wright-Patterson Air Force Base, Ohio
1	Commanding General (WCRE) Wright Air Development Center Wright-Patterson Air Force Base, Ohio
2	Commanding General (WCRET) Wright Air Development Center Wright-Patterson Air Force Base, Ohio
1	Commanding General (WCREC) Wright Air Development Center Wright-Patterson Air Force Base, Ohio
2	Commanding General (WCLR) Wright Air Development Center Wright-Patterson Air Force Base, Ohio
1	Commanding General (WCLRR) Wright Air Development Center Wright-Patterson Air Force Base, Ohio
2	Technical Library Commanding General Wright Air Development Center Wright-Patterson Air Force Base, Ohio
1	Commanding General (RCREC-4C) Rome Air Development Center Griffiss Air Force Base Rome, New York
1	Commanding General (RCR) Rome Air Development Center Griffiss Air Force Base Rome, New York

2	Commanding General (RCRW) Rome Air Development Center Griffiss Air Force Base Rome, New York
6	Commanding General (CRR) Air Force Cambridge Research Center 230 Albany Street Cambridge 39, Massachusetts
1	Commanding General Technical Library Air Force Cambridge Research Center 230 Albany Street Cambridge 39, Massachusetts
2	Director Air University Library Maxwell Air Force Base, Alabama
1	Commander Patrick Air Force Base Cocoa, Florida
2	Chief, Western Division Air Research and Development Command P. O. Box 2035 Pasadena, California
1	Chief, European Office Air Research and Development Command Shell Building 60 Rue Ravenstein Brussels, Belgium
1	U. S. Coast Guard (EEE) 1300 E Street, N. W. Washington, D. C.
1	Assistant Secretary of Defense (Research and Development) Research and Development Board Department of Defense Washington 25, D. C.
5	Armed Services Technical Information Agency Document Service Center Knott Building Dayton 2, Ohio

1	Director Division 14, Librarian National Bureau of Standards Connecticut Avenue and Van Ness St., N. W.
1	Director Division 14, Librarian National Bureau of Standards Connecticut Avenue and Van Ness St., N. W.
1	Office of Technical Services Department of Commerce Washington 25, D. C.
1	Commanding Officer and Director U. S. Underwater Sound Laboratory New London, Connecticut
1	Federal Telecommunications Laboratories, Inc. Technical Library 500 Washington Avenue Nutley, New Jersey
1	Librarian Radio Corporation of America RCA Laboratories Princeton, New Jersey
1	Sperry Gyroscope Company Engineering Librarian Great Neck, L. I., New York
1	Watson Laboratories Library Red Bank, New Jersey
1	Professor E. Weber Polytechnic Institute of Brooklyn 99 Livingston Street Brooklyn 2, New York
1	University of California Department of Electrical Engineering Berkeley, California
1	Dr. E. T. Booth Hudson Laboratories 145 Palisade Street Dobbs Ferry, New York
1	Cornell University Department of Electrical Engineering Ithaca, New York

1	University of Illinois Department of Electrical Engineering Urbana, Illinois
1	Johns Hopkins University Applied Physics Laboratory Silver Spring, Maryland
1	Professor A. von Hippel Massachusetts Institute of Technology Research Laboratory for Insulation Research Cambridge, Massachusetts
1	Director Lincoln Laboratory Massachusetts Institute of Technology Cambridge 39, Massachusetts
1	Signal Corps Liaison Office Massachusetts Institute of Technology Cambridge 39, Massachusetts
1	Mr. Hewitt Massachusetts Institute of Technology Document Room Research Laboratory of Electronics Cambridge, Massachusetts
1	Stanford University Electronics Research Laboratory Stanford, California
1	Professor A. W. Straiton University of Texas Department of Electrical Engineering Austin 12, Texas
1	Yale University Department of Electrical Engineering New Haven, Connecticut
1	Mr. James F. Trosch, Administrative Aide Columbia Radiation Laboratory Columbia University 538 West 120th Street New York 27, N. Y.
1	Dr. J.V.N. Granger Stanford Research Institute Stanford, California